NTNU
Norwegian University of
Science and Technology

An Experimental Study of Thermal Properties of Permafrost Soils

Una Helene Haug Bratlie

Civil and Environmental Engineering
Submission date: July 2018
Supervisor: Gustav Grimstad, IBM
Co-supervisor: Arne Instanes, UNIS

Norwegian University of Science and Technology
Department of Civil and Environmental Engineering

NORWEGIAN UNIVERSITY OF SCIENCE AND TECHNOLOGY
DEPARTMENT OF CIVIL AND ENVIRONMENTAL ENGINEERING

Report Title: **An Experimental Study of Thermal Properties of Permafrost Soils**	Date: **26.07.2018** Number of pages (incl. appendices): 156	
	Master Thesis	x

Name: Una Helene Haug Bratlie

Professor in charge: Professor Gustav Grimstad (NTNU)

Other external professional supervisor: Professor II Arne Instanes (UNIS)

Abstract:
Soil is a multiphase porous media, and its complexity increases when the soil freezes. The high compressive strength of frozen soil has been utilized by geotechnical engineers in construction of frozen earth structures. However, in permafrost settings, the upper layer of the soil is subject to seasonal thawing/freezing and is associated with stability problems. The thickness of this seasonally active layer is dependent on thermal properties of the soil, and the changes in these properties with temperature. Therefore, thermal properties of the soil must be evaluated in frozen ground engineering design.

Thermal conductivity is essential for the heat transport in the ground, and reliable data on the thermal conductivity is required. Very often such information is not readily available. The solution is to perform field investigations and laboratory work in order to obtain index parameters. From the obtained soil parameters, the soil thermal conductivity can be estimated from existing empirical equations and analytical models. This process could be inaccurate and time consuming. Hence, direct and efficient methods to directly measure the thermal conductivity are desired.

In this thesis, a KD2 Pro Thermal Properties Analyzer has been used to directly measure the thermal properties of frozen and unfrozen core samples from Adventdalen, Svalbard. Laboratory investigations of the soil were performed at the University Centre in Svalbard (UNIS). Index tests include the estimation of water content, bulk density, dry density, density of solids, salinity, organic content, degree of saturation, and grain size distribution.

The thermal properties from KD2 Pro measurements were compared to average diagrams based on Kersten's (1949) empirical equations for thermal conductivity. Surface and ground temperature data from a thermistor string installed in lower Adventdalen have been collected and plotted with time and depth. Back-calculations of thermal diffusivity from temperature data were performed using thermistor string data.

Finally, a one-dimensional geothermal model was used to investigate the ground thermal regime response to climate changes. The model was created with a finite element program called PLAXIS and used known thermal and physical properties as input parameters for the soil. The model was run for the period 2016-2017, and the results were validated with ground temperature data from the thermistor sting. The same model set-up was used to simulate two future scenarios in 2090; RCP2.6 and RCP8.5.

Keywords:

1. Frozen ground engineering
2. Thermal conductivity
3. Ground temperature profile
4. Adventdalen

UNIS

Polar night in Longyearbyen, Svalbard. Credit: Leonard Magerl.

Preface

This paper is a master's thesis in Geotechnical Engineering at the Norwegian University of Science and Technology (NTNU) as part of the MSc program in Civil and Environmental Engineering. The laboratory work was carried out as a guest master student at the University Centre in Svalbard (UNIS) and in cooperation with the Norwegian Geo-Test Sites (NGTS) project during the spring semester of 2018.

Professor Gustav Grimstad at NTNU and Professor II Arne Instanes at UNIS have been the supervisors.

Trondheim, 26.07.2018

Una Helene Haug Bratlie

Acknowledgments

I would like to thank the following people and institutions for their support:

Gustav Grimstad - For providing help and guidance during the work of the thesis at NTNU.

Seyed Ali Ghoreishian Amiri - For assistance and discussions of the thermal analysis in PLAXIS.

Arne Instanes - For giving me the opportunity to work with an interesting topic and for providing help and guidance during this work.

Graham Lewis Gilbert and Anatolii Sinitsyn - For providing ideas, insight and expertise that greatly assisted the research and laboratory work at UNIS.

The University Centre in Svalbard (UNIS) - For hosting me as a guest master student and for providing me with laboratory equipment and work space during my stay at UNIS.

The Norwegian Geo-Test sites (NGTS) project - For letting me be involved in the project and for providing me with economical support.

My fellow NTNU students - For motivation, help, and relevant discussions.

U.H.H.B

Abstract

Soil is a multiphase porous media, and its complexity increases when the soil freezes. The high compressive strength of frozen soil has been utilized by geotechnical engineers in construction of frozen earth structures. However, in permafrost settings, the upper layer of the soil is subject to seasonal thawing/freezing and is associated with stability problems. The thickness of this seasonally active layer is dependent on thermal properties of the soil, and the changes in these properties with temperature. Therefore, thermal properties of the soil must be evaluated in frozen ground engineering design.

Thermal conductivity is essential for the heat transport in the ground, and reliable data on the thermal conductivity is required. Very often such information is not readily available. The solution is to perform field investigations and laboratory work in order to obtain index parameters. From the obtained soil parameters, the soil thermal conductivity can be estimated from existing empirical equations and analytical models. This process could be inaccurate and time consuming. Hence, direct and efficient methods to directly measure the thermal conductivity are desired.

In this thesis, a KD2 Pro Thermal Properties Analyzer has been used to directly measure the thermal properties of frozen and unfrozen core samples from Adventdalen, Svalbard. Laboratory investigations of the soil were performed at the University Centre in Svalbard (UNIS). Index tests include the estimation of water content, bulk density, dry density, density of solids, salinity, organic content, degree of saturation, and grain size distribution.

Plots of index and thermal properties with depth, were created to investigate dependencies and trends. The tested soils are well-sorted deposits, dominated by fines. The upper part of the depth profile is dominated by high water content, which is a result of accumulation of water due to freezing and thawing processes. The thermal properties have small variations over the profile. However, an increase in thermal conductivity with higher water content in frozen state is observed. The impact of salinity and organic content on the thermal conductivity was not possible to investigate.

The thermal properties from KD2 Pro measurements were compared to average diagrams based on Kersten's (1949) empirical equations for thermal conductivity. The comparison showed that thermal conductivity from Kersten's (1949) diagrams are lower than the values obtained by the modern KD2 Pro Thermal Properties Analyzer. Uncertainties are associated with procedure and results for both methods. Hence, more data is needed to argue that the KD2 Pro is a more efficient, accurate and straightforward method to obtain values for thermal conductivity than the average diagrams.

Surface and ground temperature data from a thermistor string installed in lower Adventdalen have been collected and plotted with time and depth. In agreement with literature, the attenuation of temperature with depth was shown by a phase lag, or illustrated by a whiplash curve. The seasonal thawed layer in lower Adventdalen is estimated to be approximately one meter in thickness. The mean annual ground temperature is about -5.2°C. Back-calculations of thermal diffusivity from temperature data were performed using the thermistor string plots. The approach met some challenges, but the result was in agreement

with the direct measurements with the KD2 Pro Thermal Properties Analyzer.

Finally, a one-dimensional geothermal model was used to investigate the ground thermal regime response to climate changes. The model was created with a finite element program called PLAXIS and used known thermal and physical properties as input parameters for the soil. The thermal boundary condition at the surface was adapted from present and future air temperature data. The model was run for the period 2016-2017, and the results were validated with ground temperature data from the thermistor sting. The PLAXIS model showed unexpected results regarding the depth of thaw of the upper soil layer. The PLAXIS model overestimated the active layer with about one meter. However, the model showed good agreement with the thermistor string data in deeper layers due to the bottom boundary condition. The same model set-up was used to simulate two future scenarios in 2090; RCP2.6 and RCP8.5. Both climate scenarios indicate a warming of the Earth's surface. Increased thickness of the active layer was seen in both scenarios, with the RCP8.5 initiation the deepest thawing depth. However, conclusions must be considered with great caution due to the simple procedure and many assumptions.

Sammendrag

Jord er et flerfaset porøst materiale med økende kompleksitet i frossen tilstand. Den høye trykkfastenheten til frossen jord har blitt utnyttet av geotekniske ingeniører til utbygging av kalde områder. Imidlertid, i områder med permafrost er det øverste jordlaget påvirket av periodisk frysing og tining og er assosiert med stabilitetsproblemer. Tykkelsen på dette aktive laget (jordlaget påvirket av sesongmessige variasjoner) er sterkt avhengig av jordas termiske egenskaper, og endringer i disse egenskapene med temperatur. Det er derfor viktig at analyse av termiske egenskaper inkluderes i design av bygg og konstruksjoner i og på frossen jord.

Termisk konduktivitet (varmeledningsevne) er en essensiell materialkonstant for hvordan varme transporteres i bakken. Pålitelige data for termisk konduktivitet er nødvendig, men slik informasjon er dessverre ikke alltid tilgjengelig. Løsningen er å utføre felt - og laboratoriearbeid for å innhente indeksparametere. Disse indeksparametere kan bli satt inn i empiriske likninger og analytiske modeller for beregning av varmeledningsevnen til jorda. Da denne prosessen kan være unøyaktig og tidkrevende, ønsker man å finne direkte og mer effektive metoder for måling av jordas termiske ledningsevne.

I denne masteroppgaven har en håndholdt KD2 Pro Thermal Properties Analyzer blitt brukt til direkte måling av termiske egenskaper av frosne og ufrosne kjerneprøver fra Adventdalen, Svalbard. Laboratorieundersøkelsene av jorda er utført på Universitetssenteret på Svalbard (UNIS). Laboratorieundersøkelsene av jordmaterialet inkluderer estimering av vanninnhold, tyngdetetthet, saltinnhold, innhold av organisk materiale, metningsgrad og kornstørrelsesfordeling.

Indeks- og termiske egenskaper er presentert med dybde for å undersøke sammenhenger og trender. Materiale er dominert av finstoff, og karakterisert som velgradert. Den øvre delen av profilet har et høyt vanninnhold på grunn av akkumulasjon av vann/is som et resultat av fryse- og tineprosesser. Videre har de termiske egenskapene liten variasjon over profilet, men det observeres en økning i termisk konduktivitet med høyere vanninnhold i frossen tilstand. Sammenhengen mellom saltinnhold, organisk innhold og termisk konduktivitet kan ikke påvises.

De termiske egenskapene fra KD2 Pro-målinger er sammenlignet med verdier hentet fra diagrammer basert på Kerstens (1949) empiriske ligninger for varmeledningsevne. Sammenlikningen viste at termisk konduktivetet fra Kerstens (1949) diagrammer er lavere enn de verdiene som er oppnådd ved direkte måling med det moderne KD2 Pro instrumentet. Usikkerhet knyttes til prosedyre og resultater ved begge metode, og datagrunnlaget er for tynt til å hevde at KD2 Pro er en mer effektiv, nøyaktig og lettvint metode for å anskaffe verdier for termisk konduktivitet enn diagrammene.

En termistorstreng (temperaturmåler) installert i permafrost i Adventdalen, Svalbard gir informasjon om overflate og bakketemperaturer, og data herfra er samlet og plottet med tid og dybde. I samråd med faglitteratur avtar og dempes temperaturen med dybden, noe som kommer til uttrykk ved faseforsinkelser, eller illustrert av en whiplash-kurve. I Adventdalen, antas det aktive laget å ha en tykkelse på en meter og gjennomsnittlige årlige

bakketemperaturen er ca. -5.2 °C. Tilbakeregninger av termisk egenskaper fra temperaturdata har blitt utført ved analyse av termistorstrengplottene. Beregningene møtte noen utfordringer, men resultatet samsvarte godt med de direkte målinger gjort med KD2 Pro instrumentet.

Til slutt ble en endimensjonal geotermisk modell laget i elementmetode programmet PLAXIS. Modellen skulle undersøke termisk respons fra klimaendringer, og brukte kjente termiske og fysiske egenskaper som jordparametere. Den termiske grensebetingelsen ved overflaten ble tilpasset nåtidens og fremtidens lufttemperaturer. Modellen ble kjørt for perioden 2016-2017, og resultatene ble sammenliknet og validert med målte bakketemperaturer fra termistorstrengen. PLAXIS-modellen viste uventede resultater angående tykkelsen av det aktive jordlaget, og overestimerte det med ca. en meter. Modellen viste imidlertid likhet med termistorstrengdata i dypere lag på grunn av randbetingelsene i bunnen av jordpolygonet. Det samme modelloppsettet ble brukt til å simulere to fremtidige klimascenarier i 2090; RCP2.6 og RCP8.5. Begge klimascenarier indikerte oppvarming av jordas overflate, og økt tykkelse av det aktive laget ble sett i begge scenarier. RCP8.5 vil medføre mest tining. Konklusjonene må imidlertid vurderes med stor forsiktighet på grunn av den enkle prosedyren, tynt datagrunnlag og mange antagelser.

Table of Contents

List of Tables

List of Figures

List of Symbols

γ	unit weight of soil
ω	frequency of the annual signal
ρ	bulk density
ρ_d	dry density
ρ_s	density of solids
A	cross-section area
A_s	surface temperature amplitude
A_z	temperature amplitude at depth z
c	heat capacity
c_a	apparent heat capacity
c_i	heat capacity of the ice
c_u	heat capacity of unfrozen water
c_s	heat capacity of the solid
C_v	volumetric heat capacity
C_{vf}	volumetric heat capacity of frozen soil
C_{vu}	volumetric heat capacity of unfrozen soil
C_{vw}	volumetric heat capacity of water
D	thermal diffusivity
e	void ratio
G_s	specific gravity
I	surface freezing/thawing index
k	thermal conductivity
k_f	frozen thermal conductivity
k_{un}	unfrozen thermal conductivity
L	volumetric latent heat
L'	mass latent heat of water
M	total mass of soil
M_i	mass of ice
M_s	mass of solids
M_{uw}	mass of unfrozen water
M_w	mass of water
n	porosity
p	period
q	heat per unit length
Q	amount of heat flow
S_r	degree of saturation
t	time
t_{max}	the day when maximum temperature occur
ΔT	temperature change
T	temperature
T_m	mean (annual) surface temperature
T_{max}	maximum temperature

T_{min}	minimum temperature
$T_{s,t}$	surface temperature
T_z	limits of the temperature swings
$T_{z,t}$	temperature at any depth and time
v_a	phase speed of the annual wave
V	total volume
V_p	volume of pores
V_s	volume of solids
V_w	volume of water
w	water content
w_i	ice content
w_u	unfrozen water content
$w_{N=25}$	25 blows in the liquid limit test
$w_{N=100}$	100 blows in the liquid limit test
X	specimen thickness
z	depth
Z	depth of frost penetration

Abbreviations

ASTM	American Society for Testing and Materials
ALT	Active Layer Thickness
AT	Air Temperature
CALM	Circumpolar Active Layer Monitoring
CRREL	Cold Region Research and Engineering Laboratory
IPCC	Intergovernmental Panel on Climate Change
MAAT	Mean Annual Air Temperature
MAGT	Mean Annual Ground Temperature
MAST	Mean Annual Surface Temperature
NCAR	National Center for Atmospheric Reseach
NGTS	Norwegian Geo-Test Sites
OM	Organic Matter
ppt	parts per thousand
RCP	Representative Concentration Pathway
ST	Surface Temperature
UNIS	the University Centre in Svalbard
USCS	Unified Soil Classification System
USDA	United States Department of Agriculture
ZAA	Zero Annual Amplitude

Chapter 1

Introduction

Permafrost is ground (soil or rock) that remains at or below 0°C for two or more consecutive years. The identification of permafrost is conducted solely on the basis of temperature and not on the physical state of moisture in the ground. Due to the effect of soil particles and presence of pore-water solutes, the freezing point of water may be depressed several degrees below 0°C (Andersland and Ladanyi, 1994). Permafrost is therefore not necessarily frozen and the permafrost may be unfrozen, partially-frozen and frozen depending upon the state of the ice/water content (French, 2007).

Soil in frozen state is characterized by high compressive strength and has been utilized by engineers in construction of frozen earth structures such as stabilization of excavations, foundation support, and to temporarily control groundwater flow. When the ground freezes, interstitial the water turns into ice, termed pore ice. Ice acts as a bonding agent, increasing the soil strength by combining the strength of adjacent soil particles and preventing seepage.

On the other hand, frozen ground can also lead to engineering challenges. Permafrost derives much of its geotechnical significance from the presence of ground ice. Permafrost is overlain by a seasonally unfrozen zone termed the active layer. In fine-grained soils, this top few meters of permafrost are characteristically ice enriched (Guodong, 1983). The formation of complex terrain features and zones of ice-enriched ground may lead to difficult and expensive construction problems. One reason for this is that water expands as it freezes in the ground. Fine-grained frost susceptible soils will experience frost heave and increased lateral passive earth pressure. Secondly, changes in air temperature and flow of water may supply heat to the soil, initiating thawing which results in reduced soil strength and thaw settlements. To assess stability, information about the soil conditions, groundwater, and ground temperature regime are important.

Moreover, the thickness of the active layer is sensitive to changes in summer air temperature (Andersland and Ladanyi, 1994). Increase in active layer thickness results in

ground-ice degradation, initiating geomorphic change in permafrost landscapes. Ground-ice melt results in thaw subsidence and thermokarst in flat terrain and can lead to landslide in sloping terrain. Consideration of the response of the active layer to seasonal freezing and thawing must be considered in permafrost engineering design. Geothermal analyses are required to investigate the effect of construction work, the structure and climate scenarios on the ground - thermal regime. The heat balance below the surface can be further employed to predict the thickness of the active layer. Consequently, the depth of frost and thaw rely on reasonably accurate values of thermal properties, in particular thermal conductivity. Appropriate estimation methods for thermal properties are required for these kinds of analyses.

Figure 1.1: Map of permafrost distribution in the Arctic. Regions of isolated, sporadic, discontinuous, and continuous permafrost are shown. (Adapted from Brown et al. (1998)).

Seasonal and permanently frozen ground are characteristics of cold regions. With exception of a high-altitude, alpine environments, the cold regions of the world are centered around the poles. The isotherm for 0°C mean temperature during the coldest month of the year, or a seasonal frost penetration of 300 mm once in 10 years, are generally accepted southern limits of the cold region on the Northern Hemisphere (Bates and Bilello, 1966). Resultingly, the southern limit extends to about 40 (deg) N in the Northern Hemisphere (Andersland and Ladanyi, 1994). Furthermore, more than half of the landmass in the Northern Hemisphere have some seasonal frozen ground (NSIDC, 2017). The active layer is thickest close to the Southern limit. Its thickness varies from year to year, depending on controls such as snow cover, vegetation, slope orientation, air temperature etc. Permafrost

underlies 20 - 25 % of the land surface on Earth, and can occur everywhere over a large area continuous, or in a discontinuous pattern under the ground surface. Permafrost thickness is not constant, thinning gradually toward the lower latitude in contrast to the active layer (Andersland and Ladanyi, 1994). Figure 1.1 highlights the permafrost distribution on the Northern Hemisphere.

The temperature at which soil freezes depends on the soil types content of minerals, organic material, and water. A common assumption is that the mean annual ground temperature (MAGT) must be at least -3°C for permafrost to exist (Andersland and Ladanyi, 1994). In addition, does the presence of a water bodies affect the thermal regime of permafrost. The variations in distribution, thickness and temperature of permafrost is not constant with present-day climate. As the temperature changes, alterations of the thermal regime and thermal properties of frozen ground are seen. "General circulation models indicate that climate warming will be amplified at high latitudes, and this would likely increase the thickness of the active layer and/or result in ground subsidence" (Humlum, 2018). Moreover, climate change and increased temperatures in the Arctic result in thawing of permafrost, decreased sea ice and glacier ice mass, and shifted biological indicators (Kurylyk and Watanabe, 2013). Also construction in permafrost areas will change the thermal regime and thus degrade the permafrost table. Construction will change the soil structure and boundary condition, and heated buildings may give off heat to the soil underneath. New research to increase the knowledge about these topic is therefore vital and will be an essential focus for future investigations in cold regions (Anderson et al., 1976).

Thermal properties of the soil matrix include thermal conductivity, heat capacity, thermal diffusivity, latent heat (and thermal expansion/contraction) (Andersland and Ladanyi, 1994). For assessing the quantity of heat transported in the soil, the thermal conductivity is essential. The thermal conductivity is considered for steady-state condition problems (i.e. no change of temperature with time). In transient heat problems, the thermal diffusivity arises, and the latent heat of fusion dominates in phase change situations (Williams and Smith, 1991). Thermal conductivity and thermal diffusivity are related by the volumetric heat capacity of the material. In geotechnical problems, heat capacity can give information about the duration of the heating or cooling process under a given supply, as well as the cost implications thereof.

The focus in this thesis rests on determining the thermal conductivity, which is essential for the heat transport. To determine this property of soil, unfrozen and frozen, computational, laboratory and/or field approaches can be applied. The steady-state guarded hot plate method (GHP) to measure soil thermal conductivity is an example of an commonly used experimental method. Likewise, the probe method is an example of a transient measuring method which is suitable both in the field and in the laboratory. Additionally, several scientists have tried to simulate processes that are not measurable or required much effort in order to determine the thermal conductivity of soils. Such models use physical parameters obtained from laboratory work.

The thermal properties of soil are dependent on degree of saturation, density, water content and soil type (Farouki, 1981). Information about soil classification, the strata and soil properties can be obtained from boring and sampling. The soil heat capacity can be directly

inferred if the soil composition is known. On the other hand, determination of the thermal conductivity is more challenging as it not only depends on the soil. Other parameter are for example the vegetation cover of the soil, water movement within the soil or the sun radiation. In most situations, the solution is to perform field investigations and laboratory work in order to obtain soil parameters. From the obtained soil parameters, the soil thermal conductivity can be calculated from existing empirical equations and analytic models. This process could be cumbersome and very time consuming. For engineering purposes, more simple and efficient methods to measure the thermal conductivity are desired.

One reliable modelling method that has so far been used for determining the thermal conductivity, for both unfrozen and frozen soils, is the Kersten (1949) method. The thermal conductivity tests by Kersten (1949) were undertaken using a cylindrical guarded hot plate apparatus. His equations are based on index properties such as water content, degree of saturation and dry density. However, the method is limited by neglecting quartz content and unfrozen water content, which both influence the thermal conductivity of the soil. Furthermore, Farouki (1986) conducted a thorough review of many empirical and semi-empirical models, among them Johansen's model (1975). His model used data provided by Kersten (1949) and developed the normalized thermal conductivity concept applicable for both frozen and unfrozen soils (Côté and Konrad, 2005). In recent times, studies to evaluate and improve the accuracy of these models have been undertaken (Barry-Macaulay et al., 2015). In particular, Aleksyutina and Motenko (2017) used a commercially available thermal needle probe (KD2 Pro Thermal Properties Analyzer) to perform direct measurements of the thermal conductivity of soil samples for characterization of frozen and thawed deposits. From such measurements it is possible to perform an investigation of the relation between thermal conductivity obtained from direct measurement and soil index properties. However, there are few sources for direct testing of thermal conductivity in frozen soils, and a standard testing procedure has not yet been established (Aleksyutina and Motenko, 2017).

The interest of testing in Arctic conditions and research on problems related to permafrost soils has increased. In June 2016, the Norwegian Geo-Test Sites (NGTS) research consortium was started, with one of five test sites established in permafrost on Svalbard. The Norwegian Geo-Test Sites (NGTS) project is a Research and Development (R&D) program and is a comprehensive cooperation between the Norwegian geotechnical engineering community. Involved are the Norwegian Geotechnical Institute (NGI), NTNU, SINTEF, UNIS and the Norwegian Public Roads Administration. The test sites are developed as field laboratories for testing, verification and control of new methods and equipment for site investigations and foundation engineering (NGI, 2016). By the end of the operating phase of 20 years, the test sites will be used as benchmarks for federal and private developers, research institutes and academia and by industry. The goal is that that results and data generated at the sites will be included in development and improvement of geotechnical and foundations engineering methods. To identify geotechnical parameters for permafrost soils, laboratory investigations will be performed. The geothermal regime is monitored by thermistor strings at the site. UNIS/SINTEF are coordinators for the two permafrost sites on Svalbard and Arne Instanes is the coordinator for the work performed there. In this thesis, soil from the site located in lower Adventdalen will be investigated.

1.1 Problem Definition

This master project is an experimental study and includes evaluation of methods to determine the thermal properties of frozen soil from Adventdalen, Svalbard. Results from the experimental work are used in modeling the thermal response of permafrost to changes in air and surface temperatures. The specific objectives are:

1. To review previous studies of the thermal properties of permafrost soil;
2. To present examples of experimental and computational methods for determining thermal properties of frozen and unfrozen soils;
3. To present a depth profile of index and thermal properties for a typical permafrost soil in lower Adventdalen;
4. To study the relation between changing temperature and thermal properties in soils by investigating frozen and unfrozen thermal properties;
5. To compare methods (direct measurement, index properties, and back-calculation using temperature data) for estimating thermal properties in frozen (and unfrozen) soils;
6. To create a temperature profile for a borehole in lower Adventdalen, by using data from a thermistor string;
7. To perform geothermal modelling to investigate the thermal response of seasonal frozen ground to changes in air temperature in Adventdalen.

1.2 Limitations

The study is limited to one borehole in Adventdalen. In order to assess the wider applicability of these results, similar studies may be required at more locations within Adventdalen. However, a sedimentological model, detail the infilling of the Adventdalen (Gilbert et al., 2018), indicates that soil conditions within the Adventdalen study site should be relatively uniform.

The measurements using the KD2 Pro Thermal Properties Analyzer were performed on only two temperatures; The temperature for the unfrozen tests where chosen to be that of the room temperature in the laboratory (ca. 23°C), while the cold lab was set to -10°C. This was done due to an underlying assumption that the unfrozen water content at -10°C is small, and the measuring errors using the KD2 Pro Thermal Properties Analyzer were minimized. However, in Adventdalen the ground surface temperatures are observed to be approximately -5°C. The soils are saline, and unfrozen water will be present. Therefore, applying the laboratory results to the field should not go unchallenged.

Furthermore, some of the core samples where broken into pieces too small for installation of the TR-1 needle. In these cases, no thermal properties from direct measurements were obtained. Moreover, results for all laboratory testing are dependent on human accuracy. To

minimize human source of error, more testing on the same soil should be performed. The limited time in the laboratory at UNIS prevents the possibility of more extensive testing on the soils.

Moreover, it is worthy of remark that the Kersten (1949) method was selected based on available information from the laboratory testing. It is questionable whether Kersten's (1949) equations have best applicability for the soil studied. Johansen's (1975) model was eliminated due to lack of mineral composition data. In a larger evaluation of the thermal conductivity of soil from Adventdalen, the equations by Johansen (1975) could be investigated.

Furthermore, limitations with Kersten's (1949) equations apply. The diagrams for frozen thermal conductivity by Kersten (1949) do not account for unfrozen water content even though they are created for soils at - 4°C. A comparison of the direct measurements at - 10°C and the thermal properties found from index testing should therefore be supplemented by more data before conclusions are made. Addressing this limitation, back-calculation of the thermal properties, and more extensive testing should be done to evaluate the comparison.

Despite the importance of unfrozen water content in investigation of thermal conductivity of frozen soils, it is not included as a part of the laboratory work of this master thesis. The equations developed by Nybo (2017) was found to be sufficient as input parameters in the PLAXIS model. For an more extensive research and future investigation of thermal property models, determination of the unfrozen water content should be considered.

The thermal model in PLAXIS is simple and the accuracy at which reality is approximated depends highly on the expertise of the user regarding the modelling of the problem. During the time of this master thesis the introduction to the software was limited. Further study should focus on increasing the users understanding of the software, thus to obtain deeper knowledge about the effect of the input parameters.

Finally, the projected temperature data are retrieved from plausible alternative scenarios of the future, but are not predictions or forecasts. Moreover, the surface temperatures are roughly approximated, and brings uncertainty. Higher resolution results should be implemented and a more accurate procedure should be used to improve the model.

1.3 Structure of Report

This report is structured in 7 chapters, and an outline is provided here:

Chapter 1 is an introductory part that includes the background of the topic. The objectives and limitations are presented here, together with the outline of the report.

Chapter 2 is a literature review and gives complementary information about permafrost, along with physical and thermal properties of frozen soil and factors affecting the thermal conductivity of soils. The chapter is partially an extract of my project thesis in TBA4510

at NTNU, autumn 2017. The project thesis was a literature review of permafrost as a preparation for the master thesis (Bratlie, 2017).

Chapter 3 looks at different methods for measurement of thermal conductivity of unfrozen and frozen soils. The methods are examples of steady state methods and transient methods.

Chapter 4 describes the experiments performed in laboratories at UNIS. The study includes index testing, direct measurements of thermal conductivity, volumetric heat capacity and thermal diffusivity.

The results are presented, analyzed and discussed in chapter 5.

Finally, a one-dimensional geothermal model to simulate present and future temperature distributions in the ground is outlined in chapter 6.

A summary of the findings and recommendations for further work of the topic can be found in chapter 7.

Appendices include information about the soil samples tested in the laboratory, detailed descriptions of calculations performed within chapter 6, and additional data from the geothermal PLAXIS model.

Chapter 2

Literature Review

2.1 Ground Temperatures

The ground temperatures are determined by air temperatures, the heat flux from the interior of the earth and soil thermal properties. Figure 2.1 outlines how the surface temperature and ground temperature in a homogeneous material are subject to simple periodic fluctuations due to both daily and annual cycles.

This sinusoidal fluctuation of the surface temperature, $T_{s,t}$, is provided by observation data of the mean annual ground temperature, T_m and the subsurface amplitude, A_s. Equation 2.1 gives estimations for a daily and annually repeated surface temperature. t is the time, and p is the time period (i.e., 24 hours or 365 days) (Andersland and Ladanyi, 1994).

$$T_{s,t} = T_m + A_s \cdot sin\left(\frac{2\pi t}{p}\right) \tag{2.1}$$

Generally, temperature changes at the surface and at soil depth z are not in phase. A shift to the left or lag will occur as seen from figure 2.1. If for example the third week of July is found to be the warmest time of the year, this maximum temperature will occur later in deeper layers of the soil. This time delay or lag time, can be understood as the time required for the maximum temperature to diffuse from the ground surface downward to the soil depth z. Hence, for homogeneous soils with no change of state, equation 2.2 describes the temperature at any depth and time (Andersland and Ladanyi, 1994). The thermal diffusivity, D, is included and controls the rate of heat transfer from hot to cold in the material.

$$T_{z,t} = T_m + A_s \cdot exp\left(-z\sqrt{\frac{\pi}{D \cdot p}}\right) \cdot sin\left(\frac{2\pi t}{p} - z\sqrt{\frac{\pi}{D \cdot p}}\right) \tag{2.2}$$

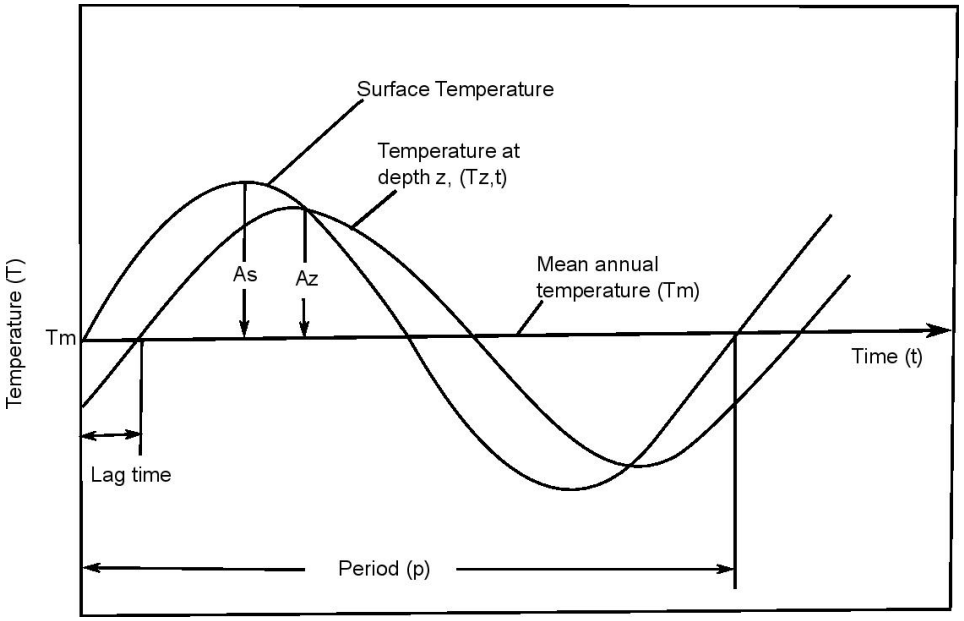

Figure 2.1: Surface and ground temperatures under homogeneous conditions. Sinusoidal fluctuation. (After Andersland and Ladanyi (1994), p. 6).

However, equation 2.1 and 2.2 are simple equations indicating trends in the ground. They can be modified significantly by the effect of soil thermal properties such as heat capacity, latent heat, thermal conductivity and thermal diffusivity, in addition to non-homogeneous soils and unsymmetrical surface temperatures resulting from vegetation, snow cover etc. (Andersland and Ladanyi, 1994).

These seasonal variation of the ground temperature with depth is often illustrated by an idealized whiplash curve as in figure 2.2.

The wave motion amplitude at each depth, A_z, reduces rapidly with increase in depth, and is given by equation 2.3.

$$A_z = A_s \cdot exp\left(-z\sqrt{\frac{\pi}{Dp}}\right) \tag{2.3}$$

The range in temperatures or limits of the temperature swings, T_z, are given by equation 2.4. It gives the maximum and minimum ground temperature for any point below ground surface, z.

$$T_z = T_m \pm A_s \cdot exp\left(-z\sqrt{\frac{\pi}{Dp}}\right) \tag{2.4}$$

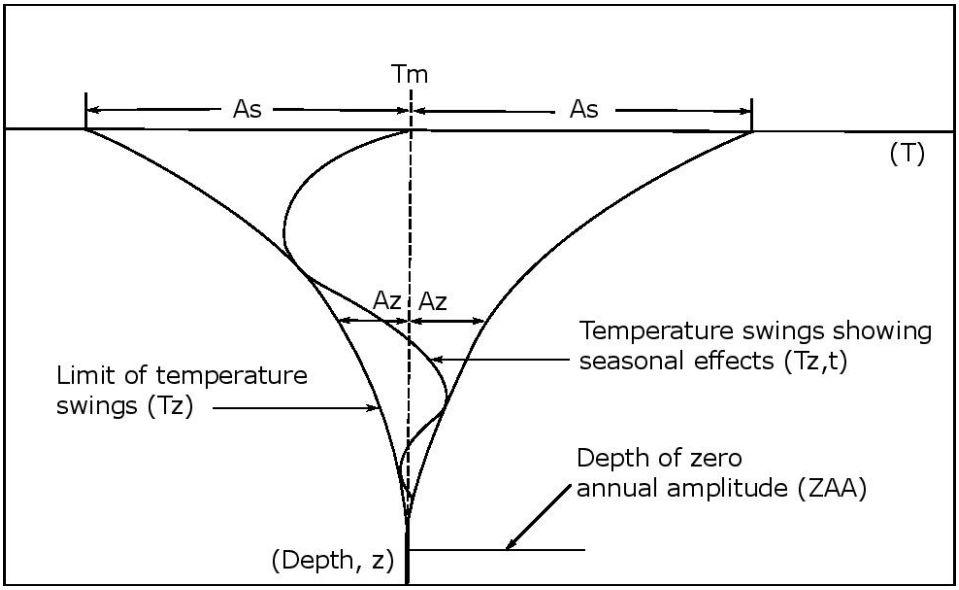

Figure 2.2: Temperature attenuation with depth in a homogeneous soil. (After Andersland and Ladanyi (1994), p.6).

2.1.1 Ground Thermal Regime

In the winter, when the temperature drops below 0°C, the water in the soil freezes by theory. The depth of freezing (0°C isotherm) is dependent on the surface freezing index (Andersland and Ladanyi, 1994). Figure 2.3 shows a vertical temperature profile of summer and winter soil temperatures, varying from T_{max} to T_{min}, in a region of permafrost.

The upper layer of the ground fluctuates between positive and negative degrees Celcius with the seasons and is termed the active layer. The thickness of this layer varies, and even in the zone of continuous permafrost, downward diffusion of heat from the surface in the summer thaws the topsoil. There are many equations for calculation of the thickness of the active layer. The Stefan equation is one of the most common (French, 2007), and is shown in its simplest form in equation 2.5

$$Z = \sqrt{\frac{2 \cdot I \cdot k}{L}} \qquad [m] \tag{2.5}$$

Z is the depth of thaw, I is the surface freezing or thawing index, k is the thermal conductivity of unfrozen soil and L is the latent heat of fusion. The two latter variables are defined in section 2.5. Where the active layer ends and turns into permafrost, a transition layer is formed. This transition layer is characterized by high ice-content and freezing and thawing on decade to century scales. The existence of this layer are related to the temperature gradient that are set up above and below, allowing moisture to migrate up or down

depending on season. Because the unfrozen water moves towards colder temperatures, there is an upward ground temperature gradient in the winter (i.e. the air is colder than the ground) (French, 2007).

As figure 2.3 shows, the temperature in the ground decreases steadily to a depth of 10 to 20 meters. The upper and lower limit, equation 2.4, are asymptotic to the mean temperature, representing the tremperatre envelope (i.e., trumpet curve). At a level of zero annual temperature amplitude (ZAA), the ground temperatures are not influenced by the surface temperatures. Deeper than this, the temperature will eventually start to increase due to heat generated in the Earth's interior. The rate of upward heat flow, is dependent on the geothermal gradient. Measured gradients (Brown et al., 1981) range from 1°C per 22 m to 1°C per 160 m.

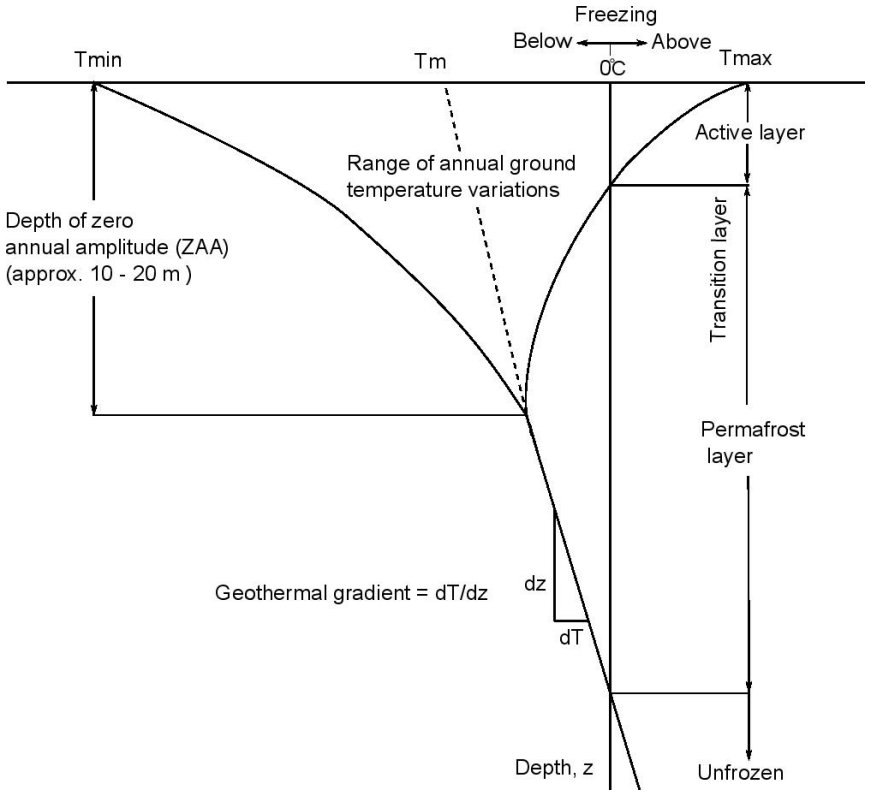

Figure 2.3: Idealized ground temperature profile of a homogeneous soil. The annual minimum and maximum temperature lines (T_{min} and T_{max}), active layer thickness (ALT), permafrost layer, depth of zero annual amplitude (ZAA) and geothermal gradient are highlighted. A projected mean annual ground temperature above the depth of zero annual amplitude (T_m) is indicated with a dotted line. (After Andersland and Ladanyi (1994), p.8)

2.2 Permafrost Features

Frost heave is a familiar and troublesome effect caused by the annual freezing of the active layer. The heave is a result of a volume increase of about 9% when water freezes. Ice lenses are formed due to free water migration by capillary action through soil pores toward the cold freezing surface. As the lenses grow they displace the soil to make room for the expanding ice. The ground surface moves upward, as well as everything on top of it. For example, differential heave is a huge problem for transportation areas. During climatically warmer periods, the active layer experience thawing. Settlement will occur due to the phase change and drainage of excess water. Specially, in the transitions between partially thawed and thawed active layer, the downward drainage path is blocked by still frozen soil and the pore-water pressure in this layer will be temporary high. Infrastructure located above this zone may experience damage (Andersland and Ladanyi, 1994).

The total annual freezing index is used to map permafrost distribution. In general, the freezing (or thawing) index are defined as the cumulative number of degree days for a given time period (Frauenfeld et al., 2007), which means number of degree-days with surface temperature below (or above) 0°C. Hence, the freezing/thawing index is a measure of ground freezing during a year. For example, areas where the thawing index is small and the freezing index is very large, indicate continuous permafrost. Likewise, if the freezing index is much lower than the thawing index one might expect only some permafrost. From the viewpoint of a geotechnical engineering, depth to occurrence of freezing and thawing in a soil will play an important role in design of for example pavements and other earth structures.

Furthermore, permafrost can occur everywhere over a large area continuous, or in a discontinuous pattern under the ground surface. The thickness of the layer varies, thinning gradually toward the lower latitude in contrast to the active layer. There is evidence of permafrost reaching the depth of 1.6 kilometer in Siberia (NSIDC, 2017). These variations in distribution and thickness are affected by factors covered by the concept topoclimate. Among the main factors are snow cover, wind, geothermal heat flow, air temperature, topography and distance to ocean (Humlum et al., 2003). In addition, does the presence of a water bodies affect the thermal regime of permafrost. While small lakes freeze completely and only influence the thawing slightly, lakes deeper than 1.5m may not freeze completely, and an unfrozen zone will extend completely through the permafrost beneath the lake (Andersland and Ladanyi, 1994).

The shape of the land is changed by the freezing and thawing process. Construction in or on frozen ground must therefore allow for changes in the thermal regime. Some of these changes may cause problems for infrastructure, while others are just odd landforms. With respect to ground ice, important features are ice wedge, pingos and thermokarst terrain. Additionally, are patterned ground dominant. Presence of these ground surface features could indicate complex underlying frozen ground conditions and layering.

2.3 Physical Properties of Soil

Soil is a multiphase porous media and its complexity increases when the soil freezes. In addition to particles, water and voids, a new solid phase, ice, is introduced to the system. Such knowledge is vital when considering geotechnical problems (Andersland and Ladanyi, 1994).

The main physical indices that are of interest for geotechnical engineers working with frozen ground are densities, water content and degree of saturation. Information about these properties are required in order to identify and classify soils. They are also influencing factors of thermal properties that will be discussed later. Figure 2.4 outlines the different constitutes of a soil elements and how it can be divided into sections of volume and mass. A general understanding is to use M for mass, and it "represents the material content of the soil. It is usually determined by weighting. V is the bulk volume and is defined as the total volume of the soil sample including open as well as closed voids" (Andersland and Ladanyi, 1994). It is important to note the section of unfrozen water in the frozen state soil element, and that mass of water is the sum of mass of ice and and mass of unfrozen water, $M_w = M_i + M_{uw}$.

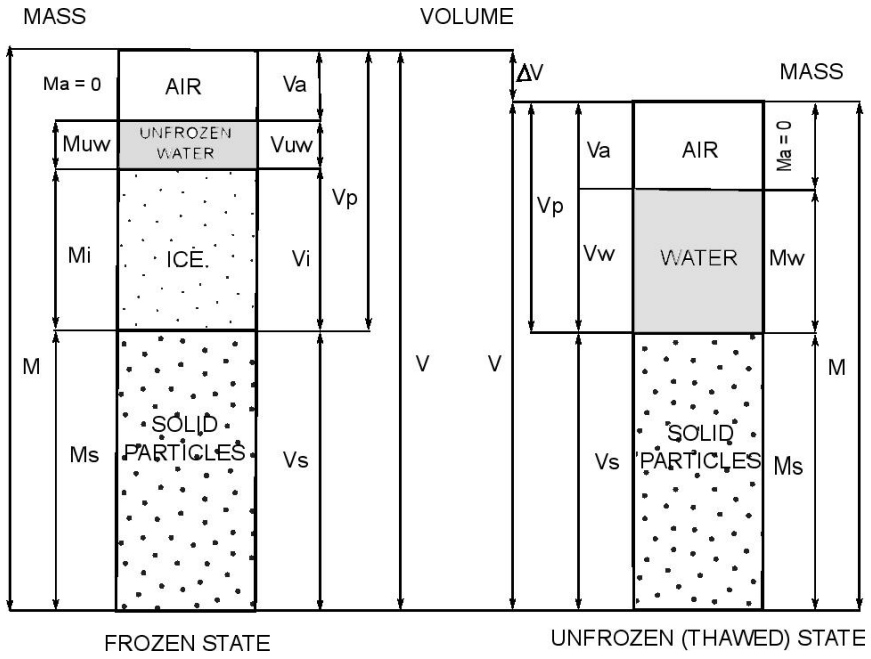

Figure 2.4: Schematic constitution of a soil element (After Andersland and Ladanyi (1994), p.25).

Using mass-volume relationship physical properties of soils can easily be calculated. In soil mechanics, density is a ratio that relates mass to volume. Bulk density (frozen or unfrozen), ρ, is defined as total mass divided by total volume; equation 2.6. The bulk

density will depend on the water, air and ice content, as well as the density of the solids. Density of solids, ρ_s, relates the mass of solids to the volume of solids. Dry density, ρ_d, relates the dry weight/solid mass to the total volume, and serves as measure for degree of compaction. The equations for ρ, ρ_d and ρ_s are shown below. The density multiplied by the gravity (g = 9.807 m/s^2) gives the soil unit weight γ (kN/m^3).

$$\rho = \frac{M}{V} \qquad \left[\frac{kg}{m^3}\right] \tag{2.6}$$

$$\rho_s = \frac{M_s}{V_s} \qquad \left[\frac{kg}{m^3}\right] \tag{2.7}$$

$$\rho_d = \frac{M_s}{V} \qquad \left[\frac{kg}{m^3}\right] \tag{2.8}$$

Low density materials will typically contain mineral such as montmorillonite and chlorite, while high values are measured for material with large amount of iron oxides or amphibole minerals. The more organic matter present in the soil, the lower density. In table 2.1 are some typical values for bulk density presented. The density of water varies slightly with temperature, while the density of ice increase with colder temperatures. A often used value for density of water is 1000 kg/m^3 at + 4°C.

Table 2.1: Characteristic bulk density values of saturated soils (From Andersland and Ladanyi (1994), p.52).

Soil Type	ρ, (kg/m^3)
Peat	1000
Mud	1000 - 1300
Clay, silt	1400- 2000
Sand, gravel	1700 - 2300
Till	2000 - 2400

In frozen soil, there will always be pores filled with ice, water or air in various proportion. The porosity, equation 2.9, indicates the voids in the soil that are available for water and/or air. It is inversely related to density. An increase in dry density, equation 2.8, thus decrease in porosity, will lead to a higher thermal conductivity. More about this in chapter 2.6. Void ratio, e, is another volumetric ratio relating volume of voids to volume of solids. See equation 2.10. Both porosity and void ratio are used to say something about the compaction of the soil. Small void ratio or low porosity indicates a dense soil.

$$n = \frac{V_p}{V} \cdot 100 = 1 - \frac{\rho}{\rho_s} \qquad [\%] \tag{2.9}$$

$$e = \frac{V_p}{V_s} = \frac{n}{1-n} \qquad [-] \tag{2.10}$$

Now, considering the mass side of the phase diagram in figure 2.4. The total water content, sometimes called moisture content when considering both the ice and unfrozen water, can be determined by equation 2.11. Hereafter, the term water content is used for both unfrozen and frozen soils.

$$w = \frac{M_w}{M_s} \cdot 100 \qquad [\%] \tag{2.11}$$

For frozen soils, it is convenient to represent water content as:

$$w = w_u + w_i \tag{2.12}$$

where w_i is the ice content and w_u is the unfrozen water. The vapor phase is usually neglected. It is well known that the amount of unfrozen water is very important in permafrost design. For some soils, water can stay unfrozen also below zero degrees, which may influence thermal and mechanical properties of the permafrost. There are many factors controlling the unfrozen water content and results are published in the literature by several researchers (Andersland and Ladanyi, 1994). Estimation of unfrozen water content from methods such as liquid limit determination and water potential determination has been conducted by other researchers (Nybo, 2017), and is not included in this thesis. The unfrozen water content w_u is defined as the mass of unfrozen water M_{uw} divided by the mass of solids M_s, see equation 2.13.

$$w_u = \frac{M_{uw}}{M_s} \cdot 100 \qquad [\%] \tag{2.13}$$

Salt content influences the freezing point depression and will increase the unfrozen water content of the soil. Thus, frost susceptibility under seasonal temperature conditions are reduced with presence of dissolved salt and the effect of salinity on creep and strength of frozen soil should be investigated (Andersland and Ladanyi, 1994).

Degree of saturation, S_r, determine the volume of voids filled with water. This means that a dry soil has $S_r = 0$ and the soil is fully saturated when $S_r = 1$. A soil is often assumed to be saturated, but for more sophisticated and accurate values, the degree of saturation can be calculated from equation 2.14.

$$S_r = \frac{V_w}{V_p} = \frac{w \cdot G_s}{e} \qquad [-] \tag{2.14}$$

where V_w is volume of water, V_p is volume of pores. However, the latter is quite difficult to measure. Hence, a correlation using water content, w, void ratio, e and specific gravity, G_s, can be useful.

2.4 Mechanical Properties of Soil

Generally, when applying a load at the surface, the underlying soil will experience increased stresses. Since frozen ground has a strength similar to that of a weak concrete, relatively large loads, foundations, can be supported. Due to small elastic deformation and creep movement, the foundations will settle. This behavior of soil must be considered in engineering design, and any analysis of the frozen-soil behavior depends on the magnitude and distribution of stresses below the foundation. Constitutive equations are used to describe the stress-strain-time relationships, frozen-soil strength, and the influence of temperature on these relationships (Andersland and Ladanyi, 1994).

2.4.1 Strength of Frozen Ground

In frozen ground, much as in unfrozen soils, the strength develops from cohesion, interparticle friction and particle interlocking. Ice-rich soils or low solids concentrations, may use the strength and mechanical behavior close to that for ice. For example, because ice creeps under extremely small stresses, the long-term strength for ice-rich soils will approach zero. Likewise, in ice-poor soils, two important parts of the strength are dilatancy and the interparticle friction. It is the ice component which creates the great strength difference between frozen and unfrozen soil. The ice content reduces with the presence of unfrozen water films on soil particles, causing a more plastic deformation. Hence, the frozen-soil strength is sensitive to strain rate, temperature, confining pressure, particle size, particle orientation and packing, and impurities in the water-ice matrix (Andersland and Anderson, 1978).

Despite many challenges with frozen ground, it is important to remember that permafrost is not always problematic, it can be a valuable asset. As discussed above, stability and strength are two beneficial aspects of frozen ground. Permafrost can provide excellent bearing capacity, work as anchorage for piling and it protects the nature from off-road operations. However, keeping the frozen ground frozen and consider the creep characteristics of frozen soil and ice, are essential considerations.

2.4.2 Creep

Creep is a time-dependent deformation, with creep rate dependent on temperature, composition (ice content), stress and stress history. In general, the constant-stress creep test gives three different creep-curve variations; primary, secondary and tertiary. See figure 2.5. For low stress levels, ice-saturated medium to high-density sands and silts (ice-poor soils) will only experience primary creep. As seen in figure 2.5, the creep is approaching some limiting deformation. Contradictory, for ice-rich clays and silts, secondary creep is a suitable approximation.

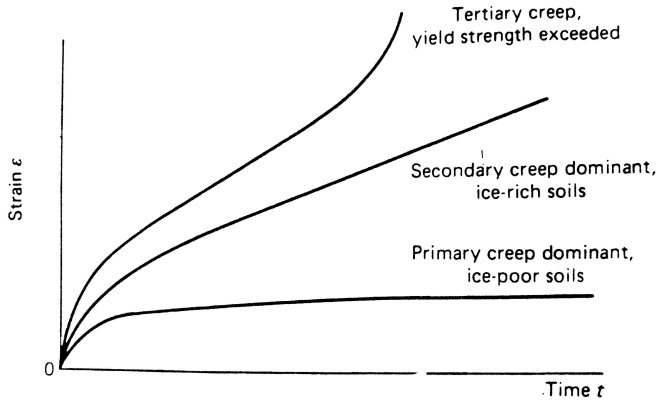

Figure 2.5: Constant stress (creep) test. The creep curve variations. (From Andersland and Anderson (1978), p. 124).

2.5 Thermal Properties of Soil

With the increased development of cold regions, methods for thermal calculations of the interference between air and ground have evolved. "The temperature field in frozen soil is governed by the heat balance equation which describes the storage and flow of heat. The heat balance equation is in its turn influenced by the thermal properties of the soil" (Carter, 1993). Consequently, understanding thermal behavior and obtaining values of soil thermal properties are helpful in many types of problems.

The thermal properties of frozen ground depend on a wide range of factors, particularly temperature, dry density, water/ice content, type of soil and degree of saturation. Additionally, as the climate gets warmer, thawing of the active layer changes the thermal properties. In fine - grained soils, the alternating cycle of freezing and thawing will leave some water unfrozen over a considerable negative temperature range. As water freezes latent heat is released, influence the ice - water phase composition and thermal behavior of the frozen soil. Resultingly, the function or/and the stability of an engineering installation will change extensively. Predictions of changes in soil temperature and unfrozen water content are of great importance.

Next, five fundamental soil properties are outlined. Thermal conductivity is extensively discussed in this thesis, due to its importance to the energy regime and energy distribution. Some typical values for thermal properties are presented in table 2.2 in the end of the chapter.

2.5.1 Latent Heat of Fusion

The amount of heat energy absorbed when a unit mass of ice is converted into a liquid at the melting point is defined as its latent heat of fusion. The same amount of heat is liberated when the water is converted into ice with no change in temperature (Andersland and Ladanyi, 1994). For a given soil;

$$L = \rho_d \cdot L' \cdot \left(\frac{w - w_u}{100} \right) \qquad \left[\frac{kJ}{m^3} \right] \tag{2.15}$$

Equation 2.15 indicates that the total water content, w and the fraction of this water that changes phase, are determined for the total energy involved in a phase change process. Water has a mass latent heat at 0°C of 333.7 kJ/kg and is given by the variable L'. ρ_d is the dry soil density. In soil such as sand and gravels the unfrozen water content might be very small, and can be assumed to be zero.

It is observed that the ground temperature remain close to constant when ground freezing occurs. This is due to latent heat flux and the so-called "zero-curtain" effect, taking place in response to a thermal gradient. As long as sufficient latent heat is released upon freezing, it flows upwards a long the thermal gradient, and the temperature will not rise. When the supply of water decrease, resulting in a less ice formation, less latent heat is released and the soil is cooled. Once again, the freezing front will advance.

2.5.2 Heat Capacity

Heat capacity and specific heat, are two terms which both describe a soil's ability to absorb thermal energy. However, heat capacity is the ratio of the amount of energy absorbed to the associated temperature rise. In formulaic expression, $c = Q/\Delta T$, where ΔT is the change in temperature, and Q is the heat transfer. The specific heat of a substance is the heat capacity of that substance per unit mass (Andersland and Ladanyi, 1994).

Hereinafter, the term heat capacity is used. It is given the symbol, c, and describes the energy required to raise the temperature of a material with 1°C. The property is either presented as a mass heat capacity, c, measured in kJ/kgK or by the volumetric heat capacity, C_v (MJ/m^3K). The latter is obtained by multiplying the mass heat capacity by the bulk density, ρ, of the material (French, 2007). Equation 2.16 gives the relationship.

$$c = \frac{C_v}{\rho} = \frac{C_v}{\rho_d(1 + w)} \tag{2.16}$$

Since soil consists of various constitutes including solids, water and/or ice, and air, the soil heat capacity can be expressed as a sum of the phases for both unfrozen and frozen soil. However, an important consideration and characteristic of frozen soils, is the liquid-solid phase change. The rate at which heat is released decreases at lower temperatures as the relationship between unfrozen water and temperature decreases (Krzewinski and

Tart Jr, 1985). This means that as the unfrozen water on the particle surface change to ice, the release of latent heat that is given off on cooling or absorbed on warming must be included. Hence, an equation for the apparent specific heat capacity was demonstrated by Anderson et al. (1973). In this model, equation 2.17, the apparent heat capacity c_a is expressed as a sum of the soil constitutes, neglecting the gas phase, but including a term accounting for cooling warming transition (Andersland and Ladanyi, 1994). Because the heat capacity is temperature dependent, the heat capacity for soils is found to decrease when the temperature gets colder. This is seen in relation with the water content of the soil under sub-zero temperatures, and ice having lower c than water.

$$c_a = c_s + c_i(w - w_u) + c_u w_u + \frac{1}{\Delta T}\int_{T_1}^{T_2} L\frac{\partial w_u}{\partial T}dT \quad \left[\frac{kJ}{kgK}\right] \tag{2.17}$$

As an alternative, the volumetric heat capacity for mineral soil, unfrozen and frozen, can be calculated from equation 2.18 and equation 2.19, respectively. Here, the values 0.17, 0.5 and 1.0 are specific heats of mineral, ice and water, defined as the ratio of the their heat capacity to that of water (Andersland and Ladanyi, 1994).

$$C_{vu} = \frac{\rho_d}{\rho_w}\left(0.17 + 1.0\frac{w}{100}\right)C_{vw} \tag{2.18}$$

$$C_{vf} = \frac{\rho_d}{\rho_w}\left(0.17 + 1.0\frac{w_u}{100} + 0.5\frac{w - w_u}{100}\right)C_{vw} \tag{2.19}$$

C_{vw} = 4.187 MJ/m^{3}K and is the volumetric heat capacity of water. ρ_d and ρ_w are the unit mass of dry soil and water, respectively.

2.5.3 Thermal Conductivity

Thermal conductivity is a substance's ability to transfer heat through a material by conduction. Thermal energy in the soil is under normal circumstances mainly transferred by conduction, even though other mechanisms also may contribute to the heat transfer (Farouki, 1981). This observation justifies that the term conductivity is used.

Considering a prismatic element of soil, as shown in figure 2.6, equation 2.20 defines the soil thermal conductivity, k, after Fouriers law as:

$$k = \frac{Q \cdot X}{A \cdot \Delta T} \qquad \left[\frac{W}{mK}\right] \tag{2.20}$$

The temperature drops from T_1 to T_2, and the thermal energy or heat, Q, flows through the thickness, X, perpendicularly to the cross-section, A, at a steady rate.

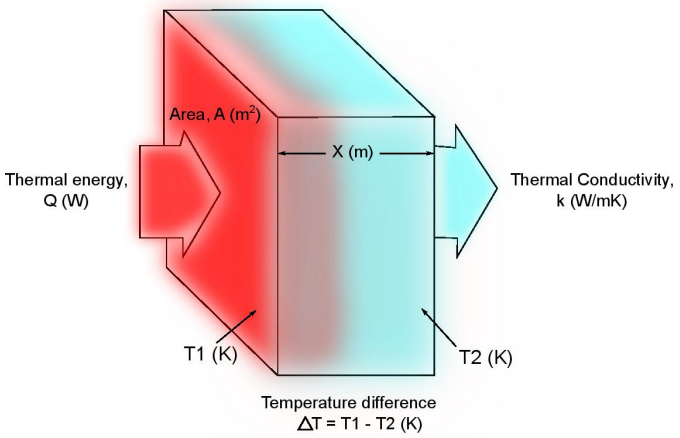

Figure 2.6: Heat flow through a soil element.

The thermal conductivity is together with moisture content, a factor controlling the rate at which the soil freeze. Soils have different thermal conductivity due to the variation of values of their basic components, among other water content, degree of saturation, porosity, mineral composition, temperature and bulk density. Section 2.6 takes a closer look at these factors.

Furthermore, methods for measuring and estimating thermal conductivity, chapter 3, are of prime importance in the numerical simulation of heat transmission through soils. For example, installation of ground source heat pump systems will be facilitated and optimized by efficient design by accurate estimation of a soil's thermal conductivity. The prediction methods are also useful for calculation of heat loss through basements and slabs and for prediction of thawing of the active layer in the future.

2.5.4 Thermal Diffusivity

The rate of which heat is transferred from the hot side to the cold side in a material is called thermal diffusivity, D. It is defined as the ratio between the thermal conductivity, k, and the density, ρ, and mass heat capacity, c. The three parameters are related through the relation in equation 2.21 (Andersland and Ladanyi, 1994).

$$D = \frac{k}{\rho \cdot c} \qquad \left[\frac{m^2}{s}\right] \tag{2.21}$$

If the thermal diffusivity of a substance is high, it means that thermal energy moves rapidly through it because of quickly conduction of heat relative to its volumetric heat capacity (C_v = $\rho \cdot c$). From experimental data, is it observed that D for ice is much higher than for water. This characteristic result in that frozen soil will have a higher diffusivity than the same soil in the thawed condition. It also indicated that the average temperature of a saturated frozen soil will increase more quickly and to greater extent than that of a mass of unfrozen soil under the same initial condition and equal dimensions. In other words, the two factors are "the higher thermal conductivity of the frozen soil and the lower specific heat of the ice as compared with liquid water" (Farouki, 1981).

2.6 Factors Affecting the Thermal Conductivity of Soil

Factors affecting soil thermal conductivity include water content, degree of saturation, dry density, mineral composition, shape and distribution of soil grains, unfrozen water content and pore water chemistry. Soil is a natural material composed of solid particles surrounded by pore space filled with water (ice) and usually air.

With regards to heat transfer by thermal conduction water content and degree of saturation are of prime importance. As defined in chapter 2.3, water content is the quantity of water contained in the soil, while degree of saturation is the percentage of the voids filled with water. The increase of thermal conductivity as the saturation level increase, can be seen as three stages. Firstly, at low saturation, water only coats the soil particles. Little or no water fills the voids or gaps between the soil particles. When the particles get fully coated with water, a further increase in water content fills the voids. The water films that are created between the soil particles in saturated soils, act as bridges for heat flow. The bridges increase the effective contact area between soil particles. Hence, the thermal conductivity increase. Finally, when the voids are completely filled with water, the sample is fully saturated and an increase in water content will not increase the heat flow, neither the thermal conductivity (Becker et al., 1992). Moreover, complications develop due to boundary conditions. A soil with a given water content does not have a unique thermal conductivity value. Soil sample disturbance could change the boundary conditions and cause a water redistribution. Such effects must be taken into consideration before reporting thermal conductivity or confidently applying laboratory results to field conditions (Farouki, 1981). Additionally, changes in the pore water's chemistry are known to alter the thermal properties. In general, an increase in the pore water salt concentration leads to a decrease in the thermal conductivity of the material.

In frozen soils, the presence of unfrozen water is found to be a major factor in the thermal behavior of the soil. Especially, if there is moisture migration to the freezing front, the freezing front will take longer to penetrate into a soil with a larger water content because a greater amount of latent heat has to be extracted. Knowledge about the relationship between unfrozen water content measured during freezing, and the suction characteristics obtained during drying, permits prediction of the amount of pore water that remains unfrozen below 0°C (Williams, 1964). Further elaboration of unfrozen water theory is not a part of this master thesis.

Even though the soil thermal conductivity generally varies little with temperature, at the ice front the thermal conductivity is subject to a dramatic change between unfrozen and frozen states, due to ice having a conductivity approximately four times that of water (Farouki, 1981). In the freezing process of fine-grained soils, smaller capillaries mean a sharp increase in the curvature of the water/ice interface. The ice - cementation is observed to increase the interfacial heat transfer with a consequent increase in the thermal conductivity. Therefore, heat transfer at the contacts or interfaces has been recognized as very important for the overall thermal conductivity of frost susceptible ground. This means that even in a high conductivity mineral soil, the limiting factor is the contact conduction, and the interfacial effects (i.e. solid/liquid, liquid/air, solid/air, solid/solid) maintain their importance to heat transfer (Farouki, 1981). Moreover, with an increase in water content for unfrozen and increasing ice content for frozen soils, the thermal conductivity approaches the values of water and ice respectively. The same is apparent for porosity close to zero, and the conductivity tends toward that of the solid particles.

The structure of the soil, often referred to as packing, is essential with regards to heat flow and imposed temperature gradient. For determination of the thermal conductivity of the soil, inspection of the distribution of grain sizes of a soil is essential. For convenience, naturally occurring soils are in many situations subdivided into those with a framework skeleton and those without. The first group are the coarse-grained soils with solid-to-solid contact, while the latter includes the fine-grained soils with water films between the particles (Farouki, 1981). In the field, soils often contain a mixture of the different mineral particles sand, silt and clay. A wide range of grain sizes (well-sorted material), result in a denser soil and increased number contact points. From the relationship in equation 2.22 it is illustrated that an increase in dry density, ρ_d, is associated with a decrease in porosity, n. Because soil particles are more thermally conductive than other the soil constituents, air and water (ice), a larger heat flow path gives better heat transfer across the contact points inducing a higher thermal conductivity. This is also why the heat flow in granular material is more effective than in fine-grained soils.

$$\rho_d = (1 - n)\rho_s \qquad \left[\frac{kg}{m^3}\right] \tag{2.22}$$

With regards to shape, spherical grains give lower coordinate number, i.e., number of contact points, and lower porosity than rhombohedral packing. The aggregation of particles in fine-grained soils must be considered, in addition to an evaluation of the disturbance of the material. Mineral composition will also influence the thermal conductivity. For example, quartz is a mineral with greater thermal conductivity than plagioclase, feldspar or pyroxene. Hence, materials dominated by the quartz minerals will have the same high thermal conductivity properties. Sands will generally show higher k - values resulting from the predominant quartz composition in contrast to the micaceous clays (Johansen, 1975).

Table 2.2: Some typical values of thermal properties for various materials (Adopted from French (2011); Johnston (1981); Williams and Smith (1989))

(A)Thermal conductivity of various material

Material	Thermal conductivity k [W/mK]
Air	0.024
Water	0.605
Ice (at 0°C)	2.23
Snow	
Loose, new	0.086
On ground	0.121
Dense	0.340
Sand, dry	1.1
Clay, dry	0.9
Organic material	
Peat, dry	0.05
Peat, saturated unfrozen	0.50
Peat, saturated frozen	2.00

(B) Heat capacities of various materials

Material	Heat Capacity c [kJ/kgK]	Volumetric Heat Capacity C [MJ/m^{3}K]
Air	1.000	0.00125
Water	4.187	4.187
Ice	2.094	1.88
Soils minerals	0.710	1.875
Organic soil	1.674	2.52
Polystyrene insulation	1.000	0.435
Concrete	0.895	2.01
Asphalt	1.674	2.52

(C) Thermal diffusivities of various materials

Material	Thermal Diffusivity D [m^2/s$\cdot$ 10^{-7}]
Water	1.45
Fresh Snow	3.3
Ice	11.9
Granite	15
Limestone	7
Dolomite	20
Sandstone	10
Shale	8
Quartzite	45

Chapter 3

Methods for Determining Thermal Properties

In order to determine the thermal properties of soils laboratory methods, in-situ procedures or theoretical and/or empirical models can be applied. The main properties of concern are thermal conductivity and thermal diffusivity, these being interrelated by means of volumetric heat capacity, equation 2.21. The former governs the steady state condition, while the latter applies to the case where the temperature is time dependent.

3.1 Experimental Methods

The method selected for measuring thermal properties should be appropriate for the general type of material and the temperature range for which the material will be used. There are several laboratory and in-situ methods of measuring thermal conductivity which are considered as suitable for use with soils. Limitations in measuring methods will occur. For example, for measuring the thermal conductivity, there will, in unsaturated soils, be moisture migration resulting from the temperature gradient across the soil sample being tested in the laboratory. In-situ, the soil generally experience smaller temperature gradients.

For most soil types, except those containing coarse gravel and rock debris, good quality samples of frozen soil can be obtained when appropriate equipment are available. Thermal disturbance must be minimized during drilling and sampling, but frozen soil is in general much less susceptible to mechanical disturbance compared to the same unfrozen sample. The use of laboratory rather than field investigations is therefore preferred. However, limitations such as preservation and scaling challenges apply, and field investigations are therefore still of interest (Farouki, 1981).

The methods presented in this chapter are examples of the two existing classes of methods for measure the thermal conductivity; steady-state methods and transient methods.

3.1.1 Steady State Methods

The concept of steady state methods require that the sample or soil portion being tested is subject to a stationary heat floe when the measurements are made. A steady state technique analyses a material in completely equilibrium, and the signals process is constant. Reaching this equilibrium could take considerable time and is considered a disadvantage to the method.

The Guarded Hot Plate Test

One of the most important and used methods for measuring the thermal conductivity of soils are the guarded hot plate (GHP) test (Farouki, 1981). It dates back to 1912 and the method has undergone many improvements and modification. The principle of the method involves a monitored one-dimensional heat flux through a specimen (Yüksel, 2016) and detailes can be found in ASTM Standard C177, "Standard Test Method for Steady-State Heat Flux Measurements and Thermal Transmission Properties by Means of the Guarded-Hot-Plate Apparatus".

The guarded hot plate setup is comprised of cold plates, a hot plate, a system of guard heaters and thermal insulation. There are different apparatuses available based on a two-specimen apparatus or a single specimen apparatus. The CRREL-apparatus (Cold Region Research and Engineering Laboratory) following the American Society for Testing and Materials (ASTM) specifications is an example of the former and is the most common configuration. A simple illustration is shown in figure 3.1.

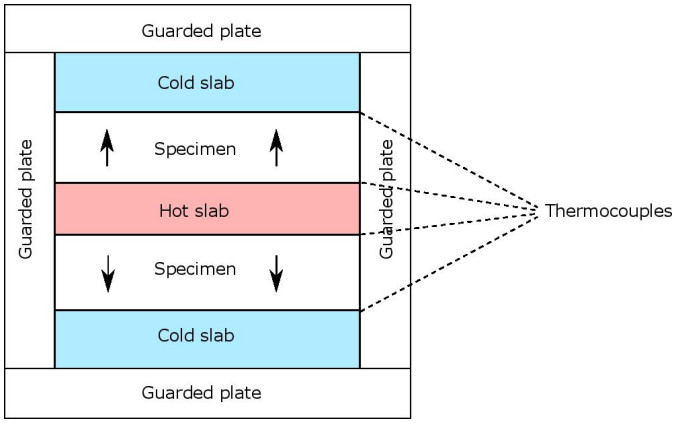

Figure 3.1: The guarded hot-plate method establishes one dimensional heat flow through a pair of specimens.

The installation has two identical test specimens that are placed above and below a flat plate main heater, in a symmetrical arrangement. An outer guard heater surrounds the system in such way that horizontal heat loss is eliminated and the heat flow only acts vertically up and down the test specimens. The outer surface of the specimens is covered by adjacent liquid-cooled heat sinks. In a two-specimen arrangement, the heat loss from the hot plate can be controlled effectively. The thermal conductivity is calculated from equation 2.20.

Heat Flux Meter (HFM)

The heat meter test could be an in-situ technique and applied in the field. The thermal conductivity is found directly by measuring the temperature at two points in the soil and the heat flow between them. The measuring equipment is called a heat flux meter (HFM) or a soil heat flux sensor (Scott, 1964). To start the recording a heat impulse of known intensity is applied at the surface. The increase in temperature in a shallow layer as a result of the applied heat i recorded. A heat flux plate, thin flat, rigid plate with known thermal conductivity, is inserted in the soil with the larger surface in the plane perpendicular to the heat flow direction. The HFM measures the applied heat flux density and the temperature gradient across the thickness of the meter (Watts et al., 1990). The HFM-method has been performed among other by Van Wijk and Bruijn (1964). It is found that due to its simplicity and the need of few supplementary measurements, the method is well suited for long-term assessment of heat flux density (Fuchs, 1986). The method follows ASTM C518, "Standard Test Method for Steady-State Thermal Transmission Properties by Means of the Heat Flow Meter Apparatus".

3.1.2 Transient Methods

Transient methods are non-steady state, and the technique records a measurement during the heating process. This means that the temperature varies with time. In comparison to the steady state methods transient methods can be made relatively quickly.

The Probe Method

The thermal probe, needle or hot wire method can be applied in situ or in the laboratory. The method is rapid and the procedure of inserting the thin probe into the soil to be tested cause little disturbance. The equipment consists of a heater (wire, needle, probe) producing thermal energy at a constant rate, and an element sensing the temperature. The surrounding medium will cause a rise in temperature of the probe, the rate dependent on the medium's thermal conductivity. "The theory of the probe method is based on the theory of the line heat source placed in a semi-infinite, homogeneous and isotropic medium" (Farouki, 1981). Effects moisture migration and axial heat loss might develop for long experimental times. Hence, the maximum measuring time should be 20 min and the rise in temperature should not exceed 4°C (Farouki, 1981). Other criterion are related to sample

radius, temperature gradient and probe design. Careful interpretation is required, especially close to the freezing front.

Point-Source Method

The point-source method is comprised of recording the voltage variations of a thermistor and variable resistor in a measuring circuit over a period of time. From the measured voltage values, variations in temperature and heat production with time for the thermistor are calculated. Thermal diffusivity, thus thermal conductivity is determined by inverse analysis based on equation 2.21. In contrast to the probe method, the typical large-sized samples make it easier to control the water content. Additionally, the thermal resistance produced between the soil sample and the probe inserted and movement of water occurring due to high temperature are reduced.

3.2 Modeling Thermal Conductivity

In section 2.6, factors affecting soil thermal conductivity were discussed. Density, water content, texture, mineralogy and temperature can all influence the heat flow in soils. "Not surprisingly, with so many variables controlling the thermal conductivity, many theories and models have been developed to predict the thermal conductivity of soils" (Barry-Macaulay et al., 2015). Both theoretical and empirical model exist. Additionally, some are called semi-empirical models due to empirical modification of theoretical models (Farouki, 1986). There are mainly three simple concepts that are used as the basis for prediction of soil thermal conductivity. These theoretical models are based on parallel and series heat flow, providing equations for an upper or lower limit of prediction of soil thermal conductivity. With the assumption that the liquid and solid phases are grouped together in blocks, equation 3.1 for heat flow in parallel and 3.2 for a series flow model.

$$k = nk_w + (1 - n)k_s \tag{3.1}$$

where n is the porosity k_w and k_s are thermal conductivity of liquid and solid phase, respectively.

$$\frac{1}{k} = n\frac{1}{k_w} + (1 - n)\frac{1}{k_s} \tag{3.2}$$

Finally, a geometric mean equation, which yields values between the parallel and series models can be expressed as:

$$k = k_w^n k_s^{(1-n)} \tag{3.3}$$

Soil thermal conductivity models have been reviewed and evaluated by several researchers. As stated in the introduction, a thorough survey of many empirical and semi-empirical

models was conducted by Farouki (1986). Applicability and conditions under which some of the methods should be used, is presented in table 3.1. It must be acknowledged that none of the methods in table 3.1 offer a unified methodology for estimation of soil thermal conductivity applicable to a wide range of soil types and conditions (Fricke et al., 1992). In the light of thermal conductivity models relevant to ground freezing and the framework of this master thesis, next section is dedicated to an elaboration of Kersten's (1949) equations and average diagrams.

Table 3.1: Applicability of Prediction Methods (Data from Farouki (1986); Adopted from Fricke et al. (1992))

State	Texture	Saturation	Method
Unfrozen	Coarse Grained	0.015 - 0.100	Van Rooyen and Winterkorn (except for low-quartz crushed rock)
		0.100 - 0.200	De Vries
		0.200 - 1.000	Johansen
		0.000 - 1.000	Gemant (sandy silt-clay)
		saturated	Johansen, De Vries, Gemant
Unfrozen	Fine Graiend	0.000 - 0.100	Johansen (underpredicts by 15 %)
		0.100 - 0.200	Johansen (underpredicts by 5%)
		0.200 - 1.000	Johansen
		saturated	Johansen, De Vries, Gemant
Frozen	Coarse Grained	0.100 - 1.000	Johansen
		saturated	Johansen, De Vries
Frozen	Fine Grained	0.000 - 0.900	Kersten
		0.100 - 1.000	Johansen
		saturated	Johansen, De Vries

3.2.1 Average Thermal Conductivity Diagrams by Kersten (1949)

In many thermal problems it is appropriate to assume an average thermal conductivity of the ground. This is based on the knowledge about natural soils as an in-homogeneous material and the large variability over relatively short distances. "Kersten (1949) conducted tests on natural soils and crushed rock from which empirical equations for thermal conductivity k were developed. Farouki (1981) converted these equations into SI units with k (W/mK) expressed in terms of water content, w (%) and dry density ρ_d (g/cm^3)" (Andersland and Ladanyi, 1994).

Soils are generally described as either coarse grained (gravel and sand) or fine grained (silt and clay). The thermal conductivity for coarse grained soils (silt-clay content $< 20\%$) can be calculated from equation 3.4 and 3.5 for unfrozen (+4°C) and frozen (-4°C) soils, respectively.

$$k_{un} = 0.1442 \cdot (0.7 \cdot logw + 0.4)(10)^{0.6243\rho_d} \tag{3.4}$$

$$k_f = 0.0109 \cdot (10)^{0.8116\rho_d} + 0.00461 \cdot (10)^{0.9115\rho_d} \cdot w \tag{3.5}$$

For fine-grained soils (50 $\%$ or more silty-clay), equation 3.6 and 3.7 are valid for unfrozen and frozen soils, respectively.

$$k_{un} = 0.1442 \cdot (0.9 \cdot logw - 0.2)(10)^{0.6243\rho_d} \tag{3.6}$$

$$k_f = 0.001442 \cdot (10)^{1.373\rho_d} + 0.01226 \cdot (10)^{0.4994\rho_d} \cdot w \tag{3.7}$$

Thermal conductivity is highly influenced by quartz content, which is most dominant in coarse grained soils. Silts and clays often composed of other minerals. Kersten's (1949) equations do not take into account variations in quartz content. To find the thermal conductivity for soils having a composition between the sand-group and the silt-clay group, interpolation between the two sets on equations might give acceptable results.

The equations by Kersten (1949) are based on results from steady-state methods and uniform temperature gradient. His laboratory work involved testing unfrozen and frozen soil samples of finite thickness, 10.8 cm, and a ΔT of 5.6°C across the sample. The samples were allowed to condition thermally until constant heat-flow condition are attained (Penner et al., 1975). However, such conditions can induce thermally activated diffusion of water in both frozen and unfrozen state (Hutcheon, 1958). Difficulties in the thermal conductivity measurements are imposed by the ice-water ratio. Hence, an important influencing factor of the thermal conductivity, is the unfrozen water content, equation 2.13. In Kersten's (1949) equations this is not accounted for. However, he reported that his equations give values with less than 25$\%$ deviation from measured values.

One of the objectives of this master thesis is to evaluate this statement. Harlan and Nixon (1978) summarized the work done by Kersten (1949) by plotting his equations. The resulting diagrams are shown in figure 3.2 for coarse grained soils, and figure 3.3 for fine grained soils. For determination of soil thermal conductivity one should obtain information about soil type, water content, dry density and degree of saturation by laboratory investigations. Chapter 4 present the results from laboratory testing of the soil from lower Adventdalen, Svalbard.

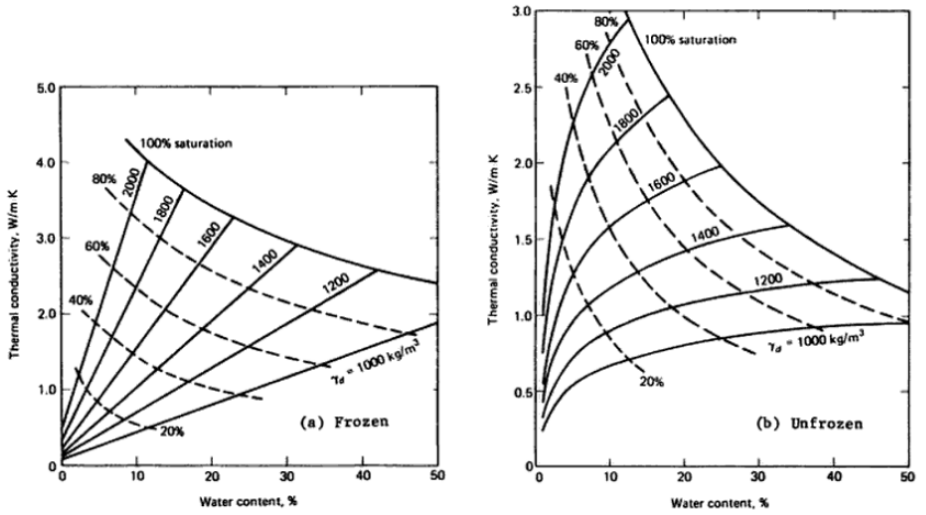

Figure 3.2: Average thermal conductivity for sands and gravel: (a) frozen; (b) unfrozen. (From Harlan and Nixon (1978))

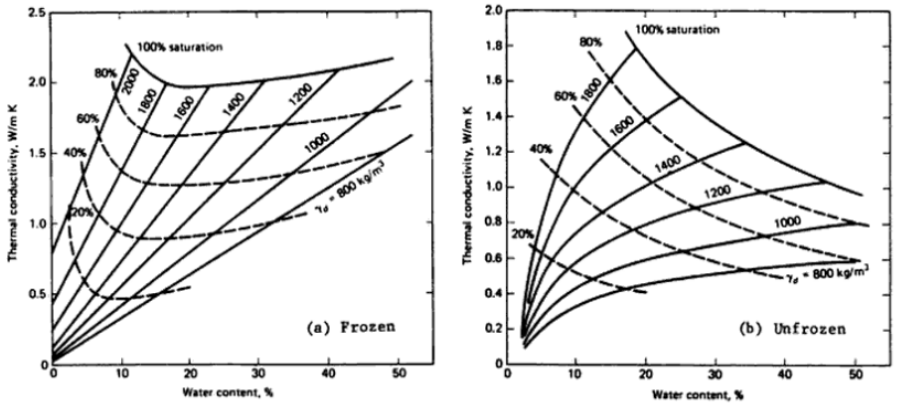

Figure 3.3: Average thermal conductivity for silt and clay soils: (a) frozen; (b) unfrozen. (From Harlan and Nixon (1978))

3.3 Thermal Properties from Back-Calculation Using Temperature Data

If soil sampling and parameters from laboratory testing are not available, the ground thermal properties can be estimated from temperature data. Since the heat transfer in permafrost occurs largely through conduction, the temperature in permafrost can be treated by applying Fouriers law (Carslaw and Jaeger, 1959).

Thermal diffusivity, the rate of heat transfer from hot to cold in a material, in the zone of seasonal temperature variations can be calculated in two ways:

- The first methods is in terms of the amplitude decrease with depth, equation 2.3; $A_s exp\left(-z\sqrt{\frac{\pi}{D \cdot p}}\right)$. The thermal diffusivity is:

$$D_a = \left(\frac{\omega h^2}{(ln\frac{A_1}{A_2})^2}\right) \tag{3.8}$$

  where ω is the frequency of the annual signal (ω = 2π/p), h is the distance between two thermistor sensors. A_1 and A_2 are the amplitudes of the upper and lower temperature sensor, respectively.

- The second method is in terms of the phase lag with depth using the last term in equation 2.2; $sin\left(\frac{2\pi t}{p} - z\sqrt{\frac{\pi}{D \cdot p}}\right)$. The thermal diffusicity is:

$$D_p = \frac{h^2}{2\omega\delta^2} \tag{3.9}$$

  where δ is the phase lag between the upper and lower temperature sensor (Isaksen et al., 2000).

The thermal diffusivity, D, thermal conductivity, k and volumetric heat capacity, C_v are all related (equation 2.21) (Isaksen et al., 2000).

In chapter 4, back-calculation of temperature data from lower Adventdalen is presented and discussed.

3.4 KD2 Pro Thermal Properties Analyzer

Since Fourier published the "Theorie Analytique de la Chalour" in 1822, several scientific works related to thermal properties have been presented using the relationship between heat flux and temperature gradient. Recently, Decagon Devices has developed the KD2 Pro Thermal Properties Analyzer that uses transient line heat source theory. Hence, the method falls under the non-steady state classification. The manufacture claims that the transient

method outperforms other technique because its fast, and limits moisture migration which changes the thermal properties of the material (Meter Environment, 2018).

The KD2 Pro logger is a hand-held controller device used to measure the thermal properties of soil. See figure 3.4. Dependent on the choice of sensor, single needle sensor or dual-needle sensor, one are able to measure thermal conductivity, volumetric heat capacity, thermal diffusivity and resistivity. The KD2 Pro system follows the specifications outlined in ASTM D5334-14. "Nevertheless, it is not clear how to obtain the required reliability and accuracy in the measurements since neither the standard nor manufacturer's user manual include any method or recommendation for that" (Rubio, 2013). The content of following sections are adapted from the operator manual for the KD2 Pro. Deviations and own experiences are discussed in chapter 4.

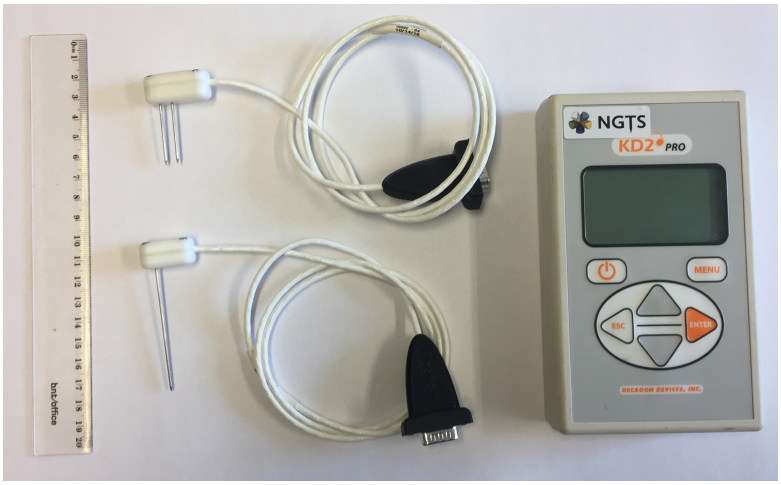

Figure 3.4: The logger and the two needles most appropriate for measuring thermal properties of soil; the SH-1 (dual) and TR-1 (single).

3.4.1 The Choice of Sensor

The sensor kit comes with three different probes. The KS-1 and the TR-1 are both single needle sensors used to measure the thermal conductivity and thermal resistivity in different mediums, employing an infinite line heat pulse method (ILHP) (Rubio, 2013). The third probe, SH-1, is a dual-needle probe, which is able to measure volumetric heat capacity, thermal diffusivity in addition to thermal conductivity and thermal resistivity. The dual-needle sensor employs the dual-needle heat pulse method (DNHP). The theory are discussed in subsection 3.4.3.

The large TR-1 single needle sensor is designed for use in soil, rock, concrete and other granular materials. The needle is 10 cm long and 2.4 mm in diameter. The relatively large diameter and longer heating time (5 min default) of the TR-1 sensor, minimize errors from contact resistance in solid samples with pilot holes or granular samples. The TR-1 sensor

measures samples with higher thermal conductivity in the range of 0.1 to 4.0 W/mK with accuracy $\pm 10°$C. The KS-1 probe (6 cm long, 1.3 mm diameter) applies a smaller amount of heat, making it more suitable for insulating material and liquids.

The dual needle SH-1 sensor is also compatible with most solid and granular materials. The needles are quite small, 3 cm long and 1.3 mm in diameter, spaced 6 mm apart. The SH-1 sensor is less suitable for soil thermal conductivity, but measures volumetric heat capacity from 0.5 to 4 MJ/m^{3}K with accuracy $\pm 10°$C at conductivity above 0.1 W/mK. For thermal diffusivity, the values should be in the interval 0.1 to 1 mm^2/s.

3.4.2 Installing the Sensors

The needle is installed by inserting it all the way into the material. A pilot hole should be drilled in hard soils, such as frozen samples. To provide optimal contact between the sensor and material, grease or a thermal compound can be used to fill the pre-drilled hole. To avoid errors, a minimum of 1.5 cm of material parallel to the sensor in all direction must be allowed for, due to the heat pulses coming from the needle.

3.4.3 KD2 Pro Theory

For more than 50 years, the transient line heat source method has been used by researchers to measure the thermal conductivity of porous material. The equipment used for this measurements is typically a needle with a heater and a temperature sensor inside. While a current passes through the heater, the system monitors the temperature of the sensor over a finite time interval. Today, the probes could also come as dual probe systems, with the heater and temperature sensor placed in separate needles. In this way one are able to obtain the relationship between time and temperature yielding information about diffusivity and heat capacity as well as conductivity.

Accurate measurements require good thermal contact between the measured medium and the sensor. An ideal sensor would therefore have a very small diameter and a length 100 times its diameter. In this way the sensor will be in intimate contact with the ambient material and heating and cooling temperatures can be recorded. In an ideal situation, the composition of the material and the temperature should stay constant during the measurement. However, real sensors fall short of these ideals. First of all, a needle with the ideal diameter would be too fragile for use in most applications. Secondly, constant temperature is generally not achievable in outdoor environments. Thirdly, when testing moist, unsaturated soils the water content in the region around the needle will move away from the heat source, thus altered from the in-situ condition. Finally, the hole made by the probe, will be exposed to contact resistance between the sensor and the material.

The KD2 Pro is designed to optimize measurements of thermal properties relative to the issues outlined above. The heating time is kept short to minimize thermally induced water movement and reduce the time required for taking the measurement. The water movement and free convection are also minimized by limiting the heat input. In order to use short

heating times and low heating rates, high resolution temperature measurements are necessary. Decagon's KD2 Pro resolves temperature to $\pm 0.0001^{\circ}$C in temperature. Additionally, built in algorithms analyze measurements made during a heating and cooling interval. The algorithm applied depends on the type of needle sensor, single or dual-needle. The two algorithms are based on Carslaw and Jaeger (1959) and Jaeger (1956) line heat source analysis.

3.4.4 The Dual-Needle Algorithm

Heat is applied to one of the needles for a set time, t_h. The temperature is measured in the monitoring needle, 6 mm distant, during the heating time and cooling period that follows. The processing of the readings involve subtracting the ambient temperature at time 0, multiplying by 4π and dividing by the heat per unit length, q. A non-linear least square procedure is used to fit the resulting data to the following equations:

$$T^* = b_0 t + b_1 E_i(\frac{b_2}{t}) \tag{3.10}$$

$$T^* = b_0 t + b_1 \left(E_i(\frac{b_2}{t}) - E_i \left[\frac{b_2}{t - t_h} \right] \right) \tag{3.11}$$

where

$$T^* = \frac{4\pi(T - T_0)}{q} \tag{3.12}$$

In the equations above, E_i is the exponential integral, b_0, b_1 and b_2 are the constant to be fitted. T_0 is the temperature at the start of the measurement and q is the heat input. Equation 3.10 applies for the first t_h seconds, while the heat is on. When the heat is off, equation 3.11 is applied.

In order to compute the thermal conductivity and thermal diffusivity, equation 3.10 is fitted to the transformed data. The correct values of b_0, b_1 and b_2 are the ones which minimize the sum of squares of error between the equations and the measurements. Finally, the thermal properties are found from following equations:

$$k = \frac{1}{b_1} \tag{3.13}$$

$$D = \frac{1}{b_1} \tag{3.14}$$

3.4.5 The Single Needle Algorithm

Heat is applied to a single needle for a time, t_h. During this time the temperature change in the needle is monitored. In addition, a time equal to the heating time, t_h, after heating is measured. The total time is called the Read Time (RT), where heat is applied for half of this time. Temperature during heating is computed from equation 3.15:

$$T = m_0 + m_2 \cdot t + m_3 \cdot ln(t) \tag{3.15}$$

where m_0 is the surrounding temperature during heating, m_2 is the rate of background temperature drift and m_3 is the slope if a line relating temperature rise to logarithm of temperature. The equation for cooling is represented below as equation 3.16.

$$T = m_0 + m_2 \cdot t + m_3 \cdot ln(\frac{t}{t - t_h}) \tag{3.16}$$

The thermal conductivity is computed from equation 3.17

$$k = \frac{q}{4\pi m_3} \tag{3.17}$$

Since the equations for the single needle are long-time approximations to the exponential integral equations, 3.10, the early-time data during heating and cooling are ignored. Advantages with this approach are better representation of thermal conductivity due to elimination of contact resistance effect in early-time data, and the equation 3.15 and 3.16 are solved by linear least squares giving a solid and definite result.

3.4.6 Previous Tests and Results

The KD2 Pro Thermal Properties Analyzer, with the correct choice of sensor, is designed to be measure thermal conductivity of both unfrozen and frozen soil samples. The theory, error analysis and application have been well documented for unfrozen soils. It may be asserted, however, that few studies of sub-zero thermal conductivity experiments are available. Of the studies performed using the KD2 Pro in characterization of frozen soils, three interesting results are presented in the following paragraphs.

The first study is performed by Sun et al. (2016), and uses the KD2 Pro to characterize subzero-temperature thermal properties of seasonally frozen soil in China. In the study, organic loamy sand from the active layer was repacked into PVC cylinders and carefully adjusted and balanced for accurately determination of water content, volume and temperature. Note that the tested samples had a wide range of water contents. The thermal properties measurements were recorded during a cooling process (from 0°C to -20°C) and subsequently a heating process from (from -20°C to 0 °C), and repeated three times.

The results from the study revealed a similar response pattern to changing temperatures below -2°C for both apparent volumetric heat , C_v, and the apparent thermal conductivity,

k. Thus, under the same water contents. See figure 3.6 and 3.5. It is seen that the response pattern from unfrozen to frozen thermal values is not linear. This is due to the latent heat released in phase transition of unfrozen water and ice. "The asymptotic characters of the C_v- and k-values are at the vicinity of the initial temperature of phase transitions, indication that both properties are particularly sensitive to changing soil temperatures at the range of -2°C to 0°C" (Sun et al., 2016). Moreover, latent heat may be the most important contributor to the great drop in cooling process of heat capacity and thermal conductivity when temperatures near 0°C. The results also indicated both volumetric heat capacity and thermal conductivity tend to increase with soil water content within the same subzero temperature Sun et al. (2016).

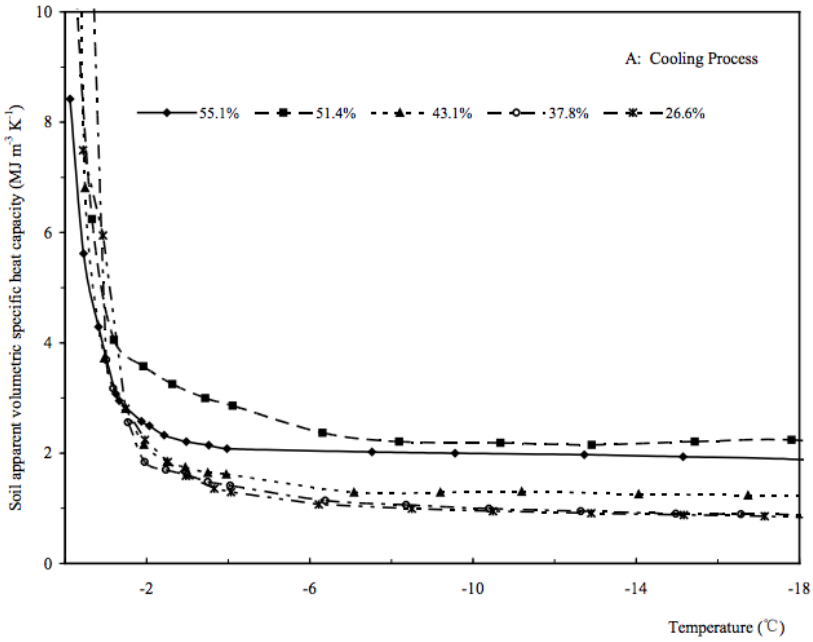

Figure 3.5: Soil apparent volumetric heat capacity changes with different moisture content in cooling processes (From Sun et al. (2016)).

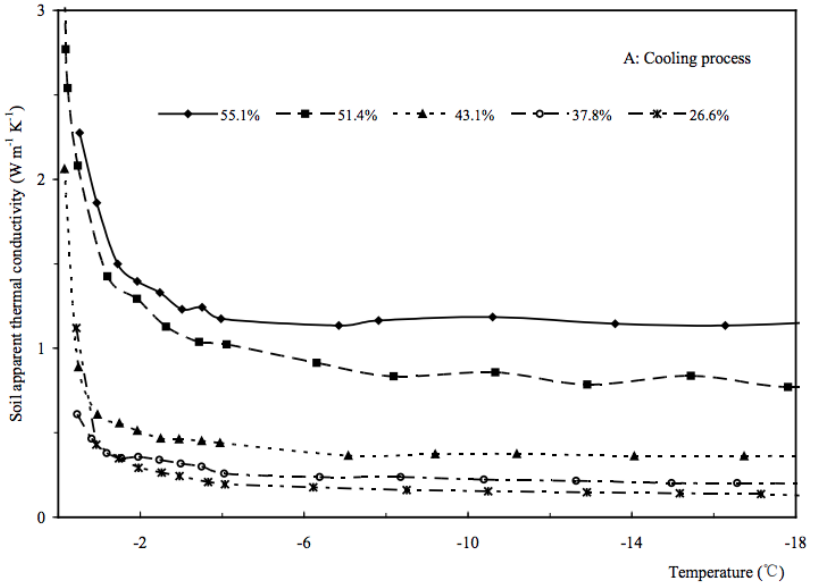

Figure 3.6: Soil apparent thermal conductivity changes with different moisture content in cooling processes (From Sun et al. (2016)).

The second study, was conducted by Aleksyutina and Motenko (2017). In the framework of an engineering and geological survey, investigation of composition, structure and properties of frozen and thawed deposits on the Baydaratskaya Bay Coast, Kara Sea were performed. The study included index parameters such as water content, density, salinity and relative content of organic matter. Additionally, thermal characteristics were investigated. In particular, heat capacity, thermal conductivity and thermal diffusivity were measured using the KD2 Pro device under laboratory conditions. Under the study, the water content and the density of the samples varied on a wide range, which made it possible to analyze the results obtained depending on the volume water content.

From the results it was seen that as the water content increase, from dry to saturated state, the thermal conductivity grows in the beginning; as seen from figure 3.7. The variation rate of thermal conductivity slows down for the frozen samples, while in the unfrozen state the k-values decrease in loams and loamy sands. For unfrozen state of these deposits, and at high values of volume water content, the thermal conductivity are close and determined by the thermal conductivity of water (k = 0.605 W/mK). Sands were characterized by the highest thermal conductivity values, and minimum values referred to peats. The impact of the organic matter is related to the lesser ability of the peat particles to conduct heat. Furthermore, the impact of salinity was found to be more manifested in the frozen state than in the thawed, resulting in a decrease in thermal conductivity of frozen loams and sands with 20 $\%$ and more. The heat capacities were found to increase with increasing volume water content for both frozen and thawed deposits, peat characterized by the highest values. However, when the values of volume water content exceeded 50$\%$, the heat capacity

of the deposit matrix exerted lesser impact on the specific thermal capacity of the deposit than the thermal capacity of water or ice.

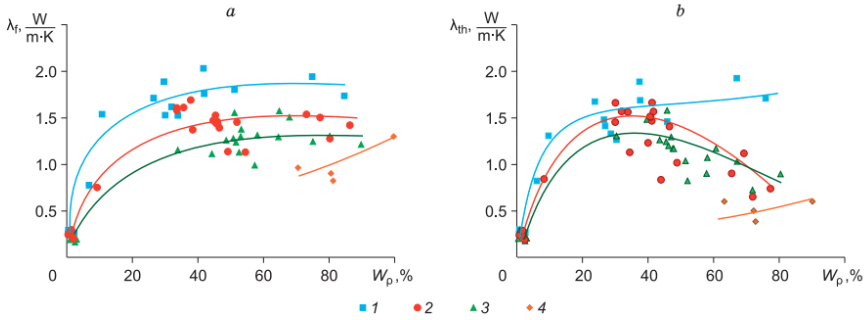

Figure 3.7: Dependencies of the thermal conductivity on volume water content of the deposits in frozen (a) and in unfrozen (b) states: 1 sands; 2 loamy sands; 3 loams; 4 peats (From Aleksyutina and Motenko (2017)).

The thermal diffusivity showed similar trends as the thermal conductivity. Lower D-values were measured in the thawed deposits than the frozen. Also thermal frozen thermal diffusivity is influenced by salinity, and revealed that salinity reduced the value by 35 - 50% (Aleksyutina and Motenko, 2017).

The final study presented essential and useful information about the application of the heated needle probe. The study was conducted by Putkonen (2003) and looked at in-situ thermal properties of ice-bearing frozen soil. He emphasized that the heated needle probe traditionally has been confounded by the energy consumption and the release resulting from the melting and re-freezing of soil ice (Putkonen, 2003). The results highlighted the unsuitability if the probe for determining the thermal properties of frozen soils at temperatures in the range of - 10°C to 0°C, due to the the solver software not accounting for unfrozen water and melting of soil ice. For determination of thermal properties below - 10°C, the heated needle probe can be used. In addition, it has was concluded that since the variability of the thermal properties is marginal between - 10°and - 2°C, it is sufficient to apply the thermal values at - 10°C for a particular soil to temperatures up to - 2°C (Putkonen, 2003).

Chapter 4

Experimental Setup

4.1 Study Site Description

4.1.1 Location

The soil sampling site is located in lower Adventdalen in western central Spitsbergen Island (Svalbard archipelago), figure 4.1. The site is a part of the Norwegian Geo-Test Site (NGTS) project. Core samples from borehole S1_A4_1 (UTM 33X 519150, 8680830; 5 m a.s.l) were collected by SINTEF in the time period 27.03.2017 - 31.03.2017. See figure 4.2 for borehole location.

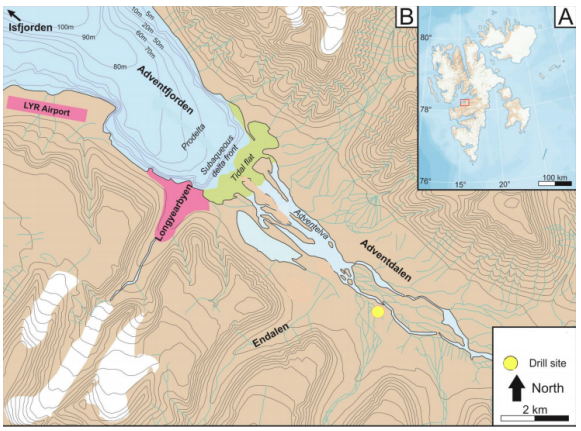

Figure 4.1: (A) Overview map of the Svalbard Archipelago (study area denoted by red box).
(B) The Adventdalen area with the NGTS site marked with a yellow circle (Modified version of figure by Gilbert (2014), fig. 1.1)

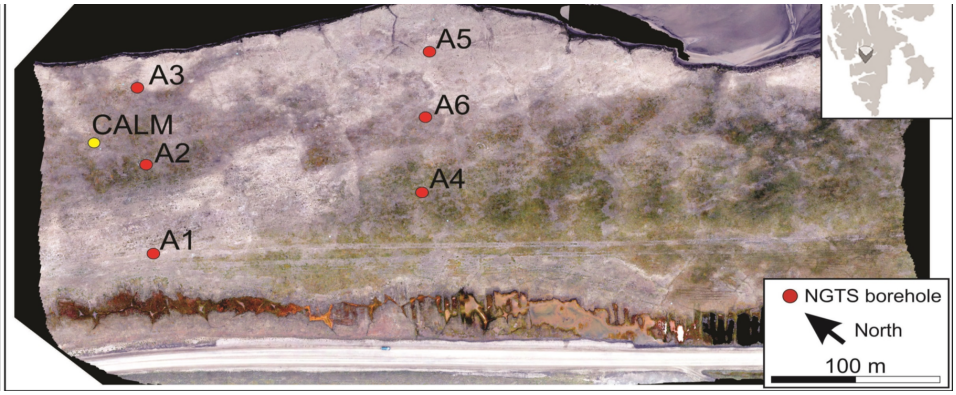

Figure 4.2: Map of borehole locations on the NGTS site in Adventdalen (S1).

4.1.2 Geology and Soil Sampling

Svalbard is located within the continuous permafrost zone (Humlum et al., 2003), and the permafrost is estimated to be approximately 107 m thick in lower Adventdalen (Gilbert, 2014). Adventdalen is a typical U-shaped glacial valley covered by unconsolidated glacial, alluvial, colluvial, marine and aeolian deposits dating to the Holocene. The permafrost in the valley floor is covered by an active layer, and the vegetation is associated with a mixture of grasses, typical for high-Arctic tundra environments (Oliva et al., 2014). The sampled soil cores are taken from a depth of 1.3 meters to 12.1 meters (top of samples) using a modified CRREL barrel. They are stored in sealed plastic bags in a cold lab (-20°C) until testing in the laboratory. Temperature data from a thermistor string close to the sampling site (CALM site) is available to a depth of 9.85 meters.

(a) Drill rig

(b) CRREL barrel

Figure 4.3: Equipment used to take the core samples out of the ground

4.1.3 Climate

The sampling site is located about 5 km from Longyearbyen at a latitude of 78°N. The climate corresponds to a polar tundra climate (ET) in the Köppen climate system. The area is dry and typified by long, cold winters, and short cool summers. However, compared to other locations at this latitude, the mean annual air temperature (MAAT) is considerably warmer. This phenomena is attributed to two geographic factors; the warm Norwegian Current and the location within the North Atlantic cyclone track. The Norwegian current contributes to the reduction or absence of sea ice in the Longyearbyen area during winter. The North Atlantic cyclone track is related to the location of the Siberian High, a cold anticyclone that forms over eastern Siberia during winter. This system results in the advection of warm, moist air to the Svalbard region (Humlum et al., 2003).

Records from Svalbard Airport Weather Station (10 km away from study site, 28 m.a.s.l) show that the mean annual air temperature (MAAT) has increased from -6.7°C in the standard normal period 1961 - 1990 to -4.6°C in the standard normal period 1981 - 2010. Only June, July and August have average air temperatures above zero. Monitoring installations for air and ground temperatures have shown large inter-annual variability, especially during winter months. However, the temperature has increased in all seasons with the strongest increase in winter and spring. The total annual precipitation recorded at Svalbard Airport Weather Station is about 191 mm of which ca. 60% is deposited as snowfall (Førland et al., 2011).

4.2 Ground Temperatures

The ground temperature data used in this master thesis is collected from a thermistor string at the CALM research site (Circumpolar Active Layer Monitoring), north east of the NGTS site (see figure 4.2). The CALM site is used due to problems with receiving data older than November 2017 from thermistor strings installed next to borehole A6 and A2 at the NGTS site. The challenges with A6 and A4 could be related to the battery in the thermistor strings. It is observed that the CALM recording at approximately 10 meters depth generally are colder than the measurements from A6 and A2 (November 2017 to April 2018), with an average of 0.42°C. For the purpose of this master thesis, these deviations are ignored. However, in future work the observations should be investigated.

The CALM program was established to forecast and observe changes in the active layer and upper permafrost. As illustrated in figure 4.4b, PVC tubing was installed to house the thermistor string. The thermistor string consists of ten temperatures sensors with variable spacing down to a depth of 9.85 meters and is pictured in figure 4.4a. The temperatures obtained were recorded hourly from January 2008.

The raw data files are examined for erroneous data such as spikes resulting from unscrewing the borehole cap or removing the string from the borehole. The data is transformed to daily average temperatures. Due to the limited air temperature data available, ground temperature data from only two years are used (January 2016 to December 2017). To create

the temperature profiles with depth and in the PLAXIS model, daily average temperatures from the last day of the month are used.

(a) Thermistor string and recorder

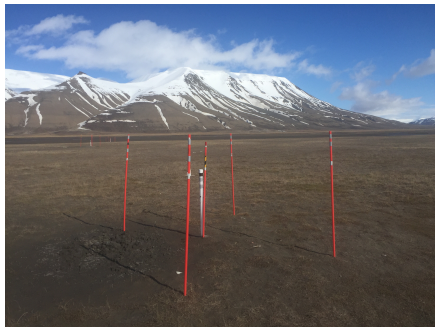

(b) Thermistor installations in Adventdalen

Figure 4.4: Thermistor string

4.3 Laboratory Investigation

In this thesis all laboratory work for index testing are performed on thawed samples and the properties are denoted unfrozen. The core samples are wrapped in cling film and kept in sealed bags to avoid loss of water by evaporation. The core samples selected for laboratory investigation have a one meter depth spacing, giving a complete soil profile with index properties and thermal data. Due to varying quality of the core samples and simplicity, no specification of the division of the core samples are undertaken. The depths presented, represent the top depth of the core samples. A illustration of the core sample division is shown in figure 4.5.

The index tests performed were water content, organic content, bulk density, density of solids, grain size distribution and salinity test. In addition, the thermal properties, in particular thermal conductivity, volumetric heat capacity and thermal diffusivity, were measured in frozen and unfrozen condition for the same soil samples.

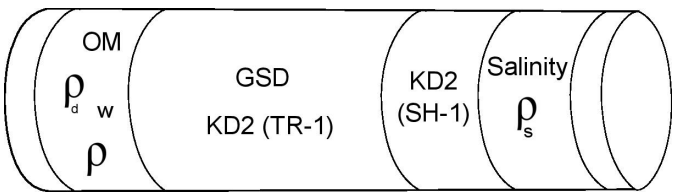

Figure 4.5: Illustrative division of a soil sample

4.3.1 Water Content

Water content or moisture content (w) is mass of water per mass of dry soil, given by equation 2.11. The water content is usually expressed as a percentage, and the method is described in detail in NS-EN ISO 17892 (2014) Part 1.

The water content is found by weighing a representative part of the soil. The sample is dried to a constant mass in an oven maintained at 105 °C to 110 °C. In most cases, drying a fine soil for 16 hours is sufficient.

4.3.2 Bulk Density

Density of soil is mass of soil per unit volume of the material, including any water or gas it contains, see equation 2.6. The methods are described in detail in NS-EN ISO 17892 (2014) Part 2.

The linear measurement method is suitable for the determination of the bulk density of a specimen of soil of regular shape, such as core samples. The specimens used are cylinders with circular cross sections. The principle of the method is to weigh a specimen of known volume.

4.3.3 Organic Content

Organic content is found by using the loss of ignition method described in NS-EN ISO 1744 (2014).

A dried sub-sample from the water content calculation is pulverised and sieved, using a 500 mm sieve (figure 4.6). Ca 20 g of the sieved material is placed on a porcelain dish and dried in the oven for two hours with the same temperature as earlier, 105°C to 110°C. After two hours the specimen is cooled to room temperature. After cooling, exactly 10.0 g of the material is placed in a crucible and dried at constant temperature of 450 °C for 24 hours. The specimen is cooled to room temperature, before it is weighed and the loss of mass is determined.

Figure 4.6: Sieving (500 mm) of dried material for organic content determination from 1.3 meter depth. The red-orange colors indicate organic matter. Small pieces of plant material are also visible.

4.3.4 Density of Solid Particles

The density of solids is defined as the ratio of solid mass (M_s) to volume of solids (V_s), equation 2.7. Density determination by pycnometer is a very precise method. It uses a liquid with well-known density, such as water. The method is described in detail in NS-EN ISO 17892 (2014) Part 3.

The fluid pycnometer method is based on the determination of the difference in the volume of liquid required to fill the pycnometer with the sample being present. The density of solid particles is calculated from the dry mass of the soil particles, divided by their volume difference.

4.3.5 Salinity

Salinity is a measure of the concentration of soluble salts in the soil and can be measured with a conductivity meter, see figure 4.7. The salinity test follows ASTM D1125 (1998) or ISO 11265 (1994).

Figure 4.7: Hand-held conductivity meter for salinity measurement

Salinity of the pore fluid (total soluble salts) is determined by conductivity method. 50 g of soil is soaked with 500 ml of distilled water and mixed well. The mixture is left for about 1 hour for the salt to dissolve completely. Measurements of the electrical conductivity are done using an electrode as part per thousand (ppt) or g/l. The conductivity meter is calibrated with a standard solution of NaCl and cleaned with distilled water before each test. The measured salinity of the mixture is used to find the salinity of the soil by solving equation 4.1.

$$S_1 = \frac{M_{salt}}{M_{w1}} = \frac{M_{w2} \cdot S_2}{M_{w1}} \tag{4.1}$$

where S_2 is the measured salinity, M_{w2} is 500ml distilled water plus the initial water content in the 50 g soil sample, M_{w1}. M_{w1} is calculated from following equation:

$$M_{w1} = \frac{w \cdot M}{(1 + w)} \tag{4.2}$$

where w is water content of the sample, and M is 50 g of soil.

4.3.6 Grain Size Distribution

For the purpose of description and explanation of soil behavior, it is convenient to make an arbitrary division of soils based on particle size. Determination of the grain size distribution of sand and coarser material is performed according to NS 8005 (1990), using sieve from the ASTM-series. Wet sieving was performed based on the assumption that the collected materials contained fines with more than 5% in the silt fraction. Samples containing mainly silt or clay are subject to hydrometer method, as described below.

The grain size distribution is determined by the following two procedures:

- Ideally a unfrozen soil sample of 230 - 300g is used. The sample is washed with distilled water and brushed on the sieves, so that the flushing water will contain the suspended fines of the material (Figure 4.8a). This suspension is used for analysis of the distribution of fines in the material. The sieves are according to ASTM E11 (2017) requirements, with the finest mesh < 75 μm. The fractions are dried in the oven at 105°C to 110°C for 24 hours before weighing.
- Hydrometer is a grain size distribution test for fine particles < 75 μm (ASTM). Hydrometer is an indirect analysis of grain distribution by measuring the density of a slurry sample (suspension), based on particles of different sizes have different sinking time in suspension (Stokes law). The hydrometer test is described in ASTM D422 (2007) and illustrated in figure 4.8b.

(a) Wet sieving of soil sample

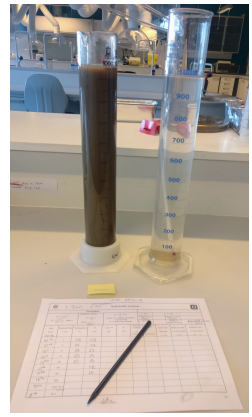

(b) Hydrometer test cylinder

Figure 4.8: Methods used for grain size distribution.

The sieves used are design after ASTM requirements, and the European soil classification standard in NS-EN ISO 14688-2 (2004) is difficult to use.

The Unified Soil Classification System (USCS) is standardized in ASTM D2487 (2017) (lab) and is used for engineering purposes. However, the USCS silt and clay classification is based on plastic properties (Atterberg Limits) and not particle size distribution. Lack of Atterberg limits and for the purpose of the PLAXIS model, the U.S. Department of Agriculture (USDA) soil classification is used for description of the soil texture. Description is found in the USDA Soil Survey Manual. Note, despite the fact that USCS and USDA are not mix and match systems (soil types are not equivalents), this thesis combines testing procedure and classification type from the two systems. This is an source of error to consider.

Moreover, several mapping schemes between the two systems are found in the literature. In particular, a mapping scheme was developed by Garca-Gaines and Frankenstein (2015). They found good consensus between all the data sources they investigated for most soil types. The conversion scheme to move from one system to another is shown in table 4.1. Despite this, it is recommend to be careful when using a mapping scheme. For high quality control, it is better to determine USCS classifications by laboratory analysis including Atterberg Limits.

Table 4.1: USDA classification equivalency in USCS classification (After Garca-Gaines and Frankenstein (2015))

USDA Classification	USCS Classification
Sand	SP
Loamy Sand	SM
Sandy Loam	SM
Sandy Clay Loam	SC
Sandy Clay	SC
Loam	CL
Silt Loam	ML
Silt	ML
Clay Loam	CL
Silt Clay Loam	CL
Clay	CH
Silt Clay	CH

4.4 Degree of Saturation and Porosity

An increase in degree of saturation of a soil will also increase the thermal conductivity. This relation is elaborated in section 2.6. Knowing the degree of saturation is therefore an important property in estimates of thermal conductivity and is one of the parameters in the diagrams by Kersten (1949), figure 3.3 and figure 3.2. Values for degree of saturation are calculated from equation 2.14.

Porosity, or the often more used void ratio, would also influence the thermal conductivity of the material. Values are obtain from equation 2.9 and equation 2.10, and are used in the geothermal model proportion in chapter 6.

4.5 Unfrozen Water Content

Laboratory testing has been carried out to observe that the melting point of water is further depressed if it includes solutes (Han, 2011). Direct measuring methods have been applied, and the results are reviewed and summarized by Anderson et al. (1973). Equation 4.3 gives a representation of the experimental data as a simple power curve. It is based on a correlation between unfrozen water content and the liquid limit of the soil. A and B are characteristic soil parameters and T is temperature expressed as a positive number in degrees Celcius below freezing. Anderson et al. (1976) developed values for the unfrozen water content parameters, A and B, based on the liquid-limit procedure.

$$w_u = A \cdot T^B \tag{4.3}$$

The agreement between measured and predicted vales is found to be excellent for several soils (Anderson et al., 1976), and unfrozen water content computed from equation 4.3 is assumed to be adequate for many engineering applications where soluble salt are absent (Andersland and Ladanyi, 1994) and there is no sophisticated measuring equipment available.

However, for Norwegian soils, equation 4.3 has shown to give misleading values. According to Nybo (2017), results obtained form the liquid limit test procedure provided lower unfrozen water content than the actual amount. In particular, soils from Longyearbyen, Svalbard, showed this tendency of underestimating the unfrozen water content, which could give too small settlement predictions and have a significant impact on potential structures on the site.

Nybo (2017) suggested more appropriate empirical formulas for Norwegian soils. The liquid limit parameters were adapted to fit the curve from water potential testing which indicated more reasonable values of unfrozen water content. Moreover, Nybo's (2017) study indicated that the liquid limit determination of unfrozen water content should be adapted to different soil types. The proposed equations for soil types on Svalbard are presented in equation 4.4 and 4.5.

$$w_{u,T=1} = 0.703 \cdot w_{N=25} - 1.67 \tag{4.4}$$

$$w_{u,T=2} = 0.657 \cdot w_{N=100} - 4.33 \tag{4.5}$$

where T = 1 and T = 2 refers to temperatures of -1°C and -2°C, respectively. $w_{N=25}$ and $w_{N=100}$ are water content corresponding to N= 25 and N= 100, where N is the number of blows required to close the standard groove in the liquid limit test.

Test Procedure

The index test program for soil from borehole S1_A4_1 at the NGTS site in Adventdalen did not include liquid limit determination. However, the soil tested by Nybo (2017) were performed on soil from a borehole at the same study site. Based on her investigation, equation 4.6 is used to estimated the temperature dependent unfrozen water content of the soil.

$$w_u = 17.32 \cdot T^{-0.6595} \qquad [\%] \tag{4.6}$$

Equation 4.6 is valid for negative temperatures, and T is temperature expressed as a positive number in degrees Celsius below freezing. A graphic representation is given by figure 4.9.

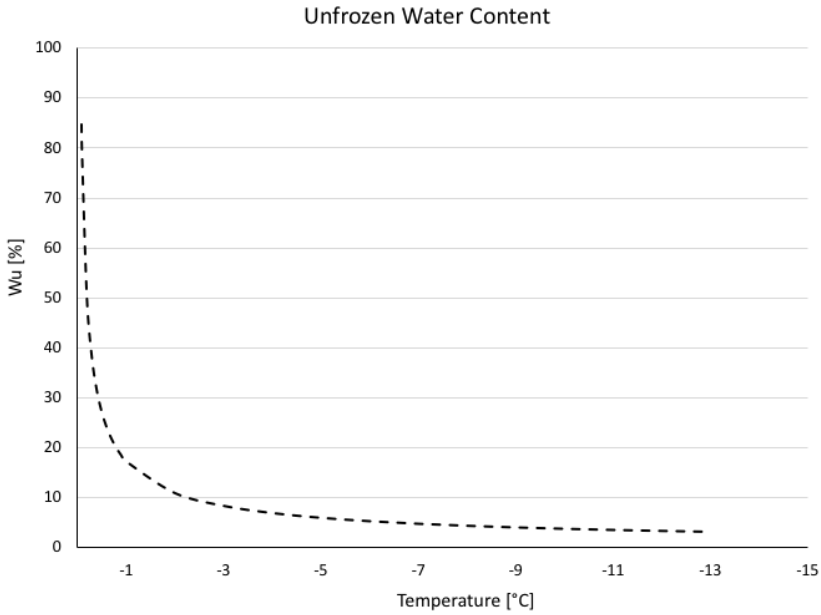

Figure 4.9: Unfrozen water content curve after Nybo (2017).

4.6 Thermal Properties of Frozen and Unfrozen Soil

Thermal properties of soils are determined by using a thermal needle probe following American standard ASTM D5334 (2014). No European standard has yet been published. The KD2 Pro Thermal Properties Analyzer (Decagon Devices, Inc.) is a useful device and is based on transient line heat source method. Dependent on choice of sensor, one are able to measure thermal conductivity, resistivity, volumetric specific heat capacity and diffusivity. The infinite heat line theory of the KD2 Pro, choice of sensor and recommend installation procedure are described in section 3.4.

4.6.1 Thermal Conductivity

As a part of the experimental testing of thermal conductivity of frozen and unfrozen soils, the TR-1 probe was chosen, due to its design characteristics. Prior to the measurements, verification (calibration) of the thermal sensor in order to check whether it was functioning properly was performed using a silicon cylinder supplied by the manufacturer. The measurements using the TR-1 needle were performed using the default settings of the device. The read time was 5 min and the power mode was high.

For unfrozen soil, usually it is adequately to follow the standard procedure discussed in

section 3.4. On the other hand, there are few resources for laboratory testing of thermal conductivity in frozen soils, and testing procedure has not yet been established. Therefore, a number of trials using different techniques were carried out to obtain results with best accuracy. The challenges were mainly related to the contact resistance between the needle and the material. Pre-drilling of holes and the use of thermal compound provided by Decagon Devices, Inc. on the needle, failed to give desired accuracy. Better results were obtained by using water instead of compound in the holes, and freezing the needle in place. Despite this, limited time and equipment made this procedure also unfavorable. Finally, it was decided to thaw the samples, measure the unfrozen thermal conductivity before freezing the samples overnight in the cold lab at - 10°C with the needle inside. This procedure gave result with error less than 1 %.

Before thawing, the frozen samples were wrapped in cling film and aluminum foil to minimize water evaporation and to support the samples for losing their cylindrical shape. Lastly, the sample was put in a plastic bag. A picture of the experimental setup is show in figure 4.10. The TR-1 needle was inserted vertically into the samples left for at least 20 min to reach temperature equilibrium. The test was started and each measurement cycle consisted of a 30-sec equilibrium time, 30-sec heating time and a 30-sec cooling time. During the heating and cooling processes, temperature measurements were made every second. Three repeated measurements, taken 15 min apart, were conducted for each sample. The same test procedure was used for unfrozen and frozen state.

Figure 4.10: Example of experimental setup for the KD2 Pro measurements. This particular sample is taken from a depth of 12.1 meters.

For the purpose of this thesis, the 12 core samples were tested for two different temperatures; one in thawed state in room temperature at +23 °C and one in frozen state in the cold lab at -10°C using the TR-1 needle. - 10°C was chosen as the frozen test temperature due to trouble with the KD2 Pro Thermal Properties Analyzer around 0°C. This observation is in agreement with previous test results, in particular Putkonen (2003) presented in subsection 3.4.6.

4.6.2 Volumetric Heat Capacity

The dual-needle probe, SH-1, is primarily designed to read volumetric heat capacity. Additional measurements are thermal conductivity, thermal diffusivity and resistivity. The purpose of measuring volumetric heat capacity was to obtain input parameters in the geothermal model in PLAXIS. The SH-1 needle was only used in the unfrozen samples (+23°C), due to logistical challenges and the objective of the experiment.

The installation of the dual-needle follows same procedure as the single needle. It was calibrated by means of a delrin block, and default setting was used. The read time was 2 min and the power mode was high. Three repeated measurements, 15 min apart, were performed. It is important to be aware of that the KD2 Pro measures volumetric heat capacity (MJ/m^{3}K), and not specific heat capacity (kJ/kgK).

4.6.3 Thermal Diffusivity

The thermal diffusivity is a secondary measurement when using the SH-1 dual-needle. The property is useful for investigations of non-steady state heat flow, and one can calculate the evolution of the soil temperature at any depth between the ground surface and the depth of ZAA by using equation 2.2. The direct thermal diffusivity recordings were compared to values obtained from back-calculation of thermistor string data.

Chapter 5

Analysis and Results

The characteristics of soil from the NGTS site in lower Adventdalen have been obtained from laboratory testing at UNIS. All investigations of the soil composition and properties presented in this chapter, have been conducted by the author in the framework of this master thesis.

5.1 Soil Classification

According to the U.S soil taxonomy classification system (USDA), the name for perennially frozen soils (permafrost) is Gelisol (Garca-Gaines and Frankenstein, 2015). From the wet sieving and hydrometer analysis, the grain size distribution chart in figure 5.1 was created. The chart includes results from all the 12 samples and indicates that the deposits are well-sorted. The soil samples are classified as either sandy loams, loam, silt loam or silt, based on the USDA soil classification system. The dominating content of silt-sized particles was characteristic in most of the samples, except the sandy loams at 3.3 m, 4.1 m, 9.3 m and 10.5 m. In these samples, the sand grain-sized fraction predominates. Only samples from 4.1 m and 9.3 m depth contained grains larger than 2.00 mm. The sample from depth 4.1 m, represented by the light green curve in figure 5.1, deviates from the other samples with a very high coefficient of uniformity, C_u (see APPENDIX A table A.4). The sample from 9.3 m depth (pink curve in figure 5.1) has a larger portion of coarse material than the other samples.

Evaluation of the deposits and their variability, supported by salinity measurements, have revealed that the upper part of the section, most likely is composed of deposits with alluvial origin, while the lower part is composed of marine saline variations.

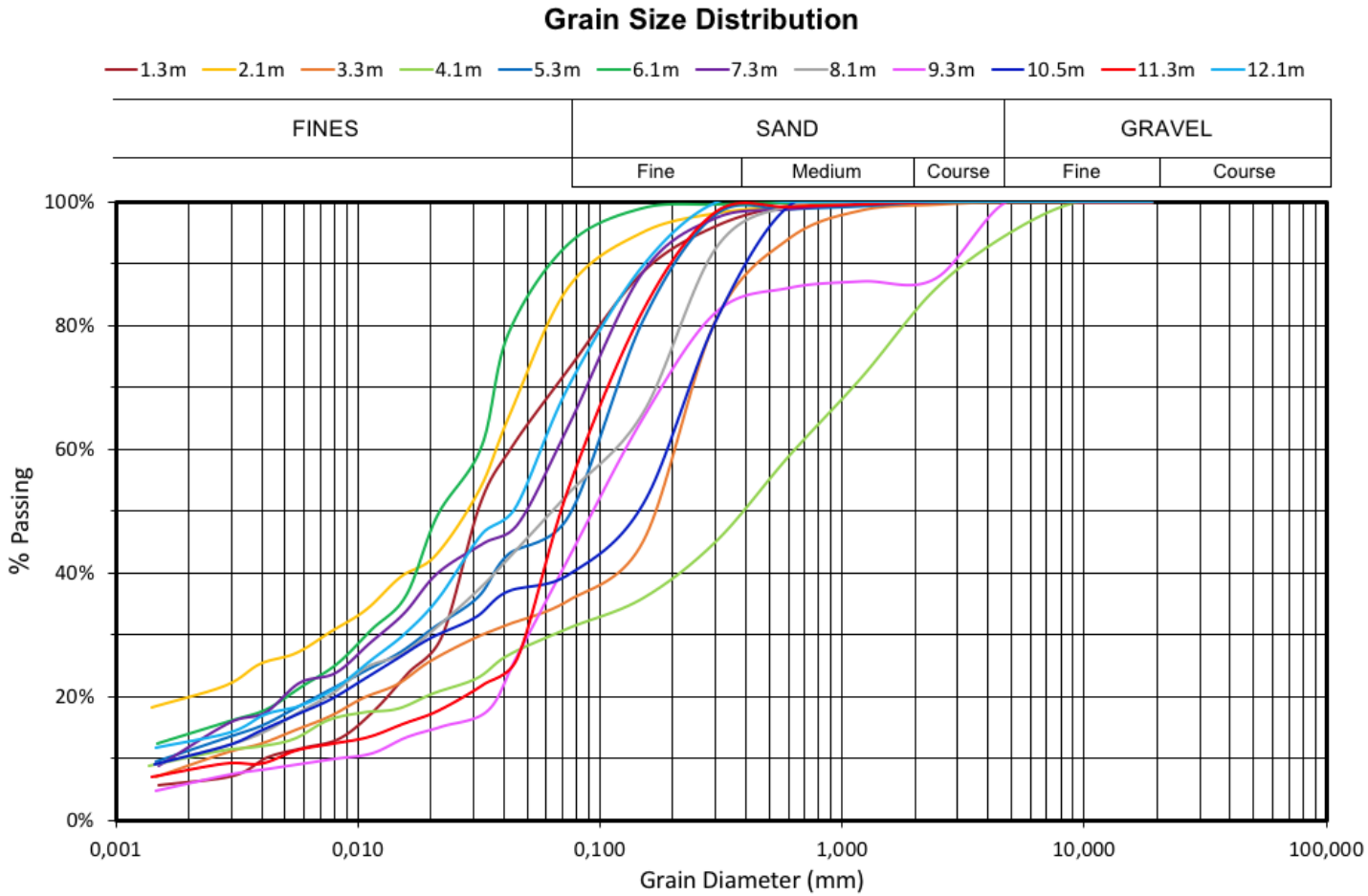

Figure 5.1: Grain size distribution curves from borehole S1_A4_1 in Adventdalen, Svalbard. The 12 core samples are from depth 1.3 m - 12.1 m.

In subsection 4.3.6, two soil classification systems were briefly introduced. It was argued that the U.S. Department of Agriculture (USDA) soil classification is used for description of the soil texture in this master thesis, due its relatively simple approach, available particle distribution and applicability to the PLAXIS software. However, for engineering purposes, in particular determining soil strength, the Unified Soil Classification System (USCS) is a better system and standardized in ASTM D2487 (2017) (lab). Therefore, table 5.1 shows the USCS classification for the soil in Adventdalen, Svalbard, based on a mapping scheme by Garca-Gaines and Frankenstein (2015).

Table 5.1: USDA classification equivalency in USCS classification for the 12 core samples from Adventdalen, Svalbard.

Depth	USDA	USCS
1.3	Silt loam	ML
2.1	Silt loam	ML
3.3	Sandy loam	SM
4.1	Sandy loam	SM
5.3	Loam	CL
6.1	Silt	ML
7.3	Silt loam	ML
8.1	Loam	CL
9.3	Sandy loam	SM
10.5	Sandy loam	SM
11.3	Sandy loam / Loam	SM / CL
12.1	Silt loam	ML

Individual grain size distribution curves and soil characteristics for each depth are tabulated in APPENDIX A.

5.2 The Results of Comparing the Deposit Characteristics by Depth

In this section, the results of studying the characteristics of frozen and unfrozen deposits, reflecting the natural variability of their composition, structure and properties, are discussed. A summary of all index parameters, thermal properties and grain size distribution are found in APPENDIX A.

5.2.1 Index Parameters

Figure 5.2 shows data from borehole S1_A4_1 in Adventdalen, Svalbard. The index properties are presented verses depth. For simplicity, all test results are plotted versus the top depth of that particular core sample.

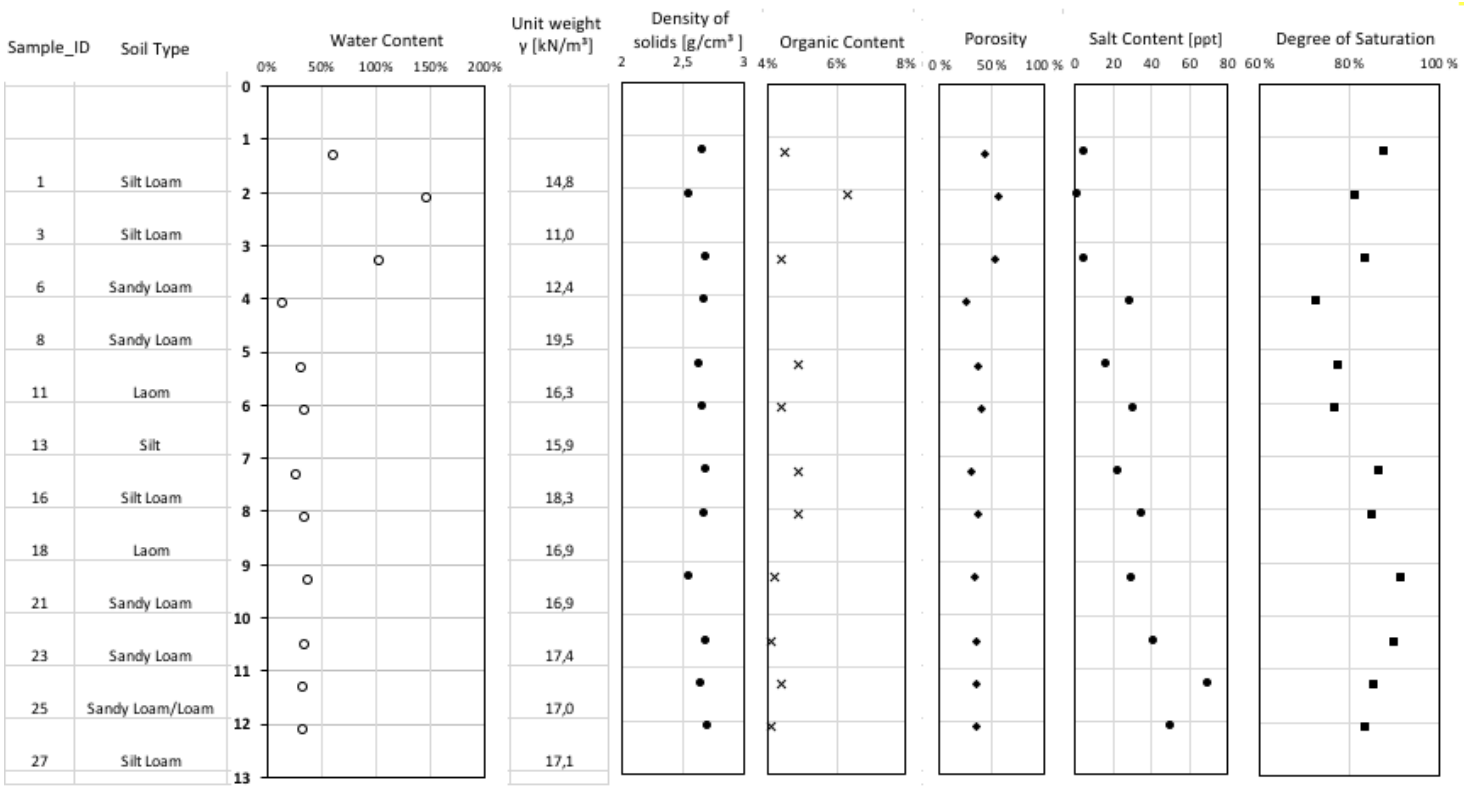

Figure 5.2: Presentation of index parameters verses depth. Borehole S1_A4_1 in Adventdalen, Svalbard.

The profile gives an overview of the distribution of soil properties from the ground surface to a depth of 12.1 meters. The upper part of the section (the first 1- 3 meters from the surface) has high water contents, 61 % - 147 %, and low unit weights, 11.0 - 14.8 kN/m^3. Peaks in water content can be explained by large visible ice lenses as shown in figure 5.3, thus, when thawing, resulting in high water contents. Large ice lenses can be seen in correlation with increased porosity, thereby lower unit weight than the rest of the profile.

(a) Core seen from the side **(b)** Core seen from the top

Figure 5.3: Core from 3.3m with larger ice lenses

The first meter or so from the ground surface is also known as the active layer. The water content in a bag sample from a borehole nearby was 31.9 % and could be used as a representative water content of the active layer in mineral soil. Most likely, the sample is taken form the middle of the active layer. This section is commonly quite dry as the moisture is pulled towards the ground surface and permafrost table during freezing.

Under the active layer, a transition zone smooths out the boundary to the permafrost as explained in section 2.1.1. Since this layer undergoes transition of freezing and thawing at much lower frequencies, it has characteristics that differ from both the active layer and the permafrost. The high water content here is a result of seasonal thawing, and will typically vary over the year, in relation to the onset of thaw in spring and with the location of the thawing front (Schuh et al., 2017). Because the layers below remain frozen, the water accumulate in top part. The transient layer is a fine conceptual model, but a bit difficult to apply when the surface is also aggrading due to sediment deposition. However, at the site in Adventdalen the transition layer could be interpreted to reach to about 4 meters. Furthermore, the soil taken from 4.1 meter has surprisingly low water content compared to the rest of the profile. A water content of 15 % could be an exception in the soil, or a human error.

In the lower part of the section, 5.3 meters to 12.1 meters, the soil has water content from 27 % to 37 %, and unit weight varying from 15.9 kN/m^3 to 18.3 kN/m^3. The soil from these depths have minor or none visible ice lenses. See figure 5.4.

Figure 5.4: Soil sample from a lower layer without large visible ice lenses.

The density of solids is in the range of 2.56 g/cm^3 - 2.70 g/cm^3. The pycnometer method is very sensitive to precision mistakes. Hence, human error or exceptions in the soil may be present. Consequently, the porosity (or void ratio) calculated based on density of solids, will follow the same trend in variability. Thus, the porosity could have low accuracy as well.

A soil cannot have saturation more than 100 %; all the pores are filled with water. In the Adventdalen soil, the degree of saturation does not have a clear pattern with variations from 73 % to 92 %. In many calculations, 100 % saturation is assumed due to simplicity and the fact that degree of saturation is a second hand calculations which is sensitive to density of solids, water content and pore distribution.

The organic content is low and had small variations, 3.6 % to 5.8 %. However, the upper layers are dominated by the highest values, which arises from proximity to surface vegetation. Organic matter (OM) in the active layer influences the thermal state. The thermal conductivity is much lower for the organic matter than for the mineral soil. Thus, heat is conducted less effective than in the mineral soil and the soil will react slower to changes in climate with the presence of OM. However, for the over all climate system, organic matter will have larger implication because of the decomposition (Kelder, 2017).

The pore-water salinity increases with depth from 1.9 ppt to 70.18 ppt. This is supported by the fact that large areas of the Arctic coast line are subjected to antecedent marine incursion. The presence of unfrozen water and significant freezing point depressions in frozen saline deposits, poses geotechnical challenges (Gilbert, 2014).

5.2.2 Thermal Properties

The properties recorded with the KD2 Pro Thermal Properties Analyzer were frozen and unfrozen thermal conductivity, thermal diffusivity and volumetric heat capacity. The former two were obtained using the single needle, TR-1, while the latter was measured with the SH - 1 dual - needle. At least three measurements with error less than 1% were taken in each sample. Figure 5.6 shows data reflecting the changeability of the characteristics of

the deposits in the unfrozen and frozen states from the ground surface to a depth of 12.1 meters.

As discussed in previous subsection, soil from 2.1 m and 3.3 m were dominated by larger ice lenses. The high ice content made it difficult to retain the shape of soil core after thawing. The samples turned into a soil slurry. A picture is shown below (figure 5.5). Values for these depth are lacking in the depth profile. Likewise, no result are available from 1.3 m, because none pieces of the core were large enough for KD2-measurements using the 10 cm TR-1 needle.

Figure 5.5: Core from 3.3 m in frozen and unfrozen state.

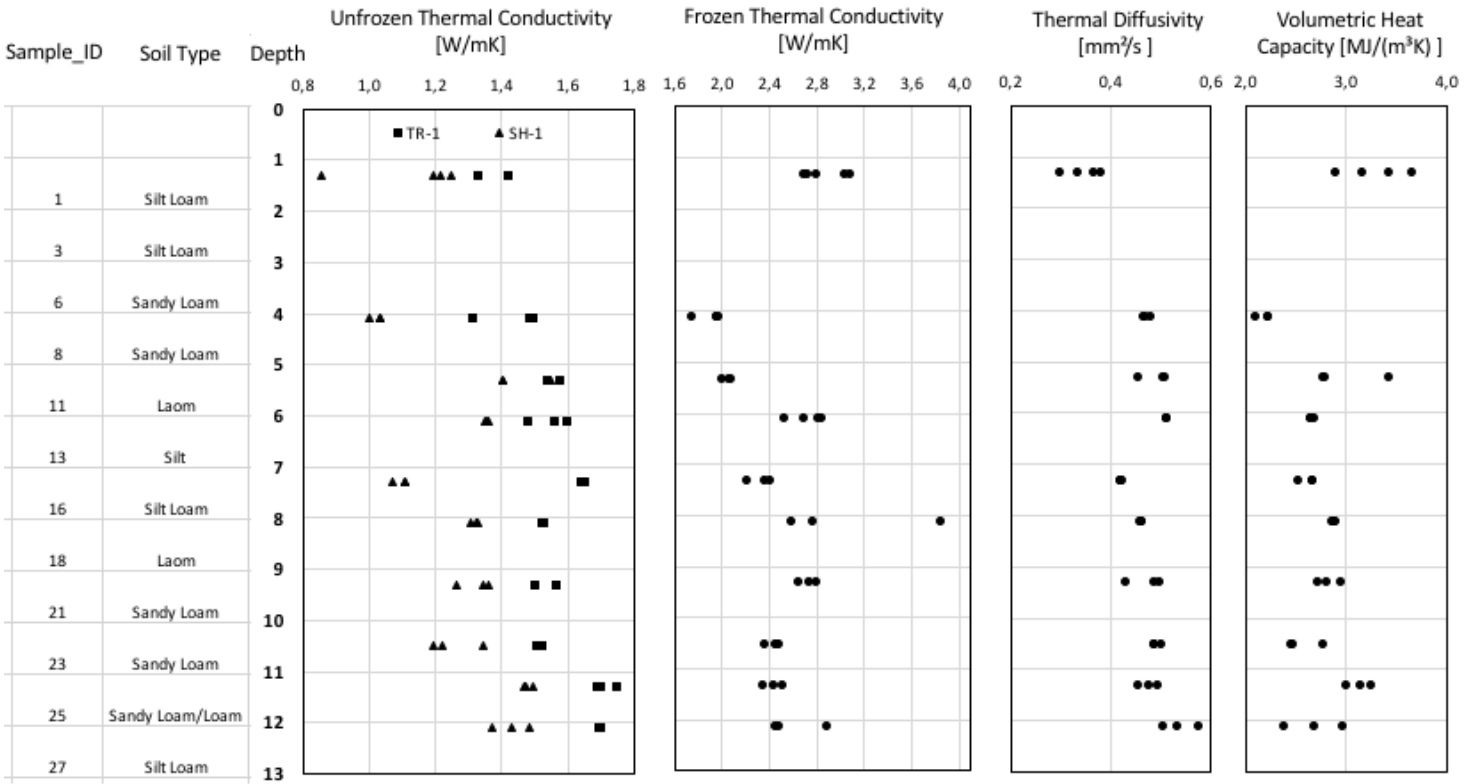

Figure 5.6: Presentation of thermal parameters verses depth. Borehole S1_A4_1 in Adventdalen, Svalbard.

The unfrozen thermal conductivity, k_{un}, is measured both by the TR-1 (square marker) and SH-1 needle (triangular marker). The values obtained with the TR-1 needle are higher than the SH-1 values for all depths. According to the manufacturer, TR-1 gives the most reliable result for soil thermal conductivity due to the measuring range. Consequently, the TR-1 values are used in the geothermal model and in the unfrozen state, the thermal conductivity is in the range of 1.329 - 1.746 W/mK. The frozen thermal conductivity measurements show values from 1.736 W/mK and up to 3.844 W/mK. In agreement with literature, the highest thermal conductivity is prominent among the frozen samples. This is caused by the four times higher thermal conductivity of ice verses water. As the water content gets close to 100 $\%$, the thermal conductivity is found to approach that of water (0.605 W/mK) and ice (2.23 W/mK), for unfrozen and frozen samples respectively. However, no conclusion can be made to support or eliminate this behaviour from the results presented here.

The variation in thermal conductivity is related to the natural variety of the deposits, therefore, it is necessary to analyze the results obtained depending on different factors. From the literature and chapter 2.6, some of the dependencies for changes in the thermal properties are water content, salinity, organic content, soil type and dry density.

The thermal conductivity has small variations over the profile. However, the trends are similar for both frozen and unfrozen measurements. The impact of organic content can not be confirmed, nor can the expected impact of salinity, and the affect by dry density is discussed in the next section. To make a distinction between thermal conductivity of the different deposits, sandy loam, loam silt loam and silt, is not possible. Nevertheless, the higher k - values in the top of the frozen sample can be seen in relation with high water content, thus ice content, and degree of saturation. Lastly, the lowest unfrozen k - values corresponding to very high water contents are in accordance with study by Aleksyutina and Motenko (2017); the thermal conductivity decreases as the volumetric water content exceeds 50 $\%$. The unfrozen water content should not have considerable influence on the thermal properties of the soil in a frozen state, due to the laboratory conditions of -10°C.

Furthermore, a slight reduction in the unfrozen volumetric heat capacity with depth is observed. This is attributed to the reduction in organic matter and water content. At 1.3 meter, the volumetric heat capacity is 3.429 MJ/m^{3}K. In the lower part, the values are as low as 2.099 MJ/m^{3}K. No relation is observed between the soil type and volumetric heat capacity.

Lastly, the unfrozen thermal diffusivity varies between 0.296 mm^2/s in the top to 0.575 mm^2/s in the bottom, indicating a slightly increase with depth. According to Aleksyutina and Motenko (2017), the thermal diffusivity is following similar trends as the thermal conductivity. Hence, one would expect a decrease in D for an increase in water content above 50 $\%$. Indeed, the lowest values should be measured in the top of the profile.

5.3 Thermal Conductivity from Direct Measurement and Index Parameters

To investigate the relation between thermal conductivity by direct measurement and from soil index properties, the average thermal conductivity diagrams based on Kersten's (1949) work are used. Because the sampled soil is dominated by fine material, the diagram for silt and clay soils is used. See section 3.2.1 for more information about the diagrams.

For the 12 core samples, index testing and direct measurements with the KD2 Pro Thermal Properties Analyzer (frozen and unfrozen) are compared. Recall that thermal values from depth 2.1 m and 3.3 m are missing. Additionally, the water contents at these depths are outside the limits of the diagrams, and are therefore not plotted in the diagrams. This fact is also applicable to soil from depth 1.3 m.

Figure 5.7 and figure 5.8 display the results for frozen and unfrozen thermal conductivity, respectively. The red markers indicate index testing results, and the blue markers are data from direct measurements. From index tests water content (w), dry density (ρ_d) and degree of saturation (S_r), are used to find the corresponding thermal conductivity from the diagrams. For some values, water content and dry density are given higher priority, due to the uncertainty related to the degree of saturation values.

The thermal conductivity values from the KD2 Pro are average values (TR-1 needle) from each depth. See APPENDIX A and table A.3 for specific values.

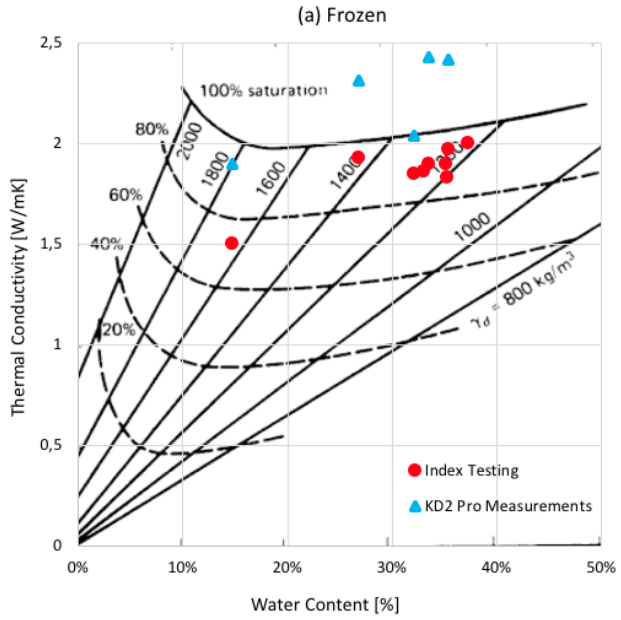

Figure 5.7: Frozen thermal conductivity of fine-grained soil. Direct measurements vs. index parameters.

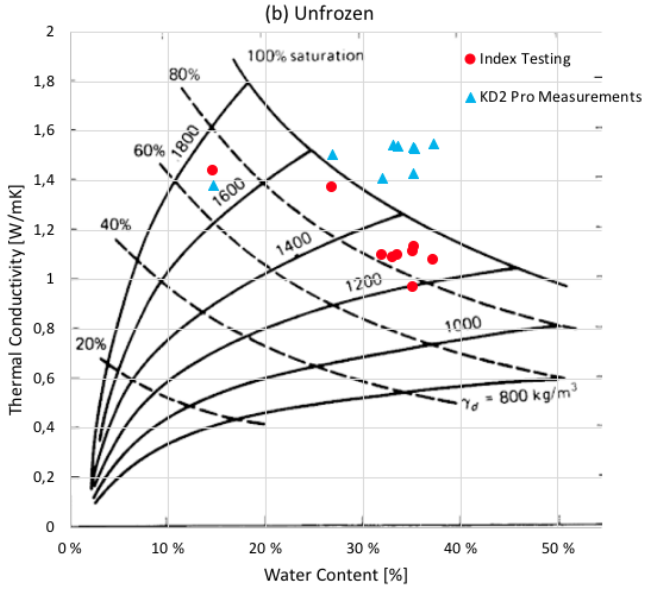

Figure 5.8: Unfrozen thermal conductivity of fine-grained soil. Direct measurements vs. index parameters.

As emphasized in section 5.2.2, the variability in thermal conductivity is related to the natural variability of the deposits. High water content in frozen samples is generally associated with higher k-values, which in good agreement with frozen state values. One can observe an increase in thermal conductivity as the saturation level increase for most of the samples, which supports the theory. However, the influence from dry density is indicated in the unfrozen diagram. High dry density, is associated with low porosity, thus a denser soil sample. With an increased number of contact points between the soil particles, and a reduction in air, water and ice with typically lower k-values than the soil particles, the thermal conductivity is expected to be higher. Two depths, 4.1 m and 7.3 m, show this behavior.

From figure 5.7 and 5.8 it is clear that the laboratory index tests give consistently lower thermal conductivity values than the direct measurements with the KD2 Pro. The only exception is found for the unfrozen value at depth 4.1 m. This observation could be a result of the unexpected low water content in the sample, seen as a source of human error or exception in the soil sample.

The disagreement in thermal conductivity values between the two methods is generally larger in frozen state than in unfrozen state. Additionally, it is observed that for the frozen state, some of the direct measurements are higher than the upper diagram limits, and more red dots than blue triangles are to be found in the plot. For the unfrozen state, all the blue markers are included. For both states, most of the KD2 Pro measurements, indicate saturation above 100 $\%$, which is impossible.

In the comparison of the results from the two methods, it is important to notice the difference in the modelling and measuring approach. The diagrams are designed after results from a steady state method, while the KD2 Pro are classified as transient method. Additionally, even though the soil from Adventdalen consists of a larger fine fraction, sands are also present. The use of diagrams for fine-grained soils could be another source of error, and interpolation between fine-grained and coarse-grained diagram should be investigated.

Moreover, another deviation between the two methods. The diagram for frozen soil is valid for soil at - 4°C, but does not account for unfrozen water which is proved by several researchers to be present at sub-zero temperatures close to 0°C (Andersland and Ladanyi, 1994). It is reasonable to think that the diagrams are simplified illustrations of the thermal conductivity only dependent on water content, dry density and degree of saturation. However, the fact that the KD2 Pro measurements are taken at - 10°C, it is assumed a negligible amount of unfrozen water. The unfrozen water content should not influence the comparison of of k - values from direct measurements and index properties.

From subsection 3.2.1, Kersten (1949) claimed that his equations gave values with less than 25 $\%$ deviation from measured values. An evaluation of this statement is presented in table 5.2.

Table 5.2: Percentage deviation between Kersten's (1949) equations and direct measurements

Depth [m]	Frozen [%]	Unfrozen [%]
4.1	21	-4
5.3	9	22
6.1	33	32
7.3	17	9
8.1	38	29
9.3	26	30
10.5	19	26
11.3	22	28
12.1	29	29

From table 5.2, it is evident that Kersten's (1949) statement is true for samples from depth 4.1 m, 5.3 m, 7.3 m and 10.5 m. However, the statement fails for 56 % of the tested samples. Based on the results in this master thesis only, no final conclusion can be drawn to verify or discard Kersten's (1949) statement. More data from index testing and direct measurements are required for a more extensive and reliable evaluation.

Discussion and Conclusion

For thermal problems in cold regions, assuming average thermal conductivity values of the ground has been found appropriate. However, looking at the results in this master thesis it can be concluded that the use of Kersten's (1949) average thermal conductivity diagram underestimates the thermal conductivity compared the direct measurements. For geotechnical design purposes, assuming too small k-values can result in underprediction of the extent of thawing during warmer periods or from structural impact. Thawing could lead to structural stability and bearing capacity problems. More investigation should be performed in permafrost soils in Adventdalen to investigate the applicability of the diagrams for development of the area. Generally, one should obtain site specific thermal conductivity values to perform more accurate thermal design in permafrost soil.

5.4 Ground Temperature Profiles from Thermistor String Installation

Figure 5.9 shows the depth penetration of variation of daily mean ground temperature from the start of January 2016 to the end of December 2017. The daily average maximum temperature for 2016 was 22.26°C on the 2nd of July and the minimum temperature was -18.96°C on the 8th of December. A_s = $\frac{22.26+18.96}{2}$ = 20.61. The mean annual surface temperature, T_m = 1.65°C. The daily average maximum temperature for 2017 was 17.37°C on the 30th of July and the minimum temperature was -20.14°C on the 27th of February. A_s = $\frac{17.37+20.14}{2}$ = 18.76. T_m = -1.39 °C.

An indication of a close linkage between surface temperature (ST), assumed to be represented by the thermistor at 0.0 meters depth, and the atmospheric climate is seen by the high frequency (irregular shape) of the curves. Moderation of the effect are caused by processes occurring at the boundary layer of vegetation, snow, mineral soil (Isaksen et al., 2000).

In chapter 2, ground temperatures were illustrated by figure 2.1 described by equation 2.1 and 2.2. It was explained that the attenuation of amplitude of the temperature variation is based on depth and phase shift. From figure 5.9, the time shift of maximum and minimum temperatures are visible; the sensor at depth 0.25 meters (dark blue) shows its maximum during middle of July whereas sensor at depth 3.0 meters (dark red) reaches its maximum in the end of January the following year. The duration of the lags between the curves in figure 5.9 are not constant. The variability is partly due to a variable distance between the temperature sensors. In general, the greater the distance between the sensors, the greater the lag between the corresponding time series (Zenklusen Mutter and Phillips, 2012).

Moreover, it is seen that the deeper the sensor is installed the smaller the influence of surface temperature variations become. This is due to the damping of the signal (Fröb, 2011), which is explained by the time the temperature needs to travel deeper in the soil profile. Hence, lower layers of the soil profile, experience small temperature variations with changing season. In correlation with theory, temperature curves follow a sinusoidal trend over the year before flattening out with depth. In particular, the thermistors installed at at 5.0 meters (light green), 7.0 meters (dark purple) and 9.85 meters (light blue) all have very stable temperatures throughout the year.

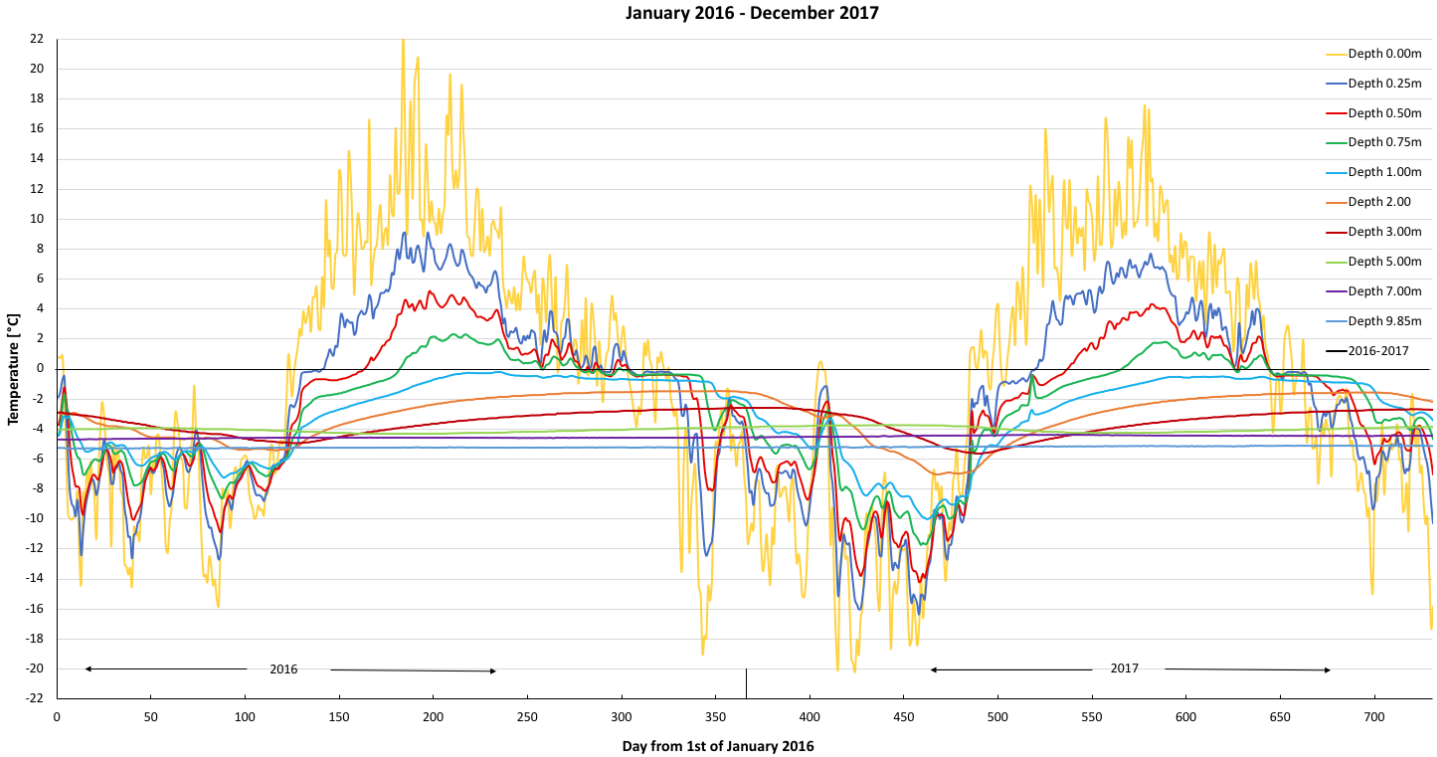

Figure 5.9: Adventdalen ground temperatures from 0.0 - 9.85 meters depth variation with time (CALM site).

In chapter 2, the seasonal variations in the ground temperature with depth were explained by a trumpet curve (figure 2.3). From the CALM thermistor string data, figure 5.10 and 5.11 are created. They show the distribution of the ground temperature on the last day of the month in 2016 and 2017, respectively. Minimum and maximum temperature lines create a temperature envelope defining the range of annual ground variations. T_{min} and T_{max} meet at the depth of zero annual amplitude (ZAA). This is where seasonal temperature variations cease to propagate and the ground temperature is constant throughout the year. In agreement with figure 5.9, the depth of ZAA is close to 10 meters. In figure 5.10 and 5.11 ZAAs are marked with red dotted lines. For both figures the temperature seems to continue decreasing past the deepest thermistor sensor. From other thermistor string installations at the UNIS East site (5km North-West) and at Janssonhaugen (15km East), the ground temperatures are found to stabilize and eventually increase due to the thermal gradient. This happens at around 15-25 meters depth, and a similar trend could be expected at the CALM site.

The mean annual ground temperature (MAGT) taken at the depth of zero annual amplitude (9.85 m) is -5.25°C in 2016 and -5.17°C in 2017. Despite the increase in temperature of by 0.08°C from 2016 to 2017, it is not sufficient to conclude that ground temperature warming is happening. Acceptance of this statement merits closer examination and more data.

In addition to zero annual amplitude, temperature profiles in time and space give information about the active layer thickness (ALT). The active layer is seasonally thawed and its thickness is important for example in foundation design. Figure 5.9 shows that the thermistors at 1.0 meter and deeper, do not experience plus degrees, hence no thawing, during the time period studied. A more accurate estimate of the active layer can be obtained from the reconstructed thermal regime or trumpet curves. In figure 5.10 and 5.11 ALTs are marked with a green dotted lines. The active layer was 0.98 meter in 2016 and 0.92 meter in 2017.

The mean annual surface temperature (MAST) calculated based on the last day of the months differ from the T_m calculated based on daily values in the beginning of the section. In 2016, the thermistor sensor at 0.0 m gives a MAST of - 0.77°C, while the MAST in 2017 is - 2.25°C.

5.4.1 Discussion and Conclusion

After processing and plotting temperature data from a single borehole in Adventdalen, it is clear that the temperature distribution in the ground fluctuates during the year. The upper 3-4 meters reflects the changes in air temperature with a greater phase lag in deeper layers. The depth of zero annual amplitude (ZAA) in lower Adventdalen, Svalbard is located at a depth of approximately 10 meters. The active layer is roughly 1.0 meter thick. Finally, literature has revealed that large variations in permafrost distribution, thickness and temperature are to be expected with present-day climate (Kurylyk and Watanabe, 2013). This is also true for Svalbard. Hence, for any building activity, soil information from one single borehole is not sufficient. More investigation of the specific building site needs to be

undertaken to provide the necessary design parameters for safe construction activity.

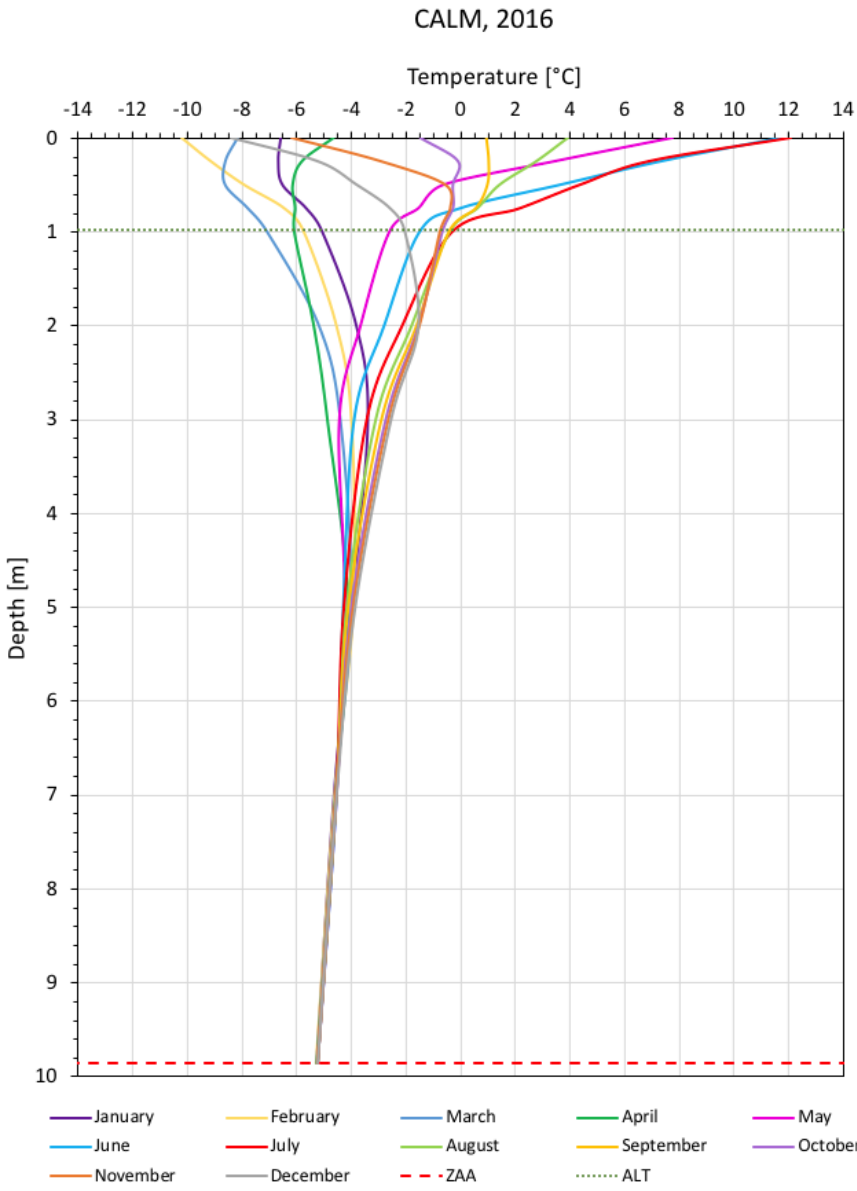

Figure 5.10: Ground temperature envelope of the CALM borehole in Adventdalen, Svalbard. Created from values from the last day of the months in 2016.

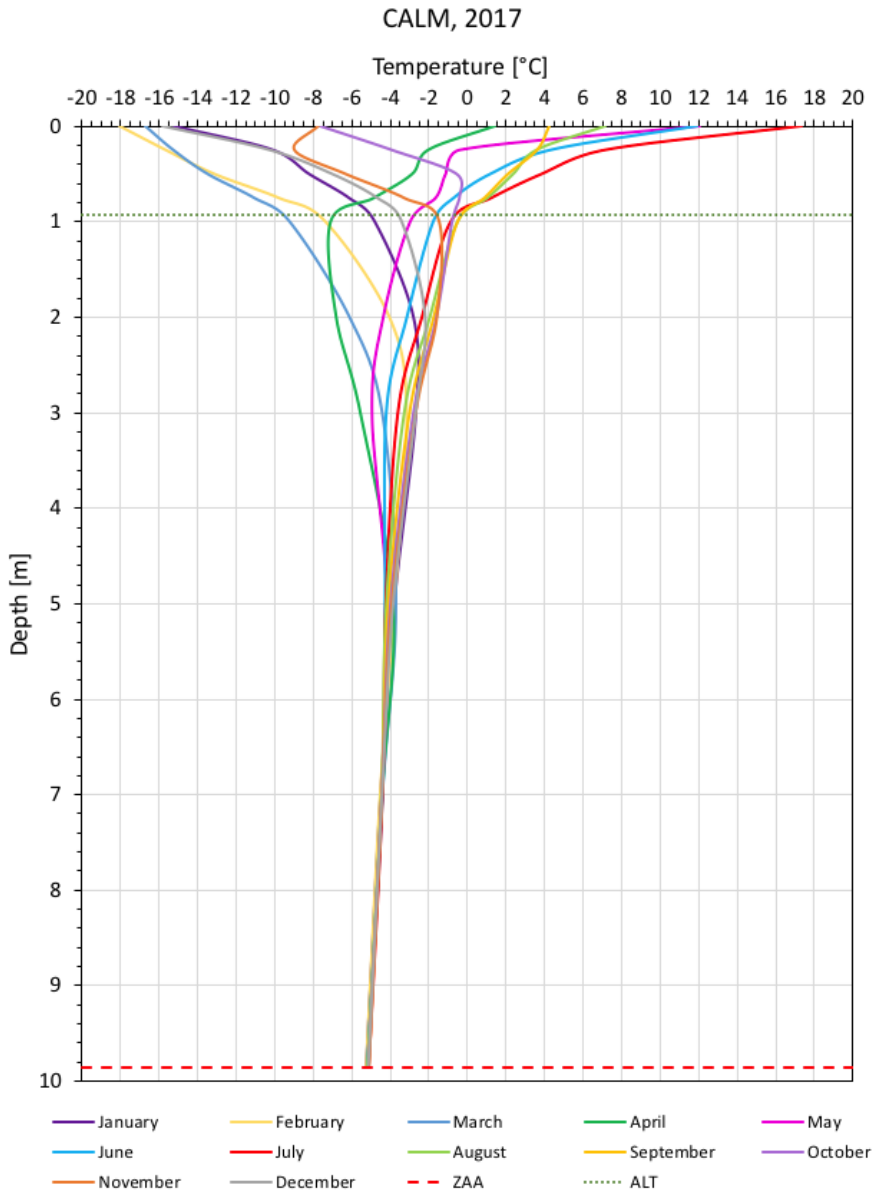

Figure 5.11: Ground temperature envelope of the CALM borehole in Adventdalen, Svalbard. Created from values from the last day of the months in 2017.

5.5 Back-Calculation of Thermal Properties from Temperature Data

Fourier's equation can be used to back-calculate thermal properties from temperature data, and the equations are presented in section 3.3. Due to the flat topography of Adventdalen, the heat flow can be treated in one dimension (Isaksen et al., 2000).

Table 5.3 shows a matrix with the calculated values for the thermal diffusivity in the uppermost 9.85 m of Adventdalen based on 1 year of data (01.05.16 - 30.04.17) from the CALM thermistor string installation. The upper right triangle shows calculations of thermal diffusivity based on the attenuation of the amplitude, D_a. The lower left triangle shows calculations of thermal diffusivity based on the phase lag D_p. It is seen from the table that the results from D_p generally are higher than those for D_a. According to Camuffo and Bernardi (1982), the difference between the two values is attributable to the fact that due to the presence of higher harmonics in the diurnal thermal wave the time lag method tends to overestimate.

Table 5.3: Calculated values for the thermal diffusivity in the uppermost 10 m of Adventdalen. In general, z is depth; A is T_{max} - T_{min} (double amplitude); t_{max} is the day when T_{max} occurred.

z	A	t_{max}	0.00	0.25	0.50	0.75	1.00	2.00	3.00	5.00	7.00	9.85
m	°C	dd.mm.yy										
0.00	29.0	05.07.16		0.35	0.24	0.25	0.23	0.24	0.36	0.35	0.50	0.64
0.25	25.4	16.07.16	0.17		0.17	0.21	0.20	0.23	0.36	0.35	0.51	0.65
0.50	21.0	30.07.16	0.13	0.11		0.26	0.22	0.24	0.40	0.36	0.54	0.69
0.75	18.0	17.08.16	0.10	0.08	0.07		0.19	0.24	0.42	0.37	0.56	0.71
1.00	15.0	01.09.16	0.10	0.09	0.08	0.09		0.25	0.47	0.39	0.60	0.75
2.00	8.0	15.11.16	0.20	0.20	0.23	0.35	0.59		1.20	0.47	0.75	0.91
3.00	6.0	25.09.16	0.29	0.31	0.36	0.49	0.70	0.84		0.33	0.68	0.88
5.00	2.0	07.11.16	0.54	0.59	0.68	0.91	1.20	1.64	2.55		2.14	1.61
7.00	1.3	30.11.16	0.75	0.82	0.94	1.19	1.50	1.93	2.55	2.55		1.35
9.85	0.6											

In D_a there are two distinct layers which appear in plotting ln(A_z) against depth, z (Figure 5.12). The first layer, 0.0 - 2.0 m is the range of the extended active layer. High frequency temperature signals are predominant in this layer as shown in figure 5.9 (Isaksen et al., 2000). The diffusivity is 0.2 - 0.4 mm^2/s . The second layer, 2.0 - 9.85m, the values fall in the range of 0.4 - 2.00 mm^2/s.

Using the phase lag, D_p, the upper layer (0.0 - 2.0 m) has a wider range of thermal diffusivity than the D_a (0.1 - 0.6 mm^2/s). In the lower layer (2.0 - 9.85 m) the values for thermal diffusivity are 0.3 - 2.6 mm^2/s.

Looking at figure 5.12, the mean thermal diffusivity, D, is determined from the slope a of a linear fit to the natural logarithm of the maximum amplitude A_Z plotted versus depth, assuming that the period is one year (Mühll and Haeberli, 1990):

$$D = \frac{\pi a^2}{p} \tag{5.1}$$

which give a mean thermal diffusivity of 0.57 mm^2/s. Based on this value, the phase speed of the annual wave (v_a = $(2D\omega)^{1/2}$) is determined to be 4.77 $\cdot$ 10^{-7} m^2/s, equal to 4.1 $\cdot$ 10^{-2} m^2/day.

In subsection 5.2.2, the thermal diffusivity was measured in the range between 0.296 mm^2/s and 0.575 mm^2/s using the KD2 Pro Thermal Properties Analyzer. The back-calculation from the temperature data gives an average value, 0.57 mm^2/s, which correlates with these measurements.

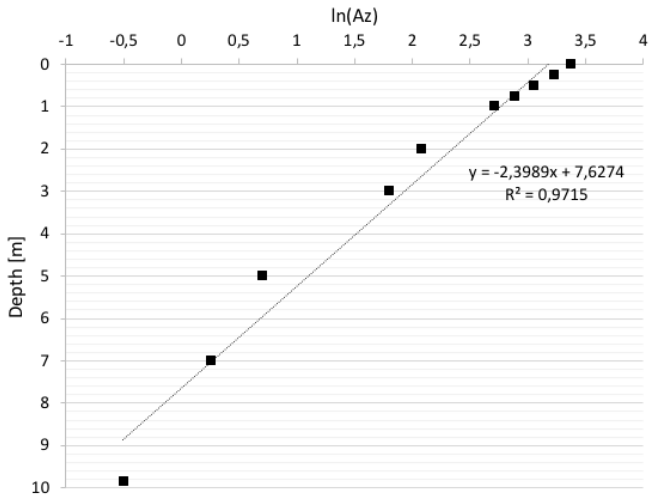

Figure 5.12: Maximum amplitude (A_z) of annual fluctuations versus depth. The mean annual diffusivity is calculated from the slope of the dotted trend line.

In subsection 2.5.4, the relation between thermal diffusivity and thermal conductivity was expressed as:

$$D = \frac{k}{\rho \cdot c} \tag{5.2}$$

where ρc = C_v (volumetric heat capacity). From the direct measurements with the KD2 Pro Thermal Properties Analyzer, the average volumetric heat capacity was 2.78 MJ/m^{3}K. Hence, from temperature data, the thermal conductivity can be calculated as 1.58 W/mK. The average thermal conductivity for unfrozen ground was measured to 1.56 W/mK with the KD2 Pro, so the two methods are in agreement.

5.5.1 Discussion and conclusion

In the present study, the amplitude and phase lag methods have been used to find the soil thermal diffusivity in the field. However, because these methods suffer from limitations due to the assumption of homogeneous soil properties, the interpretation of the thermistor string data had some challenges.

In particular, there were two main problems with the back-calculation. Firstly, it was found that the double amplitude, A, had large impact on the diffusivity, and it was difficult to identify the timing of maximum and minimum values and to get reasonable results. Hence, for the thermistors sensors closes to the surface the most outstanding peaks and valleys were ignored. Small adjustments were done to the deeper amplitudes as well, due to damping of the temperature. Secondly, in a homogeneous soil, the lag in maximum or minimum temperature should increase and decrease almost linearly. From the field data, the phase lags were difficult to detect due to extremes in the temperatures and small amplitudes with depth. Therefore, the t_{max} (the day when maximum temperature occurred) were obtained from the measured data, but to follow theory (phase lag) after best ability.

The thermal diffusivity calculated from temperature data was in agreement with the direct measurements using the KD2 Pro Thermal Properties Analyzer. However, the amplitude and phase lag methods are sensitive to choice and identification of maximum and minimum temperatures, so conclusions using the back-calculation method to determine thermal properties must be considered with great caution.

Chapter 6

Geothermal Model Proposition

A one - dimensional (1-D) geothermal model is proposed to investigate the effect of chancing air temperatures on ground thermal regime. It would be of interest to be able to predict the future ground temperatures in permafrost regions based on known thermal and physical properties of the soil, and approximated meteorological air temperature data. For the accuracy of the model, it will be compared to and validated by temperature data from a thermistor string installation in the same soil type.

The model presents a downward temperature curve based on phase changes and ground surface temperature. The modelling program used to create the model is called PLAXIS 2D and is a commercially available two-dimensional (2-D) finite element program.

The model input parameters for soil (e.g., thermal properties, unfrozen water content and index parameters) and surface boundary conditions are selected from index testing, measurements, correlations and the literature.

6.1 Background

Since the early 20th century, the mean annual air temperature (MAAT) worldwide has been rising, indicating warming of the Earth's surface. The role of surface warming on permafrost is a major concern in cold regions such as Alaska and Svalbard. Melting of permafrost causes surface destabilization and ecological changes. However, limited numbers of permafrost studies/forecasts exist (Batir et al., 2017). Consequently, it would be of interest for engineers to investigated the thermal state of the permafrost; in particular how the active layer thickness (ALT) will be affected by changing climate. The objective is to use air temperature recordings and thermal conductivity data to simulate present ground temperature profiles, but also try to forward model future active layer thickness caused by increasing air temperatures.

6.2 Heat Flow in Soils

According to the heat transfer principle, energy is transported from the high-temperature region to the low-temperature region when a temperature gradient exists in a body. Heat transfer in soils are due to conduction, vapour diffusion, radiation and convection. For engineering considerations, at macro-scale, conduction is the pre-dominating mechanism of heat flow. Conduction is caused by transfer of kinetic energy by internal molecule motion (Andersland and Ladanyi, 1994).

The temperature in the ground is an important factor in the design of frozen ground constructions. The soil behavior and characteristics changes as a result of altered temperatures. The temperature in the ground is determined by air temperatures (and surface temperature), the heat flux from the interior of the earth and soil thermal properties. Additionally, remarkable changes in the thermal regime are observed due to construction activities.

The mean annual surface temperatures differs from the mean annual air temperature, due to surface factors such as snow cover, vegetation and drainage. Surface boundary conditions for a thermal prediction model are therefore often separated into air temperature and empirical n-factors. The n-factor is the ratio of seasonal degree-day sums at the soil-surface to those in the air, and can be found from tabulated values (Andersland and Ladanyi, 1994). However, it should be stressed out that site specific n-values should be used due to large spatial and temporal variations in land-cover and temperature.

In conductive heat flow, thermal conductivity and specific heat are the primary parameters affecting the transfer of heat energy through a material. They depend on physical characteristics of the soil, including type of soil, density, water content, degree of saturation and porosity.

6.3 PLAXIS 2D; Thermal Model Setup

The model is generated using the plain strain model and linear elastic material model. Flow only is chosen as the calculation type, and thermally there is a transient heat flow. The modelling focuses on the thermal regime of the soil and does not account for any thaw settlement or frost heave. It consists of 25 phases; the initial phase, and 24 phases representing the months from January 2016 to December 2017. The lengths of the phases are according to days in the months. 2016 was a leap year, thus, 29 days in February.

The soil polygon is 1 meter wide and 12 meters high. The configuration of the soil polygon is interpreted from the laboratory work, and consists of 12 layers with thickness of 1 meter. An illustration of the model is presented in figure 6.1.

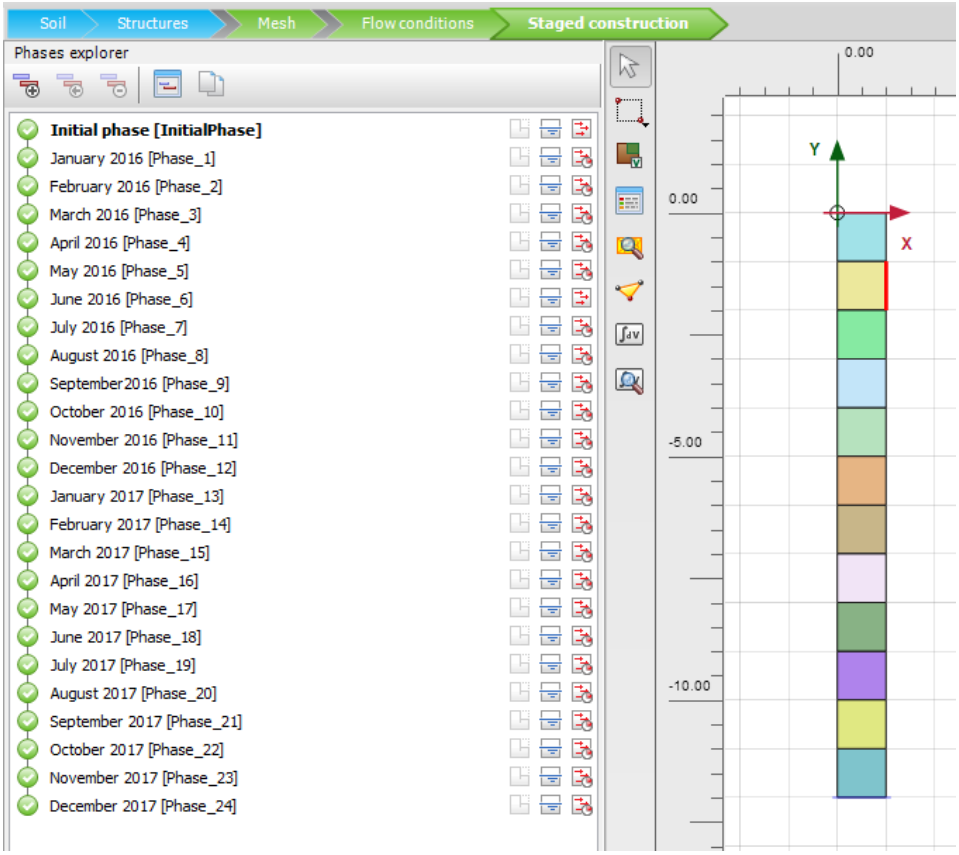

Figure 6.1: Screen shot of the geometry and phases in PLAXIS.

The material within each layer is assumed to be drained, isotropic and homogeneous. The physical material properties and grain size distribution are obtained from index testing, while the thermal properties come from KD2 Pro measurements of the unfrozen samples. Figure 6.2 shows the options for thermal material factor settings. (Note: The PLAXIS software uses λ for thermal conductivity).

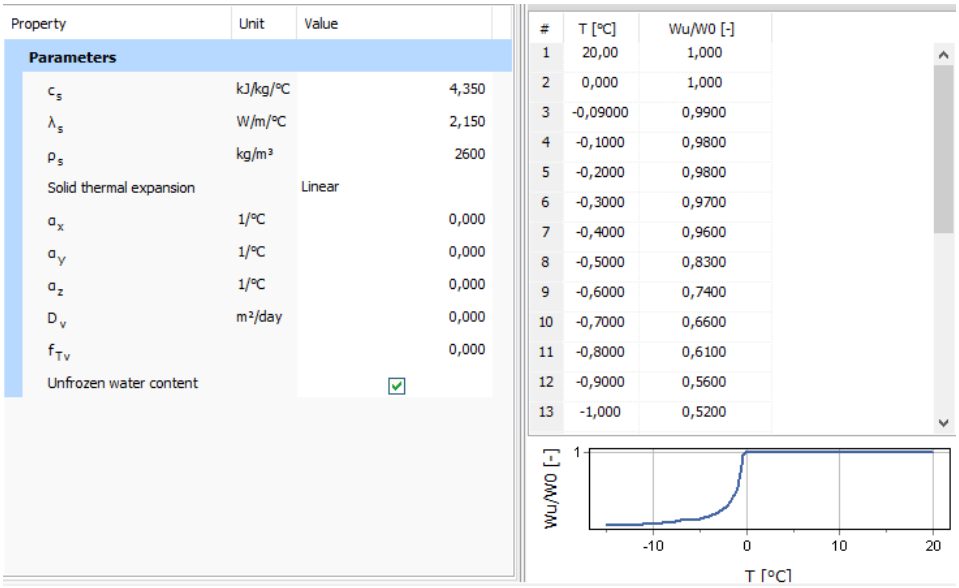

Figure 6.2: Screen shot of thermal material settings in PLAXIS.

The water properties are set to be temperature dependent and the temperature units are set to °C. The groundwater table is assumed to be at 12 meter depth, and the groundwater model is Van Genuchten. Flow parameters are set to default values. Flow boundary conditions are closed with head at the bottom.

For the purpose of this model, the mechanical properties are not significant, and are given default or random values. All deformations are set to free, with exception of the lower horizontal line that is fully fixed.

Thermally, the vertical boundary lines are closed for heat flow. The nodes along the bottom of the polygon were given a constant boundary condition of -5°C, obtained from measurements. Initially, the upper horizontal boundary is also given a constant temperature of -5°C, which is the reference temperature for January. For the rest of the phases the upper boundary conditions are temperature dependent using a unique table for each month. The tables are given as ΔT calculated from the temperature in the end of the previous phase. This temperature is also set as reference temperature in the month of the associated table. In other words, the temperature on the 31st of January is used as the reference temperature in February and upper boundary condition in February is a table of ΔT calculated from this reference temperature. The temperatures applied to the surface are obtained from air temperatures.

6.4 Choice of Parameters

6.4.1 Surface Boundary Condition

The input parameters in the model are selected from educated guesses and laboratory work. A critical input parameter in the PLAXIS model is the surface temperature (ST). To be able to estimate the future thickness of the active layer based on a meteorological prediction, a correlation between air and surface temperature must be developed.

In the literature, a common procedure to obtain the ST is to multiplied the measured air temperature (AT) by an empirical n-factor to accounts for surface boundary conditions of snow, vegetation, minerals ect. As mentioned previously, the literature suggests a large range of n-factors. After numerous trials playing with tabulated values accounting for surface factors and research for appropriate equations, none of these approaches was found to be appropriate for the temperature measurements Adventdalen. Thus, a simplified procedure for temperature correlations in Adventdalen is to adjust the air temperature to the measurements from the upper thermistor sensor at 0.0m depth, to best ability, for a time period were both parameters are known.

In figure 6.3, the orange curve illustrates the daily average air temperature from the Adventdalen Weather Station. The yellow curve is the daily average temperature recorded in the thermistor sensor installed at 0.0 meter depth. The duration of the measuring period lasts from 1st of January 2016 to 31st of December 2017 accordingly 24 months. The mean annual air temperature (MAAT) for this period was - 2.23 °C indicated by the red dotted line. The mean ground temperature (measured at 0.0m) for the period was -1.99 °C based on daily values. Based on last day of the month, this value is -1.51°C.

Surface temperatures exhibit periodic variation with the seasons and follow the pattern of the air temperature curve. Moreover, figure 6.3 shows two warmer periods with temperatures above 0°C, from approximately 1st of May until middle of November both in 2016 and 2017. During these months the surface temperature measured by the thermistor sensor at 0.0m is higher than the air temperature. The surface offset, or difference between air and surface temperature, arises from boundary conditions. Generally, snow works as an insulator in the winter, while vegetation cools the ground surface by shading it from solar radiation in the summer. ”However, since summer in permafrost environments is relatively short and vegetation is relatively limited, the insulating effect of snow dominates and ST is usually higher than AT” (Strand, 2016). This statement fits well with the recorded temperatures in Adventdalen for most of the year.

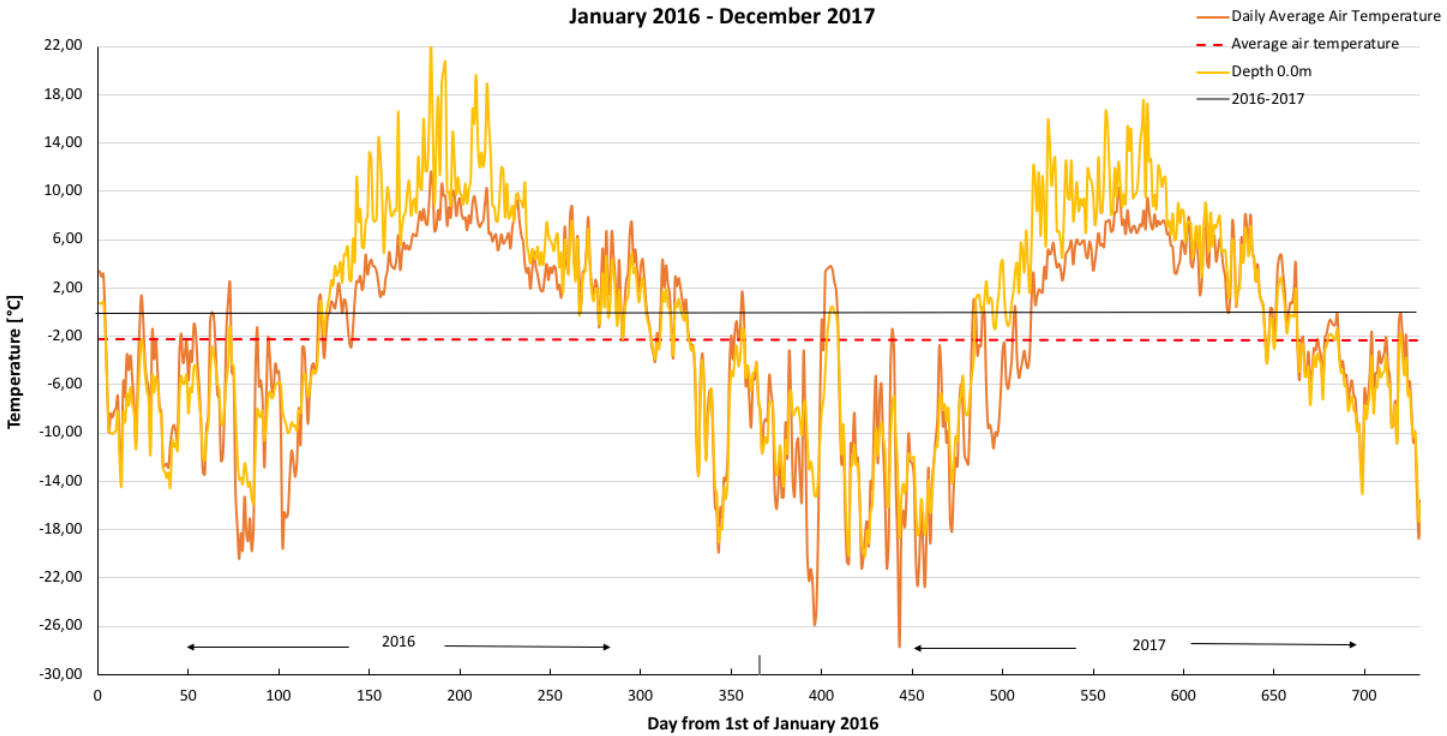

Figure 6.3: Illustration of the air temperature and temperature measured in the ground at 0.00 meter.

As explained previously, the surface temperature is a critical parameter in a permafrost model. Figure 6.4 represents a 20-day moving average of the AT and thermistor data at 0.0 meter. The moving average function smooths out the peaks and valleys and makes the data more interoperable. The yellow curve is temperatures from thermistor, while AT is the orange curve.

For the purpose of the surface boundary condition in the PLAXIS model, it is assumed that thermistor string data from 2016-2017 from 0.0 meter is a appropriate measurement of the ST, due to the good agreement in the winter months. Moreover, since the thermistor recordings are higher than the AT in the summer months, an adjustment factor of 4 is added to the AT from 1st of May to 13th of September to obtain a reasonably good fit between the two curves. The relationship for the summer months is represented by equation 6.1.

$$ST = AT + 4 \tag{6.1}$$

The red and blue arrows in figure 6.4 show were equation 6.1 is applied. The new ST is illustrated by the blue dotted line.

Finally, by the use of equation 6.1 on air temperatures from 1st of May to 13th of September in 2016 and 2017 it is possible to determine the ST at the site reasonably well. This statement is supported by comparing the average surface temperature of the 0.0 m moving average (yellow) and the ST moving average (blue) which are -1.81°C and -1.68°C, respectively. The surface temperature is assumed to have an acceptable accuracy and is suitable to be used in a simple 1-D PLAXIS model.

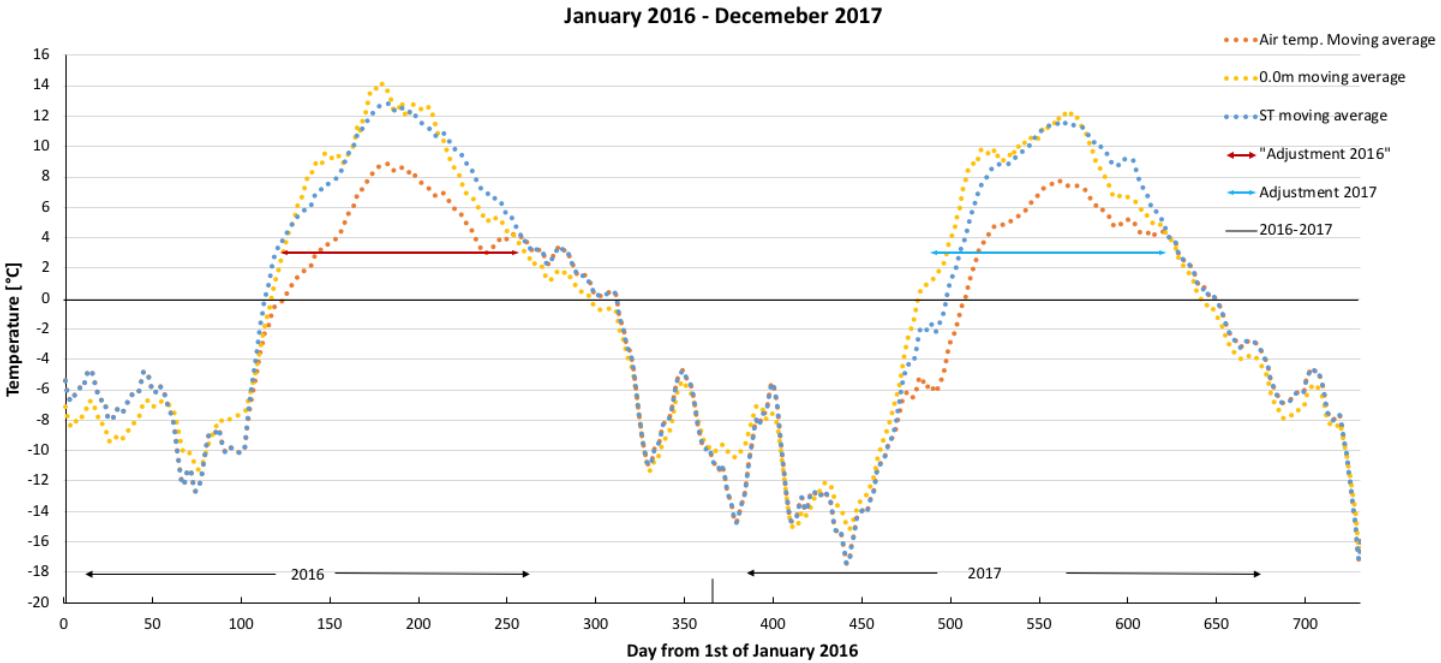

Figure 6.4: Moving average curves for air temperature, thermistor surface temperature and adjusted surface temperature for the PLAXIS model.

6.4.2 Soil Parameters

Thermal Properties

Thermal parameters are retrieved from measurements with the KD2 Pro. Table 6.1 presents values of unfrozen thermal conductivity and volumetric heat capacity for each layer. The values for layer 2 and 3 are interpreted values, due to lack of measurements. Because the high water content and porosity in these layers, the thermal conductivity is assumed to approach a k-value closer to that of water, k_w = 0.6065.

Table 6.1: Thermal properties from KD2 Pro measurements

Layer	Thermal conductivity [W/mK]	Volumetric heat capacity [MJ/m^{3}K]
1	1.39	3.28
2	0.80	3.02
3	1.00	2.88
4	1.38	2.75
5	1.41	2.53
6	1.43	2.18
7	1.51	2.58
8	1.53	2.76
9	1.55	2.99
10	1.53	2.73
11	1.54	2.69
12	1.55	2.66

Since the equations implemented in the PLAXIS software separate the soil into its compounds, water/ice, air and soil particles, the measured parameters for thermal conductivity and volumetric heat capacity for the complex soil are converted to values for soil minerals only; c_s, k_s. See APPENDIX B for calculations and specific values for each layer.

Unfrozen Water Content

Temperature dependent unfrozen water content from the equations by Nybo (2017), is applied to each layer. The unfrozen water content is presented as a ratio of the natural water content, w_0 and approaches 1 at 0°C. Figure 6.5 shows the estimated unfrozen water content curves. The equation by Nybo (2017) gives unreasonable values for the soil samples from borehole S1_A4_1 near 0°. The values for this range are not included in the graph. In PLAXIS, a linear approximation is used. Details for calculations of the unfrozen water content are explained in sections 4.6.

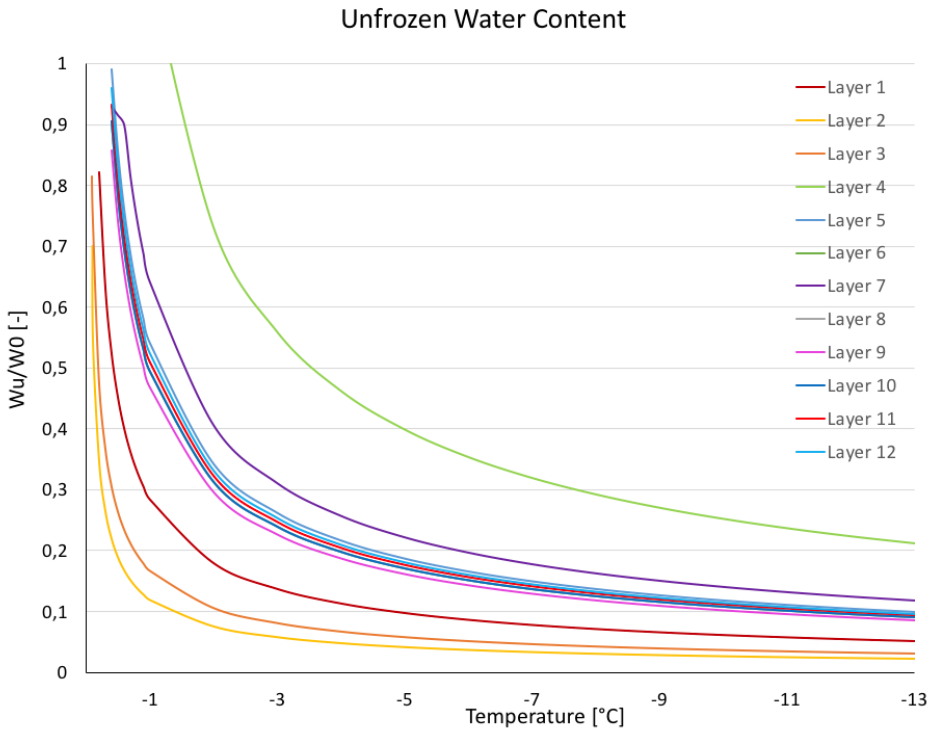

Figure 6.5: Development of unfrozen water content with temperature for layer 1 - 12.

Physical Properties

The values for the physical properties of the soil are obtained from index testing and grain size distribution. Table 6.2 gives a summary of the density of solids and soil type.

Table 6.2: Physical input parameters in PLAXIS

Layer	Density of solids (kg/m^3)	Soil type (USDA)
1	2660	Silt loam
2	2560	Silt loam
3	2700	Sandy loam
4	2680	Sandy loam
5	2640	Loam
6	2670	Silt
7	2690	Silt loam
8	2690	Loam
9	2560	Sandy loam
10	2700	Sandy loam
11	2660	Sandy loam / Loam
12	2710	Silt loam

The manual grain size distribution settings in PLAXIS follows the U.S. Department of Agriculture (USDA) soil classification system given by figure 6.6. This system is based on particle size distribution only, and commonly used because of its simplicity.

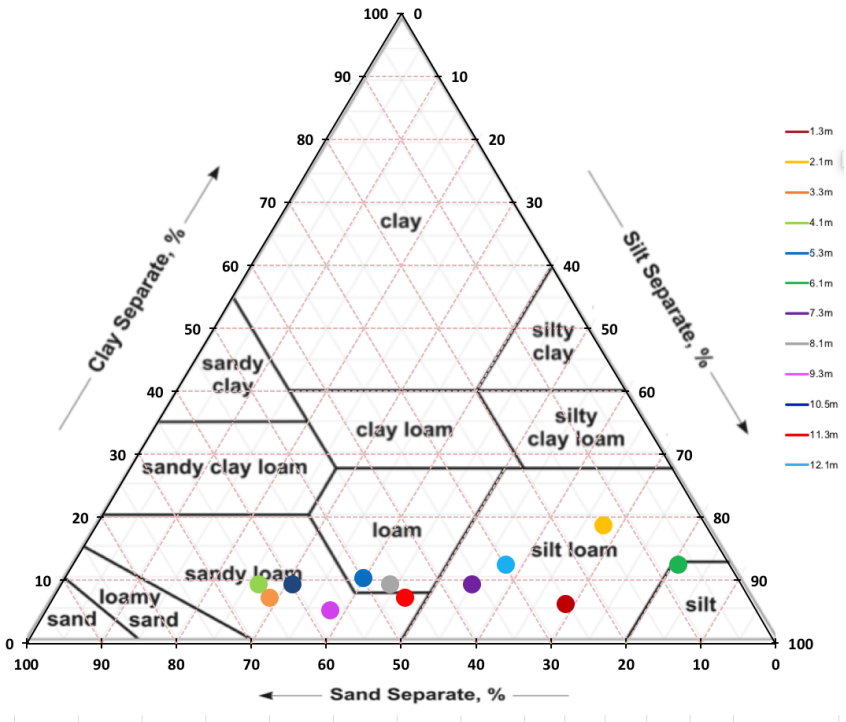

Figure 6.6: USDA soil textural triangle

6.5 Projected Climate Change Data

As displayed in figure 6.7, the mean annual air temperature on Svalbard is already changing, and the trend is expected to continue over time (Nordli, 2010).

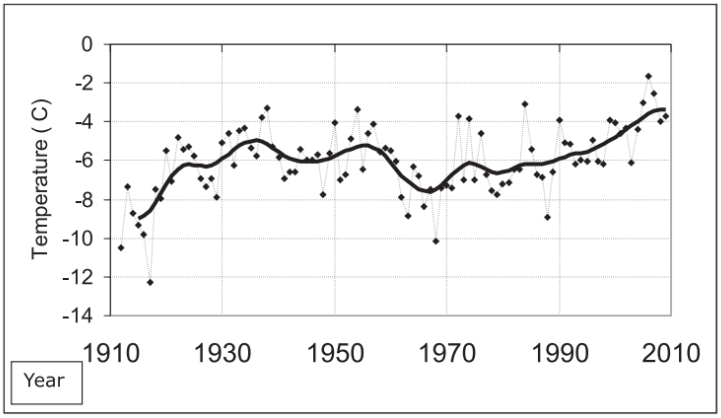

Figure 6.7: The homogenised Svalbard Airport series during the period September 1911 to December 2010 for annual values (From Nordli (2010)).

Figure 6.9 and figure 6.8 present the projected change in annual air temperature for the period 2000 - 2090 for Longyearbyen, Svalbard. The figures illustrate two alternative scenarios for future air temperatures; RCP2.6 and RCP8.5. The RCP2.6 is denoted the ”best - case” scenario, while RCP8.5 is the ”worst - case” scenario.

The temperature data is retrieved from National Center for Atmospheric Research (NCAR) using the GIS Climate Change Scenarios option (NCAR, 2012). According to NCAR, the climate change scenarios are redesigned for the Intergovernmental Panel on Climate Change (IPCC) Fifth Assessment Report. The emission trajectories are Representative Concentration Pathways (RCPs) and are labelled based on how much heating they would produce at the end of the century in watts per square meter (W/m^2). According to Inman (2011), the RCPs are representative of plausible alternative scenarios of the future, but are not predictions or forecasts (Inman, 2011).

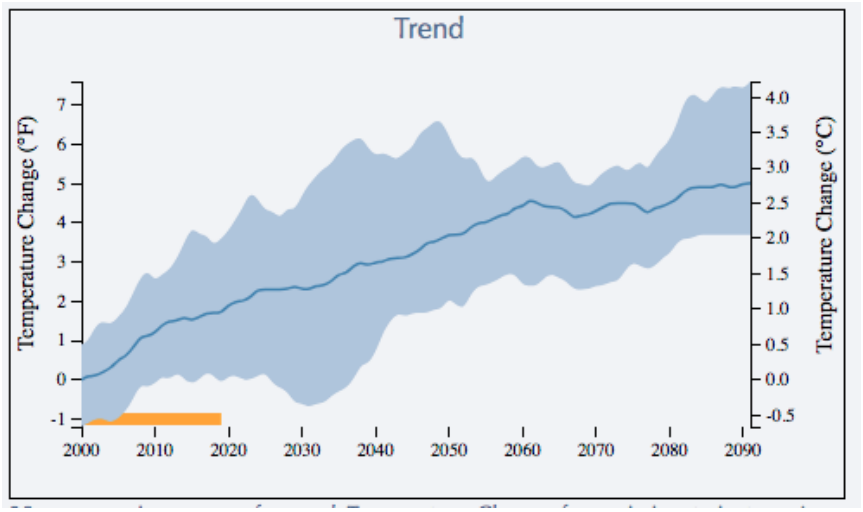

Figure 6.8: 20-year running mean of annual Temperature Change for ”best - case” emission trajectory: Low (RCP 2.6) ensemble average (dark line) and spread of ensemble members (shaded area). Values are for Longyearbyen: 78.219°N 15.64°E (Data from NCAR (2012)).

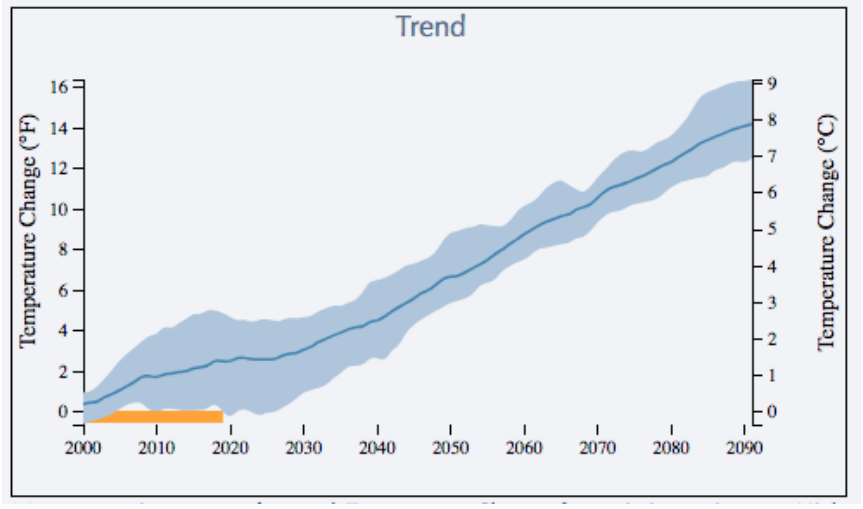

Figure 6.9: 20-year running mean of annual Temperature Change for ”worst - case” emission trajectory: High (RCP 8.5) ensemble average (dark line) and spread of ensemble members (shaded area). Values are for Longyearbyen: 78.219°N 15.64°E (Data from NCAR (2012)).

From the two climate scenarios, it is clear that, even in the best-case scenario (RCP2.6), the annual air temperature in Longyearbyen, Svalbard is increasing. Moreover, the worst - case scenario (RCP8.5), will lead to an annual air temperature increase of about 8°C in 2090, starting in year 2000.

To investigate the thickness of the active layer in the future, the surface temperatures (ST) for year 2090 are implemented in the PLAXIS model. To find these temperatures, the adjusted surface temperatures for 2016 are used as a basis. (See section 6.4.1 for details). For simplicity the NCAR-data is used directly and the increase in air temperatures from figure 6.9 and 6.8 are assumed to apply to the surface temperatures to the same extent. However, these assumptions deviates from other modelling procedures, and limit the reliability of the PLAXIS model results.

In the PLAXIS model, the year 2016 is used as the known and initial year. Since measured ground temperature data is available also for 2017, the start date of the increase is set to 1st January 2018. The total increase in temperatures, ΔT, for each scenario are 1.9°C and 6.7°C, for RCP2.6 and RCP8.5, respectively. The increase for RCP2.6 is assumed to be linear with a slope of 1.5 between 2018 and 2060. From 2060 to 2090, the slope is only 0.4. The RCP8.5 increases linearly with 6.7 for the whole period. A summary of the changes in temperature is tabulated in table 6.3.

Table 6.3: Projected increase in temperatures (From NCAR (2012)).

Model	ΔT
RCP2.6	1.9°C
RCP8.5	6.7°C

Figure 6.10 gives a graphical presentation of the increase in surface temperature for a period of 366 days. The blue line is the initial surface temperature in 2016. The green curve is the ”best - case” scenario and the red curve is the ”worst - case” scenario. For the latter, sub - zero temperatures are only occurring from March until middle of April, and from middle of November and some days into December, with exception of a few negative days the transition from January to March. For the the 2016 and RCP2.6, the whole month of January, February, March, December and most of April and November below 0°C.

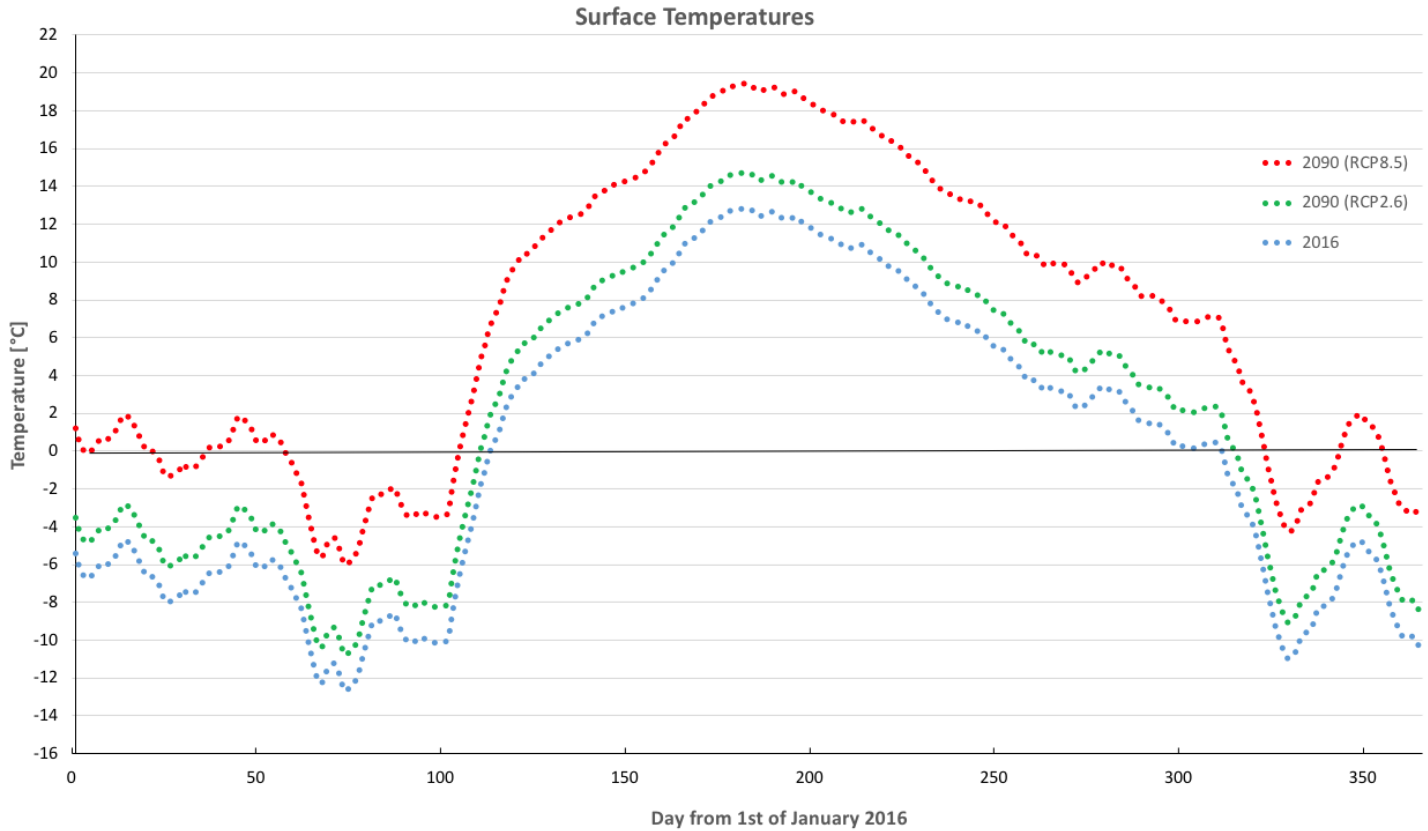

Figure 6.10: Estimated surface temperatures for the initial year 2016 and the two climate scenarios in 2090.

6.6 Results

The PLAXIS model is run on soils representing permafrost soil in lower Adventdalen, Svalbard. The output is presented showing heat flow and distribution of temperature through the soil polygon. See figure 6.11. The temperature varies from the applied surface temperature in the top to the constant temperature of -5°C in the bottom. The ST is unique to each phase, while the bottom boundary is the same for all phases. The temperature is evenly distributed in the soil. All the results are presented as temperature envelopes to a depth of 12 meters. Tabulated values for a cross-section of the profile in PLAXIS are inserted in into Excel and plotted. Results are compared with thermistor string measurements from the same soil.

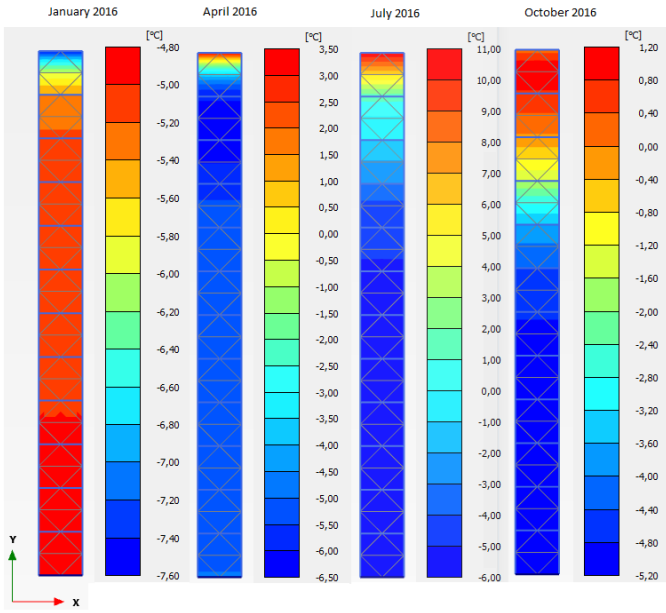

Figure 6.11: Soil polygons for four months of 2016, showing the temperature distribution with depth. The legend on the right side of the polygon shows its temperature range.

6.6.1 Present Ground Temperatures

The modelled ground temperatures for 2016 and 2017 are displayed in figure 6.12 and 6.13, respectively. The figures show the downward distribution of the ground temperature on the last day of the month for both years. To make it easier to compare and validate the results from the PLAXIS model, the months are color coded in accordance with the measured thermistor data in section 5.4.

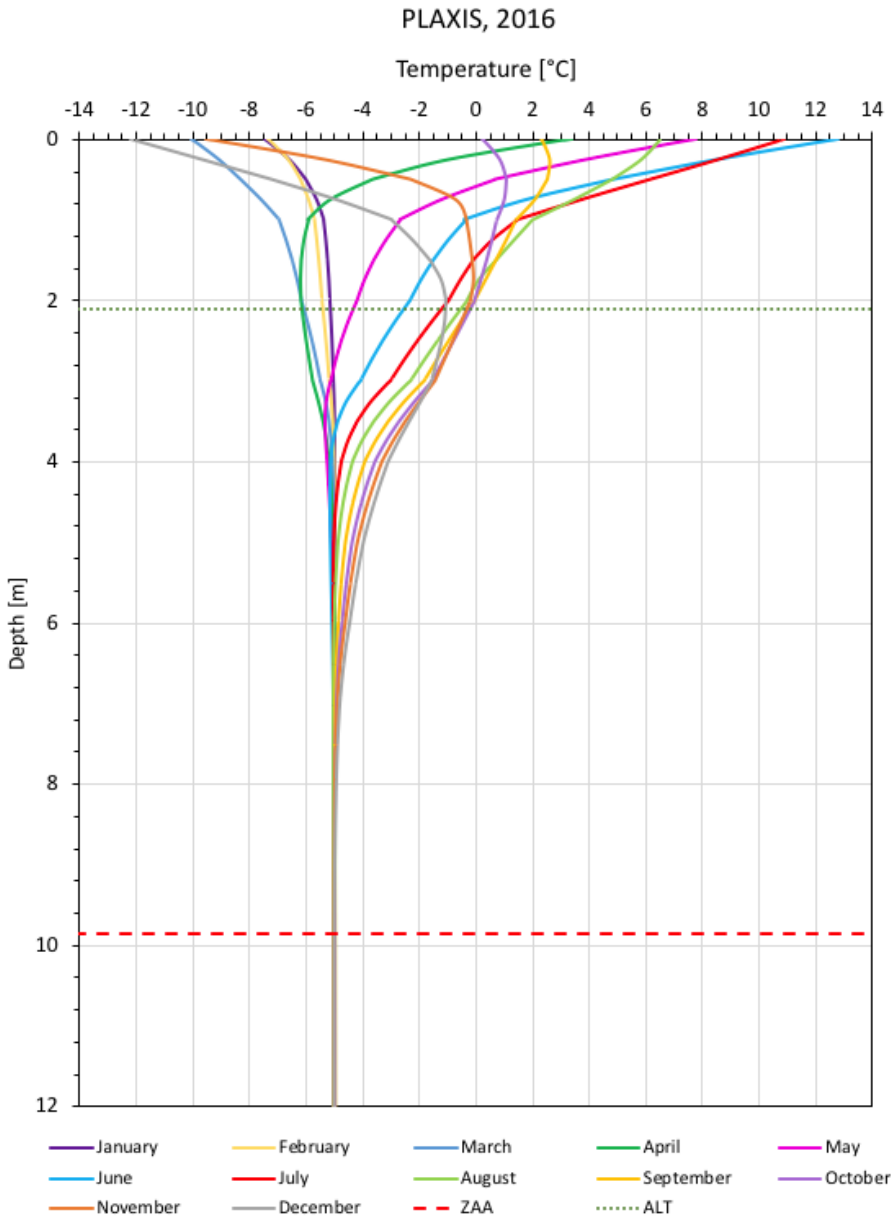

Figure 6.12: PLAXIS results. Ground temperature envelope for the last day of the month in 2016

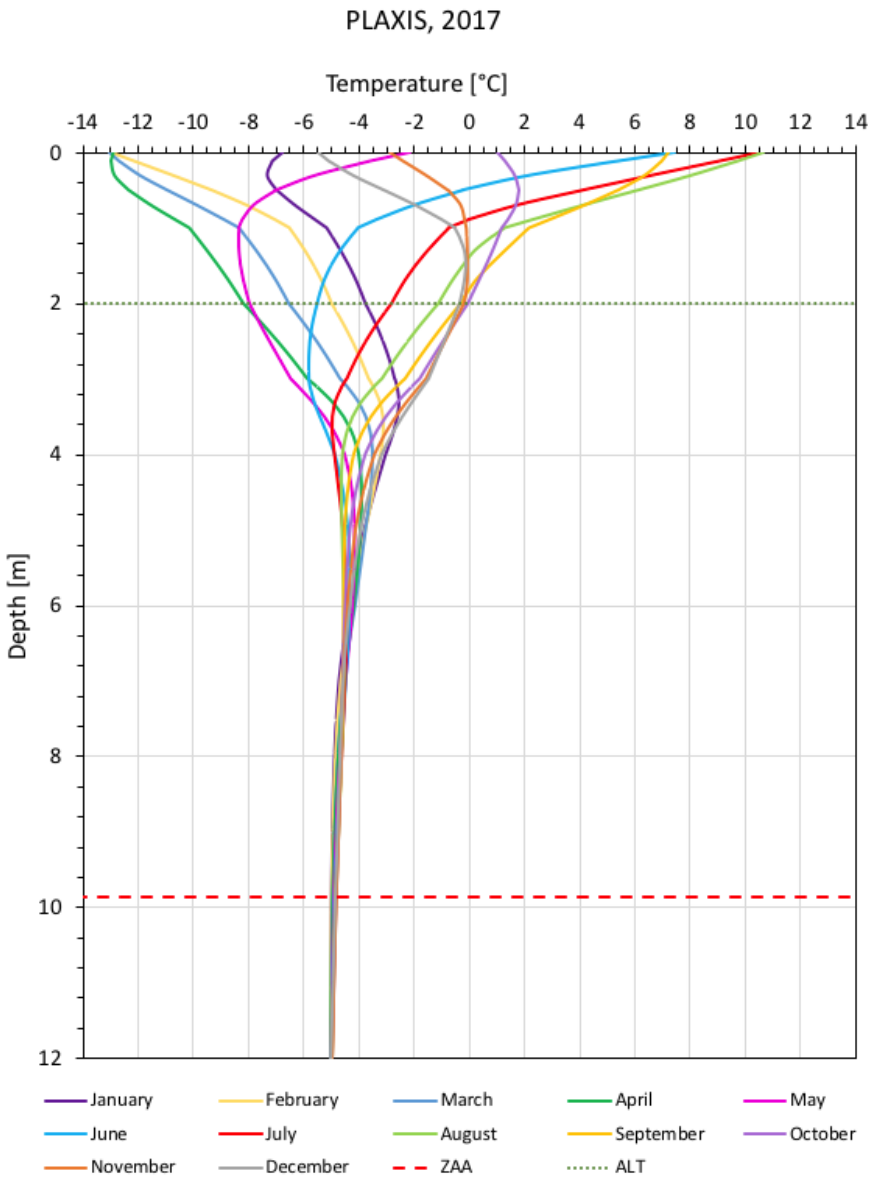

Figure 6.13: PLAXIS results. Ground temperature envelope for the last day of the month in 2017

The mean annual surface temperature (MAST) in the model are -0.23°C in 2016 and -1.61°C in 2017. The lower boundary of the active layer is indicated with a green dotted line, and is estimated to 2.1 m and 2.0 m in 2016 and 2017, respectively. The depth of zero annual amplitude is interpreted to be at 9.85 m for both years, and the mean annual ground temperature is -5°C.

6.6.2 Future Ground Temperatures

The modelled ground temperatures for 2090 are displayed in figure 6.14 and 6.15, for RCP2.6 and RCP8.5, respectively. The figures show the downward distribution of the ground temperature on the last day of the month for both scenarios. 2016 is used as the initial year, hence the results should be compared to 2016 measurements. The colors of the months are in accordance with the previous results.

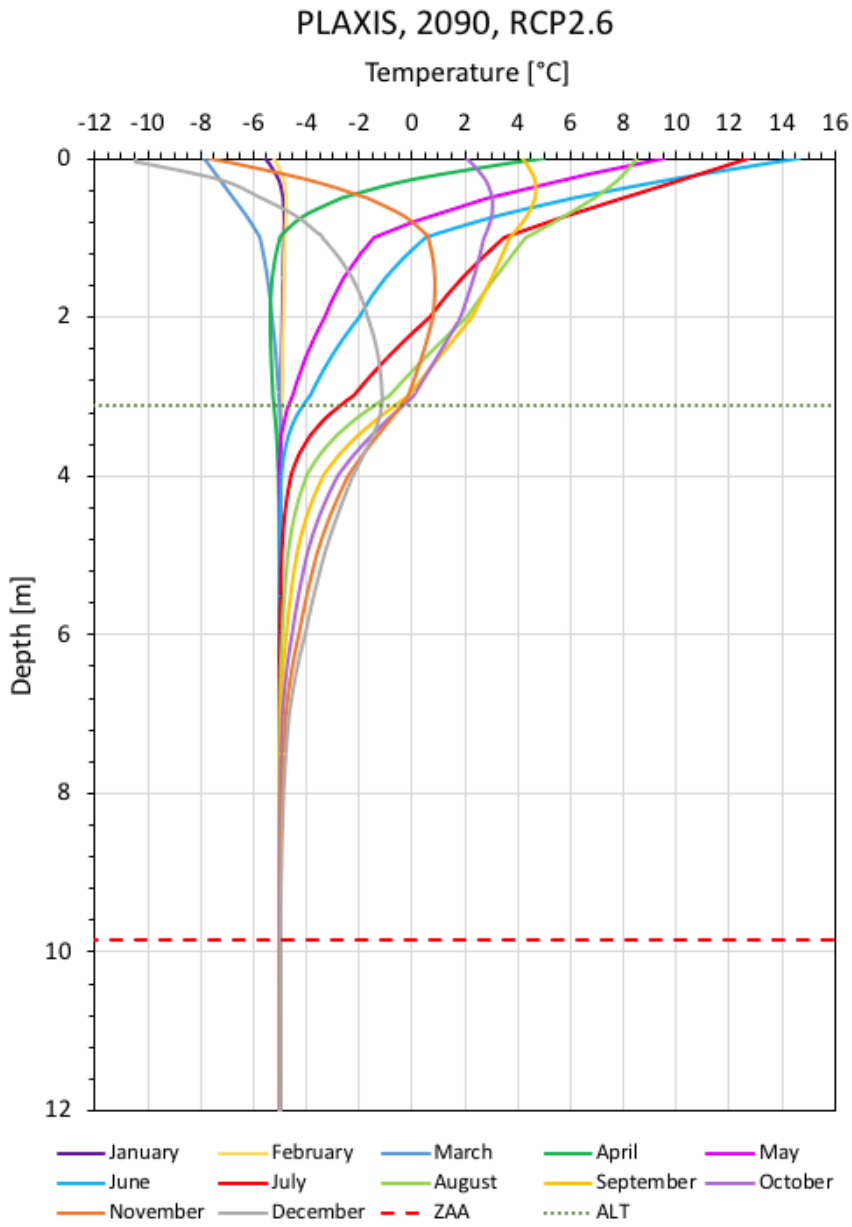

Figure 6.14: PLAXIS results. Ground temperature envelope for the last day of the month in 2090 based on the RCP2.6 scenario.

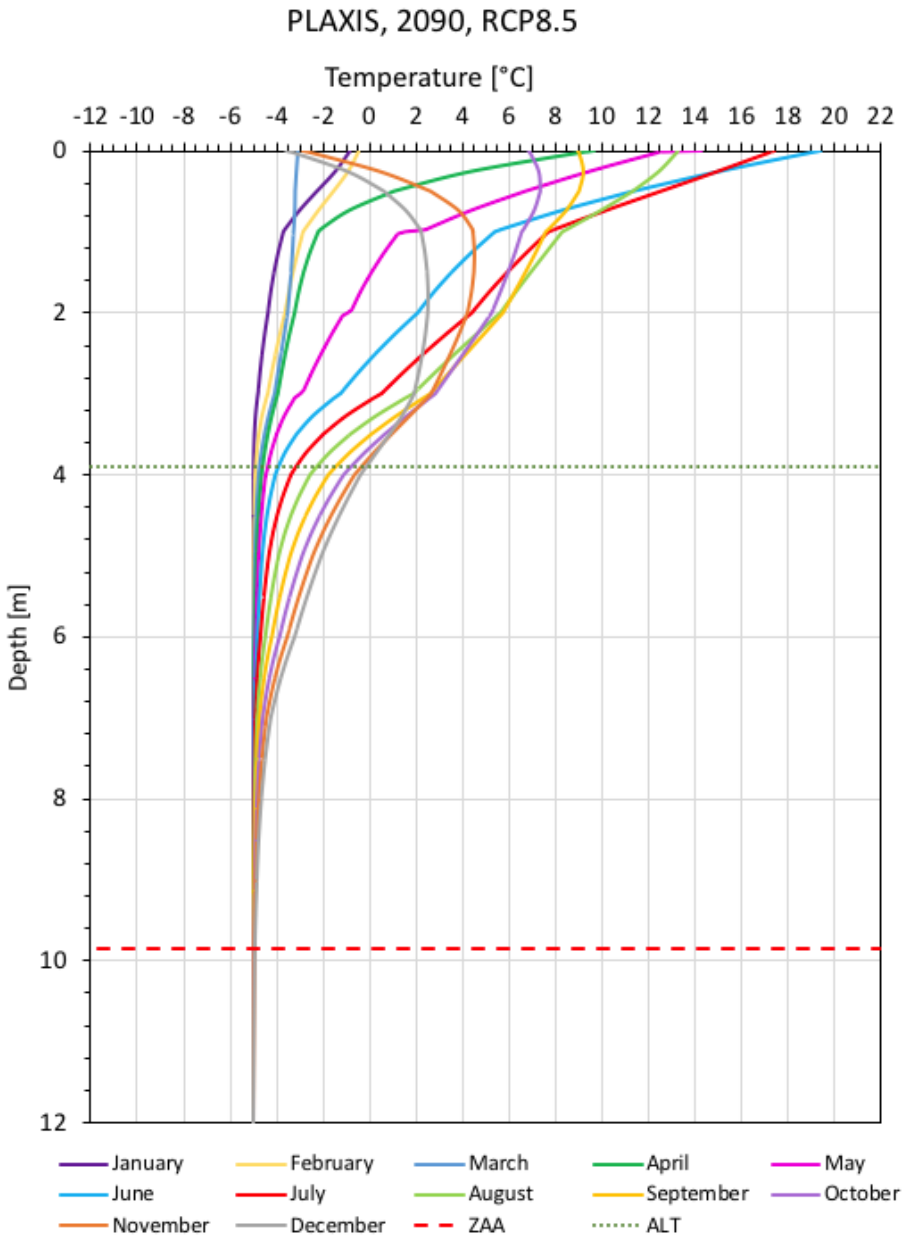

Figure 6.15: PLAXIS results. Ground temperature envelope for the last day of the month in 2090 based on the RCP8.5 scenario.

The mean annual surface temperatures (MAST) in the model are 1.65°C for RCP2.6 and

6.59°C for RCP8.5. The lower boundary of the active layer is indicated with a green dotted line, and is estimated to 3.1 m and 3.9 m for RCP2.6 and RCP8.5, respectively. The depth of zero annual amplitude is interpreted to be at 9.85 m for both years, and the mean annual ground temperature is -5°C.

6.7 Discussion and Conclusions

For both the present and future PLAXIS model, the model set-up is simplified. The soil is divided into 12 layers, with constant texture throughout each layer. In reality more variation is present, and salinity and organic content are not accounted for. The input data used in this study also brings uncertainty. All the input used in this study is produced by the author of this thesis, but no quality control is performed. In particular, uncertainly is related to the thermal properties of the soil. Moreover, the observational air temperature data for 2016 and 2017 are assumed to be of high quality. On the other hand, one can cast a serious doubt on the accuracy of the the surface boundary condition in PLAXIS for both present and future modelling. This is mainly due many assumptions and simplifications and due to lack of testing on long term temperature series.

6.7.1 Present Ground Temperatures

The most striking feature in the results from 2016 and 2017 are the differences in active layer thickness (ALT) between the measured and modelled ground temperature profiles. APPENDIX B includes a comparison of the profiles. For both years, the modelled ALT is more than double of the measured. Table 6.4 gives a summary of the active layers thicknesses. The ALT is overestimated with 1.12 m in 2016 and 1.08 m in 2017.

Moreover, it can be observed that the measured and modelled trumpet curves have a similar shape. However, the surface temperatures or start temperature for each month differ. The mean annual surface temperature, is 0.54°C warmer in 2016 model and 0.64°C warmer in the 2017 model compared to the results from the thermistor string discussed in section 5.4.

Table 6.4: Summary of measured and modelled active layer thicknesses

Year	Model	Thickness [m]
2016	Thermistor string	0.98
	PLAXIS model	2.10
2017	Thermistor string	0.92
	PLAXIS model	2.00

It could be several possible reasons for deviations between the measured and modelled temperature profiles. In figure 6.16, two surface temperatures for 2016 are presented. The blue dotted line indicates the surface temperature used in the PLAXIS model. The solid

yellow line shows the daily surface temperatures at 0.0 m measured by thermistors in Adventdalen, Svalbard. The surface temperature is thought to be a critical input parameter in permafrost models and will influence the depth of thaw. In particular, the intra-annual variations between the measured and the modelled input should be discussed. In figure 6.16, one can observe that the shape of the two curves are roughly the same. As discussed in section 6.4.1, the surface temperature implemented in the PLAXIS model is a moving average air temperature fitted to the measured surface temperature (depth 0.0 m). In figure 6.16, the blue curve is shifted a bit to the left. This shift is caused by the 20-day moving average function used in Excel and should have been adjusted for. Unfortunately, this was not discovered during modelling, and this error in the model should be correct for a closer relation between the model and reality. Because the surface temperatures do not match perfectly, the curves will give different results for the last day of the month when plotted. It could also be that the temperature peaks or valleys influence the temperature in the ground to a larger extent than assumed. Thus, it is not appropriate to use a smooth average curve. These observations indicate that the intra-annual variation could play an important role for the active layer development.

To accurately model the ALT over time, the projected surface temperature should be of a higher resolution. In this study, the estimation of the surface temperature was done manually in Excel, and was a very simple process. Additionally, a better procedure of creating trumpet curves for comparison and investigation of temperature changes would be to use monthly average values rather and temperatures from single day (e.g. last day of the month).

Secondly, the thickness of the active layer is also determined by the thermal properties of the soil. The thermal properties in the PLAXIS model are measured values of unfrozen soil samples obtained by the KD2 Pro. Uncertainty to their accuracy apply. Wrong value or combination of the thermal conductivity and heat capacity of the solid particles will change the conductive heat flow in the soil. The thick active layer in the model could be a result of overestimated thermal values, thus increased heat energy in the soil. Additionally, it would be of interst to investigate how the model deals with latent heat during active layer development and the melting of ice in the top of permafrost (transient layer).

Thirdly, the bottom boundary condition is set to -5°C, which could be an incorrect assumption. As discussed in chapter 2, the ground temperatures are affected by a geothermal gradient deep in the ground. Even though this should not influence the 12 meter deep model, the result may be somewhat twisted, and applying a geothermal gradient should be tested for further modelling.

Furthermore, frozen soil is a natural material, which is difficult to recreate with the thermal options in the PLAXIS software. Lack or not enough input data to accurately model the active layer could give results that differ from reality. Examples of parameters that are difficult to measure are the unfrozen water content and ice distribution.

The depth of zero annual amplitude (ZAA) and mean annual ground temperature (MAGT) in the model match the measurements. This is due to the bottom boundary conditions selected for the PLAXIS.

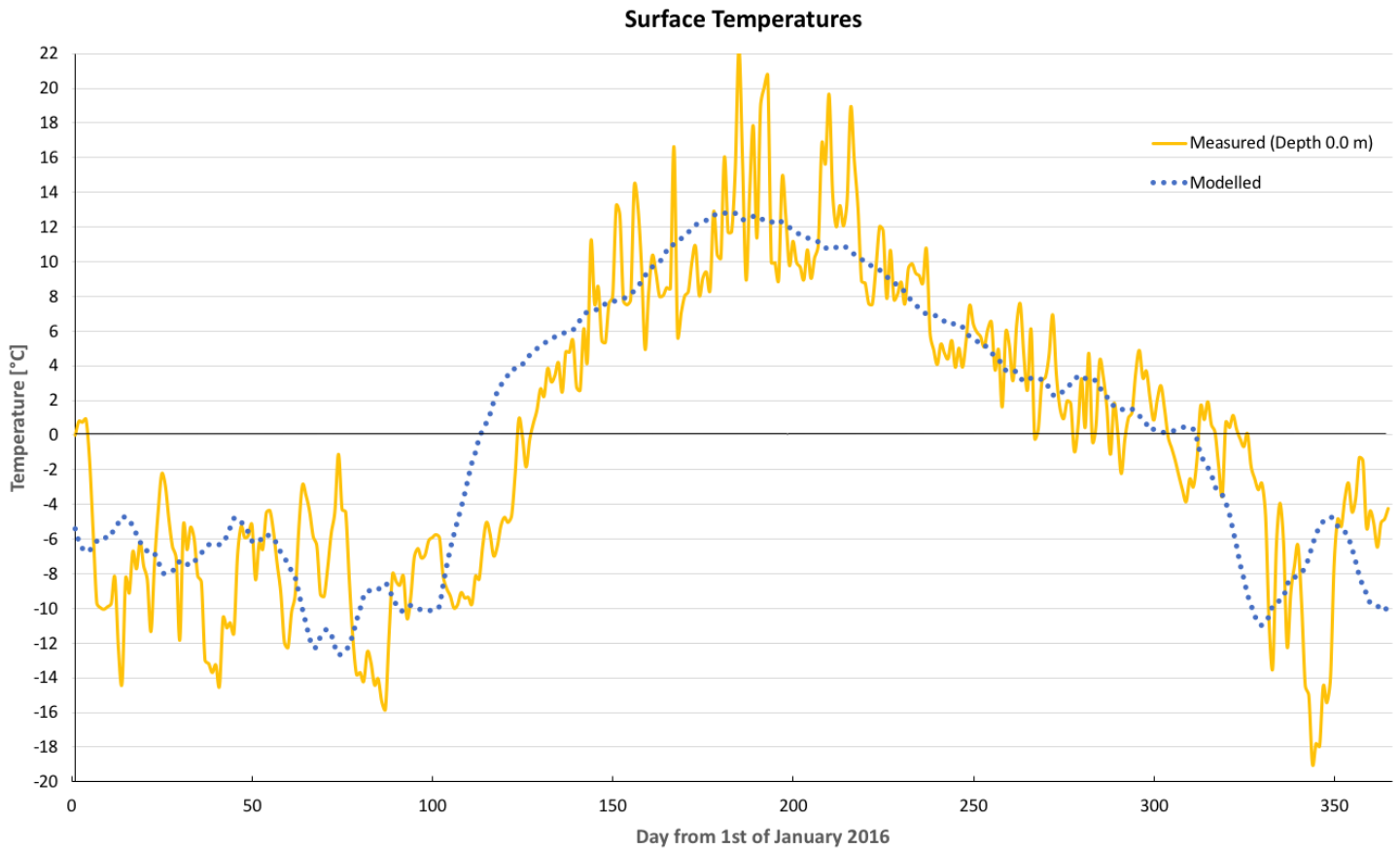

Figure 6.16: The input data in the PLAXIS model together with the observed data for 2016.

6.7.2 Future Ground Temperatures

The idea behind a simulation of the future ground temperature profile was to use the PLAXIS model to investigate changes in the thickness of the active layer as a result of climate warming. Consequently, the results from 2090 modelling are compared to modelled and measured data from ground temperatures in 2016. The result of the two possible climate scenarios in 2090 are compared in APPENDIX B.

Looking at the trumpet curves representing the ground temperature regime in 2090, the first thing that stands out is the overall increase in surface temperatures for both RCP scenarios compared to 2016. The temperature envelope is tilted and shifted to the right, with a factor reflecting the applied increase in temperature. For the ”best-case” scenario, RCP2.6, November, December, January, February and March have sub-zero temperatures in the end of their periods. This is in accordance with what is shown in figure 6.10. A similar pattern is present for RCP8.5, but the negative temperatures are closer to 0°C.

Compared to the 2016 PLAXIS model, the mean annual surface temperatures (MAST) have increased 1.88°C and 6.82°C, for RCP2.6 and RCP8.5, respectively. This correlates reasonably well with the projected increase in surface temperatures tabulated in table 6.3. The MAGTs in 2090 are modelled to be 1.65°C and 6.59°C for the ”best- and worst-case” scenario. However, it is well worth noting that assumptions and simplifications in the procedure affect the model result. First of all, the increase was assume to start 1st January 2018 and not from 2016 since ground temperature values in 2016 and 2017 are known. Secondly, the MAST from PLAXIS is calculated based on the last day of the month values. The ΔT is applied to daily values. Finally, it should be mentioned that this model is based on short-term temperature records and caution is necessary when using it for future predictions. Trends among the annual temperature fluctuations should be investigated for a longer period of time. It should also be mentioned that the mesh refinement close to the surface is to coarse, even though fine mesh is used. The denser the mesh, the closer the approximate solution gets to the observed temperatures.

Furthermore, attention should be give to the significant increase in the thickness of active layer in 2090 compared to the 2016 PLAXIS model. This observation is as expected since the surface temperature and mean annual temperature increase from 2016 to 2090. For the ”best-case” scenario the ALT increases with 1.0 m and for the ”worst-case” scenario the ALT increases with 1.8 m. This bring us to the question presented in the beginning of the chapter; if it is possible to forward model the active layer thickness as a result of increasing air temperatures. One could think that since the PLAXIS model for 2016 overestimated the ALT compared to measurements, this error would also apply to the ALT in the PLAXIS models for 2090. Moreover, adjusting for the overestimation, the ALT for the RCP2.6 scenario would be 2.12 m. The RCP8.5 scenario would initiate an ALT of 2.92 m. It is to be questioned whether these active layers are reasonable or not, due to the simple model approach, rough estimates and choice of input parameters. Nevertheless, despite the weak data collection and procedure, it is essential to realize that an increase in active layer thickness will most likely following climate warning. Additionally, future increase of extremes in temperature and precipitation will have a large impact on the ground temperature regime, thus changes in the permafrost (Isaksen et al., 2007). In the PLAXIS model, the

depth of zero annual amplitude (ZAA) and mean annual ground temperature (MAGT) in 2090 match the measurements from 2016. This is due to the bottom boundary conditions selected for the PLAXIS. Thus, it is not possible to evaluate an eventual change in the position of the zero annual amplitude (ZAA) or future mean annual ground temperature (MAGT).

No final conclusion of the future increase in the active layer thickness can be made from the PLAXIS model in this master thesis. As discussed, the geothermal model is based on a variety of assumptions and simple procedure that play a role in the final result. The future climate data and the 2090 PLAXIS model brings skepticism. One thing is the use of NCAR-data directly instead of following a downscaling procedure, but also the future reality itself creates uncertainly (Kelder, 2017). A more complex model set-up which represents the study site in a way that is closer to reality should be investigated in future studies of the ground temperature regime in Adventdalen, Svalbard.

6.7.3 Previous Studies

With the PLAXIS results in mind, it could be interesting to investigate two recent studies to see how the results compare. Firstly, a report focusing on expected climate change long-term consequences for construction and management on Svalbard was developed for Statsbygg by Eraker et al. (2018). With the recognition of a warmer climate and increased precipitation on Svalbard, the report emphasizes that attention must be given to maintenance of existing buildings and to design and foundation of new buildings. As basis for the future climatic scenarios of the Longyearbyen area, three RCP-scenarios are modelled using Temp/W, developed by Geo-Slope International LTD. The geothermal modelling indicated an active layer of about 2.5 m in 2100 for a middle high emission scenario (RCP4.5). In comparison with the PLAXIS model, this ALT lays between the predicted RCP2.6 and RCP8.5 scenarios. Thus, one may use this as evidence to support the PLAXIS results, provided that one bear in mind the limitations of the methods used to obtain it. For example, it should be pointed out that the study site are not exactly the same. Additionally, the data collection and results in the Statsbygg-report are of much higher quality than the geothermal model proposition in PLAXIS. However, both observations and the agreement between the two studies are very interesting and should be investigated further. With a more detailed and accurate temperature prediction and procedure it might be possible to use the PLAXIS model for estimation of future thawing of the active layer.

Moreover, Kelder (2017) investigated the effects of climate change and organic matter content on modelled active layer thickness and the thermal state of permafrost in Adventdalen, Svalbard in her master thesis. She used the same temperature scenarios, RCP2.6 and RCP8.5, but used a software called CoupModel which is a coupled heat and mass transfer model. The CoupModel gave continuous results for the study period from 2014 to 2100. Comparing the result from the PLAXIS model and the CoupModel is difficult, but attention should be given to the development of the RCP8.5 scenario with time. In contrast to the PLAXIS model discussed above, Kelder's (2017) model showed that a complete permafrost degradation took place around 2088. To expect a future collapse of the active layer

is very dramatic, but should be seriously investigated in further permafrost modelling and research.

All in all, one must acknowledge that there are large uncertainties related to the amount of warming in the ground temperatures, and how the heat flow will be affect. However, a general rise in ground temperatures has been observed. The increase is assumed not to pose an immediate threat to natural and human systems, but the long-term consequence could cause severe impacts on the stability of infrastructure (Isaksen et al., 2007).

Chapter 7

Summary and Recommendations for Further Work

7.1 Summary

Seasonal and permanently frozen ground are characteristics of cold regions. Soil in frozen state is characterized by high compressive strength and has been utilized by geotechnical engineers in construction of frozen earth structures. On the other hand, frozen ground can also be challenging and formation of complex terrain features and zone of ice-enriched ground may lead to difficult and expensive construction problems. The seasonal frozen layer (active layer) above the permafrost is highly sensitive to temperature changes. For assessment of the quantity of transported heat in the soil, thermal properties of the soil are of interest.

Longyearbyen, Svalbard and other cold region cities are likely to experience increased air temperatures. Thus, the surface and ground temperatures will increase leading to reduced bearing capacity and more settlement problems. These effects experienced by the active layer and permafrost should be taken very seriously in permafrost engineering design. Moreover, uncertainty is related to the extent of climate change. Geothermal modelling can serve as a good tool to explore the possible consequences of a warmer climate. Models may contribute to an overall improved understanding of the processes related to the ground thermal regime.

In this master thesis, permafrost soil from the Norwegian Geo-Test Sites (NGTS) project in lower Adventdalen, Svalbard has been investigated. Methods to determine the thermal properties of frozen (and unfrozen) soils have been presented and evaluated. The experimental part of the thesis included index testing and direct measurements of thermal properties using the KD2 Pro Thermal Properties Analyzer. All the laboratory investiga-

tions were performed at the University Centre in Svalbard (UNIS). The results from 12 core samples were presented verses depth. Furthermore, ground temperature profiles from 2016 and 2017 were created. The ground temperatures were obtained from a thermistor sting installed in a borehole in lower Adventdalen. From this data, back-calculations of the thermal properties of the soil were conducted. Finally, geothermal modelling was done in PLAXIS to simulate the present ground thermal regime, but also to look at the thermal response of permafrost to changes in air temperature in Adventdalen. In particular, the PLAXIS model was aimed to simulate the active layer thickness (ALT) and how it can be affected by changing climate.

7.2 Discussion and Conclusions

The results from the index testing indicated well-sortted deposits dominated by fines. The water content was higher in the upper part of the profile, which reflects a layer that experience thawing as a result of seasonal temperature fluctuations. Supported by the thermistor string installed in the same soil type in Adventdalen, the active layer reached to about one meter depth. The two meters of soil underneath can be interpreted as a transition layer to the permafrost table. Generally, the material is partially saturated with no clear pattern with depth. The unit weight of the soil below the transition layer was in the range of 15.9 - 18.3 kN/m^3. The organic content in the soil was low, but as expected the highest values were found closes to the surface. The salinity measurements indicated marine deposits in deeper layers.

The thermal properties were recorded by a heated needle connected to a hand - held controller designed by Decagon Devices. The KD2 Pro logger used transient line heat source theory to obtain the thermal conductivity, thermal diffusivity and volumetric heat capacity of the soil. Two types of needles were used. The TR-1 single needle for unfrozen and frozen thermal conductivity, and the SH-1 dual-needle for the other properties in unfrozen state only. The results showed that the frozen thermal conductivity, 1.736 - 3.844 W/mK, was higher than the unfrozen thermal conductivity, 1.329 - 1.746 W/mK, for all samples tested. Despite the fact that previous research has shown dependencies for changes in the thermal properties on water content, salinity, organic content, soil type and dry density, no conclusions could be drawn from the results in this master thesis. Nevertheless, the higher water contents in the top part of the frozen profile, correlated with the highest values of thermal conductivity. For the unfrozen state, and high water contents, the thermal conductivity was reduced. These trends were in accordance with the results reported by Aleksyutina and Motenko (2017). The thermal diffusivity indicated a slightly increase with depth ranging from 0.296 mm^2/s to 0.575 mm^2/s, while the volumetric heat capacity decreased and had its highest values in the top. The measured volumetric heat capacities varied between 3.429 MJ/m^{3}K and 2.099 MJ/m^{3}K.

The average thermal conductivity diagram based on Kersten's (1949) equations were used to evaluate thermal conductivity obtained from direct measurements and index properties. From index tests water content (w), dry density (ρ_d) and degree of saturation (Sr) were used. Direct measurements were obtained with the KD2 Pro Thermal Properties Analyzer.

From the analysis it was clear that it was a distinct disagreement between the two methods, generally larger for the frozen state than the unfrozen state. The average diagrams underestimated the thermal conductivity for most soil samples. The deviation between the methods was larger than 25 % for 56 % of the tested samples. Hence, it must be acknowledged that Kersten's (1949) diagrams should be used with care in geotechnical engineering in cold regions. Site specific investigation should be performed before any building activity in permafrost soils. Moreover, it can be conclude that it remains a need for more thermal conductivity measurements and data on permafrost soil to fully evaluate the used of the diagrams.

Thermal properties can be calculated from back-calculation of temperature data. By using the amplitude and phase lag methods, one can find the soil thermal diffusivity in the field. Since the methods assume a homogeneous soil and are based on temperature amplitudes and phase lag, back-calculation suffer from challenges such as identification and timing of minimum and maximum temperatures. The average thermal diffusivity calculated from the temperature data from the CALM site in Adventdalen was 0.57 mm^2/s. This giving a thermal conductivity of 1.58 W/mK, correlation very well with the direct measurements with the KD2 Pro.

In cold regions, the temperature regime in the ground is very important for the thickness and temperature of the permafrost. Thermistor string installations can give information of the annual fluctuations of the ground temperature, often represented as a trumpet curve. In lower Adventdalen, ground temperature data to a depth of 9.85 meters was obtained and plotted for 2016 and 2017. The ground temperature fluctuations over the measuring period were in agreement with literature. Indeed the temperature attenuated with depth, and the upper part of the profile experienced seasonal thawing. The temperature envelope created for 2016 had a mean annual ground temperature (MAGT) of -5.25°C taken at the depth of zero annual amplitude (ZAA), assumed to be at 9.85 meters. The MAGT in 2017 was -5.17°C. The active layer was estimated to 0.98 meter and 0.92 meter in 2016 and 2017, respectively. Finally, the mean annual surface temperature (MAST), was calculated based on the last day of the months. In 2016, the thermistor sensor at 0.0 m gave a MAST of -0.77°C, while the MAST in 2017 was - 2.25°C.

The one - dimensional PLAXIS model was created to investigate the effects of changing climate on ground temperatures. Because the active layer is sensitive to temperature variations, a critical boundary condition for the PLAXIS model was the surface temperature. A simple correlation between air and surface temperatures was used and deviations from real surface temperature values were present. Hence, the simulated ground temperature profiles in 2016 and 2017 did not fit the measurements perfectly. In particular the mean annual surface temperature differed. Furthermore, a more important and major deviation was found in the thickness of the active layer. In 2016 the ALT was modelled to be 2.1 meters and in 2017 the ALT was 2.0 meter. For both years it was a overestimation of about 1.0 meter. It is difficult to find the source causing the error, but uncertainties are related to the thermal and physical input data as well as the surface boundary condition. For example, the thermal properties obtained by the KD2 Pro could be wrong. The increase in active layer thickness can be consequence of too high values of soil heat capacity and thermal conductivity. In particular, the thermal conductivity will affect the heat flow in the soil

polygon. The modelled ZAA and MAGT were as expected due to the bottom boundary condition of the model.

The PLAXIS models for 2090 indicated two interesting features. First of all, both climate scenarios, RCP2.6 and RCP8.5, showed an increase in mean annual surface temperature that were in accordance with applied values. The temperature profiles were shifted to the left, the RCP8.5 to a larger extent than the RCP2.6. Secondly, there was an increase in the active layer thickness for both scenarios. The ALT increase is a consequence of the warmer air (and surface) temperatures assumed in the future. Adjusting for the "doubling-effect" found in the 2016 model, the ALT for the RCP2.6 scenario would be 2.12 m. The RCP8.5 scenario would initiate an ALT of 2.92 m. Changes in the ZAA and MAGT were not investigated due to the fixed bottom boundary condition. Overall, it can be concluded that climate change will have an impact on frozen soils that is crucial to include in the global climate models (Kelder, 2017).

Finally, with future thawing of the active layer and permafrost degradation, installations will become exposed to uneven settling of sediments and potential degradation. In frozen ground engineering, geotechnical considerations should include evaluation of consequences for infrastructure and buildings that are currently not resting on bedrock. If the current practice is not adapted to the warming conditions, large construction and maintenance costs of buildings and infrastructure are expected. Therefore, proper site investigation strategies and foundation practices must be developed for future development of cold regions (Eraker et al., 2018).

7.3 Recommendations for Further Work

For further work within the topic, the following points are recommended to be performed:

- For measurements of thermal conductivity of frozen soils with the KD2 Pro Thermal Properties Analyzer, routines need to be formed and established.
- Extensive testing should be performed on permafrost soils from Adventdalen, Svalbard and other permafrost regions in order to evaluate the applicability of Kersten's (1949) average thermal conductivity diagrams.
- Back-calculation of temperature data from several thermistor strings should be preformed in order to evaluate the thermal properties of a study site in the field.
- The geothermal model in PLAXIS is simple, and for more accurate simulations and results it needs to be investigated more. Especially, development of the active layer thickness should be be examined. Testing and adjustments of the input data are required to find the errors in the model. In particular, the surface and bottom boundary conditions can be improved by employing a more sophisticated correlation between air and ground surface temperature to gather complete data sets and to use a geothermal gradient. Additionally, continuous results for a time period, rather than single values, would be preferred and be of lager value for analysis of thawing of the active layer and permafrost degradation with time.

- Modelling projects of future permafrost scenarios should use high quality temperature data with high resolution and downscaling, rather than NCAR-data directly. A more complex model set-up which represents the study site in a way that is closer to reality should be investigated in future studies of the ground temperature regime in Adventdalen, Svalbard.
- Permafrost models can be more useful tools in geotechnical engineering design by including mechanical factors in addition to heat flow. In particular, load, creep and water flow would be parameters of interest. Such parameters are available in the PLAXIS software.

Bibliography

Aleksyutina, D. and Motenko, R. (2017). The composition, structure and properties of frozen and thawed deposits on the baydaratskaya bay coast, kara sea. *Kriosfera Zemli (Earth's Cryosphere)*, XXI(1):11–22.

Andersland, O. and Anderson, D. (1978). *Geotechnical engineering for cold regions*. Mcgraw-Hill College.

Andersland, O. B. and Ladanyi, B. (1994). *An introduction to Frozen ground engineering*. Chapman & Hall.

Anderson, D. M., Banin, A., and Tice, A. R. (1976). The prediction of unfrozen water contents in frozen soils from liquid limit determinations. Technical report, US Cold Regions Research and Engineering Laboratory. CRREL report 76-8.

Anderson, D. M., Tice, A. R., and McKim, H. L. (1973). The unfrozen water and the apparent specific heat capacity of frozen soils. In *Second International Conference on Permafrost, Yakutsk, USSR. North American contribution*, pages 289–295.

ASTM D1125 (1998). Tests for chemical properties of aggregates. Standard, American Society for Testing and Materials.

ASTM D2487 (2017). Standard practice for classification of soils for engineering purposes (unified soil classification system. Standard, American Society for Testing and Materials.

ASTM D422 (2007). Standard test method for particle-size analysis of soils. Standard, American Society for Testing and Materials.

ASTM D5334 (2014). Standard test method for determination of thermal conductivity of soil and soft rock by thermal needle probe procedure. Standard, American Society for Testing and Materials.

ASTM E11 (2017). Standard specification for woven wire test sieve cloth and test sieves. Standard, American Society for Testing and Materials.

Barry-Macaulay, D., Bouazza, A., Wang, B., and Singh, R. (2015). Evaluation of soil thermal conductivity models. *Canadian Geotechnical Journal*, 52(11):1892–1900.

Bates, R. E. and Bilello, M. A. (1966). Defining the cold regions of the northern hemisphere. Technical report, U.S.Amy Cold Reg.Res.Eng.Lab.178.

Batir, J. F., Hornbach, M. J., and Blackwell, D. D. (2017). Ten years of measurements and modeling of soil temperature changes and their effects on permafrost in northwestern alaska. *Global and Planetary Change*, 148:55–71.

Becker, B. R., Misra, A., and Fricke, B. A. (1992). Development of correlations for soil thermal conductivity. *International Communications in Heat and Mass Transfer*, 19(1):59–68.

Bratlie, U. H. H. (2017). *Thermal properties of permafrost*. Project thesis. Norwegian University of Science and Technology, Department of Civil and Environmental Engineering.

Brown, J., Ferrians Jr, O., Heginbottom, J., and Melnikov, E. (1998). *Circum-Arctic map of permafrost and ground-ice conditions*. Boulder, CO: National Snow and Ice DataCenter. Digital media.

Brown, R., Johnston, G., Mackay, J., Morgenstern, N., and Shilts, W. (1981). Permafrost distribution and terrain characteristics. *Permafrost engineering design and construction. Wiley, New York*, pages 31–77.

Camuffo, D. and Bernardi, A. (1982). An observational study of heat fluxes and their relationships with net radiation. *Boundary-Layer Meteorology*, 23(3):359–368.

Carslaw, H. S. and Jaeger, J. C. (1959). Conduction of heat in solids. *Oxford: Clarendon Press, 1959, 2nd ed.*

Carter, M. R. (1993). *Soil sampling and methods of analysis*. CRC Press.

Côté, J. and Konrad, J.-M. (2005). A generalized thermal conductivity model for soils and construction materials. *Canadian Geotechnical Journal*, 42(2):443–458.

Eraker, T., Rongved, J. L., Instanes, A., and Isaksen, K. (2018). Forventede klimaendringers langsiktige konsekvenser for bygging og forvaltning p svalbard. Technical report, Statsbygg.

Farouki, O. (1986). Thermal properties of soils. series on rock and soil mechanics, vol. 11. clausthal-zellerfeld.

Farouki, O. T. (1981). The thermal properties of soils in cold regions. *Cold Regions Science and Technology*, 5(1):67–75.

Førland, E. J., Benestad, R., Hanssen-Bauer, I., Haugen, J. E., and Skaugen, T. E. (2011). Temperature and precipitation development at svalbard 1900–2100. *Advances in Meteorology*, 2011.

Frauenfeld, O. W., Zhang, T., and Mccreight, J. L. (2007). Northern hemisphere freezing/thawing index variations over the twentieth century. *International Journal of Climatology*, 27(1):47–63.

French, H. M. (2007). *The periglacial environment, Third edition*. John Wiley & Sons Ltd.

French, H. M. (2011). Periglacial. In *Encyclopedia of Snow, Ice and Glaciers*, pages 827–841. Springer.

Fricke, B. A., Misra, A., Becker, B., and Stewart, W. (1992). Soil thermal conductivity: effects of saturation and dry density. In *Thermal Performance of the Exterior Envelopes of Whole Buildings V International Conference, Clearwater Beach, Florida, USA*.

Fröb, K. (2011). *Measuring and modeling of soil thermal properties and ground heat flux at two different sites at Lena Delta, Siberia*. PhD thesis, University of Leipzig.

Fuchs, M. (1986). Heat flux. *Methods of Soil Analysis: Part 1Physical and Mineralogical Methods*, 1(methodsofsoilan1):957–968.

Garca-Gaines, R. A. and Frankenstein, S. (2015). Uscs and the usda soil classification system: Development of a mapping scheme. Technical report, Engineer Research and Development Center Hanover NH Cold Region Research and Engineering Lab.

Gilbert, G. L. (2014). Sedimentology and geocryology of an arctic fjord head delta (adventdalen, svalbard). Master's thesis, University of Oslo.

Gilbert, G. L., O'Neill, H. B., Nemec, W., Thiel, C., Christiansen, H. H., and Buylaert, J.-P. (2018). Late quaternary sedimentation and permafrost development in a svalbard fjord-valley, norwegian high arctic. *Sedimentology*.

Guodong, C. (1983). The mechanism of repeated-segregation for the formation of thick layered ground ice. *Cold Regions Science and Technology*, 8(1):57–66.

Han, F. S. (2011). Geotechnical behaviour of frozen mine backfills. Technical report, University of Ottawa (Canada).

Harlan, R. and Nixon, J. (1978). Ground thermal regime. *Geotechnical engineering for cold regions*, pages 103–163.

Humlum, O. (2018). Calm site in adventdalen (accessed april 2018). `https://www.researchinsvalbard.no/project/5752`.

Humlum, O., Instanes, A., and Sollid, J. L. (2003). Permafrost in svalbard: a review of research history, climatic background and engineering challenges. *Polar research*, 22(2):191–215.

Hutcheon, W. L. (1958). Moisture flow induced by thermal gradients within unsaturated soils. *Highway Research Board Special Report*, (40).

Inman, M. (2011). Opening the future. *Nature climate change*, 1(1):7.

Isaksen, K., Benestad, R., Harris, C., and Sollid, J. (2007). Recent extreme near-surface permafrost temperatures on svalbard in relation to future climate scenarios. *Geophysical Research Letters*, 34(17).

Isaksen, K., Mühll, D. V., Gubler, H., Kohl, T., and Sollid, J. L. (2000). Ground surface-temperature reconstruction based on data from a deep borehole in permafrost at janssonhaugen, svalbard. *Annals of Glaciology*, 31:287–294.

ISO 11265 (1994). Soil quality -determination of the specific electrical conductivity. Standard, International Organization for Standardization.

Jaeger, J. (1956). Conduction of heat in an infinite region bounded internally by a circular cylinder of a perfect conductor. *Australian Journal of Physics*, 9(2):167–179.

Johansen, Ø. (1975). Thermal conductivity of soils. *PhD thesis, Norwegian Technical University, Trondheim. Also: U.S. Army Cold Reg. Res. Eng. Lab. Transl. 637, July 1977*.

Johnston, G. H. (1981). *Permafrost: engineering design and construction*. J. Wiley.

Kelder, A. M. (2017). Effects of climate change and organic matter content on modelled active layer thickness and the thermal state of permafrost in adventdalen, svalbard. Master's thesis, Department of Physical Geography, Stockholm University.

Kersten, M. S. (1949). Laboratory research for the determination of the thermal properties of soils. Technical report, Minnesota univ Minneapolis Engineering Experiment Station.

Krzewinski, T. G. and Tart Jr, R. G. (1985). *Thermal design considerations in frozen ground engineering*. ASCE Publications.

Kurylyk, B. L. and Watanabe, K. (2013). The mathematical representation of freezing and thawing processes in variably-saturated, non-deformable soils. *Advances in Water Resources*, 60:160–177.

Meter Environment (2018). Thermal properties: why the transient method outperforms other techniques (accessed may 2018). `https://www.metergroup.com/environment/articles/thermal-properties-transient-method-outperforms-techniques/`.

Mühll, D. V. and Haeberli, W. (1990). Thermal characteristics of the permafrost within an active rock glacier (murtèl/corvatsch, grisons, swiss alps). *Journal of Glaciology*, 36(123):151–158.

NCAR (2012). The national center for atmospheric research. climate change scenarios, version 2.0. community climate system model, june 2004, version 3.0 (accessed may, 2018). `https://gisclimatechange.ucar.edu/inspector`.

NGI (2016). Ngts - norwegian geo-test sites (accessed may 2018). `https://www.ngi.no/eng/Projects/NGTS-Norwegian-Geo-Test-Sites`.

Nordli, Ø. (2010). The svalbard airport temperature series. *Bulletin of Geography. Physical Geography Series*, (3):5–25.

NS 8005 (1990). Geotechnical testing - laboratory methods - grain-size analysis of soil samples. Standard, Standard Norge.

NS-EN ISO 14688-2 (2004). Geotechnical investigation and testing - identification and classification of soil - part 2: Principles for a classification. Standard, Standard Norge.

NS-EN ISO 1744 (2014). Standard test methods for electrical conductivity and resistivity of water. Standard, Standard Norge.

NS-EN ISO 17892 (2014). Geotechnical investigation and testing - laboratory testing of soil. Standard, Standard Norge.

NSIDC (2017). National snow and ice data center: All about frozen ground (accessed march, 2018). `https://nsidc.org/cryosphere/frozenground/index.html`.

Nybo, M. S. (2017). An experimental study of unfrozen water content in fine grained permafrost soils. Master's thesis, Norwegian University of Science and Technology, Department of Civil and Environmental Engineering.

Oliva, M., Vieira, G., Pina, P., Pereira, P., Neves, M., and Freitas, M. (2014). Sedimentological characteristics of ice-wedge polygon terrain in adventdalen (svalbard)-environmental and climatic implications for the late holocene. *Solid Earth*, 5(2):901.

Penner, E., Johnston, G., and Goodrich, L. (1975). Thermal conductivity laboratory studies of some mackenzie highway soils. *Canadian Geotechnical Journal*, 12(3):271–288.

Putkonen, J. (2003). Determination of frozen soil thermal properties by heated needle probe. *Permafrost and Periglacial processes*, 14(4):343–347.

Rubio, C. M. (2013). A laboratory procedure to determine the thermal properties of silt loam soils based on astm d 5334. *Applied Ecology and Environmental Sciences*, 1(4):45–48.

Schuh, C., Frampton, A., and Christiansen, H. H. (2017). Soil moisture redistribution and its effect on inter-annual active layer temperature and thickness variations in a dry loess terrace in adventdalen, svalbard. *The Cryosphere*, 11(1):635.

Scott, R. F. (1964). *Heat exchange at the ground surface*. US Army Materiel Command Cold Regions Research and Engineering Laboratory.

Strand, S. M. (2016). Ground temperature response to winter warm events in svalbard. Master's thesis, University of Oslo.

Sun, H., Liu, S., and Qin, J. (2016). Characterizing subzero-temperature thermal properties of seasonally frozen soil in alpine forest in the western sichuan province, china. *Journal of Water Resource and Protection*, 8(05):583.

Van Wijk, W. and Bruijn, P. (1964). Determination of thermal conductivity and volumetric heat capacity of soils near the surface. *Soil Science Society of America Journal*, 28(4):461–464.

Watts, D., Kanemasu, E., and Tanner, C. (1990). Modified heat-meter method for determining soil heat flux. *Agricultural and forest meteorology*, 49(4):311–330.

Williams, P. and Smith, M. (1989). The frozen earth: fundamentals of geocryology. cambridge, uk. *Cambridge University Press*.

Williams, P. J. (1964). Unfrozen water content of frozen soils and soil moisture suction. *Geotechnique*, 14(3):231–246.

Williams, P. J. and Smith, M. W. (1991). The frozen earth. *Cambridge University Press*.

Yüksel, N. (2016). The review of some commonly used methods and techniques to measure the thermal conductivity of insulation materials. In *Insulation Materials in Context of Sustainability*. InTech.

Zenklusen Mutter, E. and Phillips, M. (2012). Active layer characteristics at ten borehole sites in alpine permafrost terrain, switzerland. *Permafrost and Periglacial Processes*, 23(2):138–151.

Appendix A

Results from Laboratory Testing

Index Parameters

Table A.1: Index parameters. Densities and unit weight

SINTEF_ID	Depth [m]	ρ [g/cm^3]	γ [kN/m^3]	ρ_d [g/cm^3]	γ_d [kN/m^3]	ρ_s [g/cm^3]	γ_s [kN/m^3]
1	1.3	1.51	14.8	0.93	9.17	2.66	26.13
3	2.1	1.12	11.0	0.45	4.45	2.56	25.12
6	3.3	1.27	12.4	0.62	6.10	2.70	26.46
8	4.1	1.99	19.5	1.74	17.04	2.68	26.27
11	5.3	1.67	16.3	1.26	12.38	2.64	25.87
13	6.1	1.62	15.9	1.20	11.78	2.67	26.17
16	7.3	1.86	18.3	1.47	14.41	2.69	26.40
18	8.1	1.72	16.9	1.28	12.51	2.69	26.40
21	9.3	1.72	16.9	1.25	12.31	2.56	25.09
23	10.5	1.78	17.4	1.31	12.87	2.70	26.49
25	11.3	1.74	17.0	1.30	12.76	2.66	26.05
27	12.1	1.74	17.1	1.31	12.84	2.71	26.56

Table A.2: Index parameters

SINTEF_ID	Depth [m]	w [%]	O.C [ppt]	Salinity [%]	n [%]	Sr
1	1.3	61	4.0	4.77	43	88
3	2.1	147	5.8	1.90	56	81
6	3.3	104	3.9	5.00	53	84
8	4.1	15	4.9	28.91	26	73
11	5.3	32	4.4	16.91	37	78
13	6.1	35	3.9	30.75	39	77
16	7.3	27	4.4	23.25	31	87
18	8.1	35	4.4	35.49	36	85
21	9.3	37	3.7	29.76	33	92
23	10.5	35	3.6	41.69	34	90
25	11.3	34	3.9	70.18	35	86
27	12.1	33	3.6	50.53	36	84

Thermal Properties

Table A.3: Average values for the thermal properties

Depth [m]	k_{un} (SH-1) [W/mK]	k_{un} (TR-1) [W/mK]	k_f (TR-1) [W/mK]	C_{vu} [MJ/m^{3}K]	D [mm^2/s]
1.3	1.129	1.389	2.859	3.279	0.343
4.1	1.029	1.383	1.900	2.753	0.381
5.3	1.087	1.409	2.038	2.531	0.437
6.1	1.022	1.430	2.718	2.181	0.469
7.3	1.193	1.506	2.315	2.579	0.465
8.1	1.316	1.532	3.056	2.764	0.478
9.3	1.451	1.551	2.715	2.988	0.488
10.5	1.387	1.531	2.420	2.732	0.507
11.3	1.370	1.538	2.427	2.690	0.509
12.1	1.355	1.545	2.603	2.657	0.510

Grain Size Distribution Curves

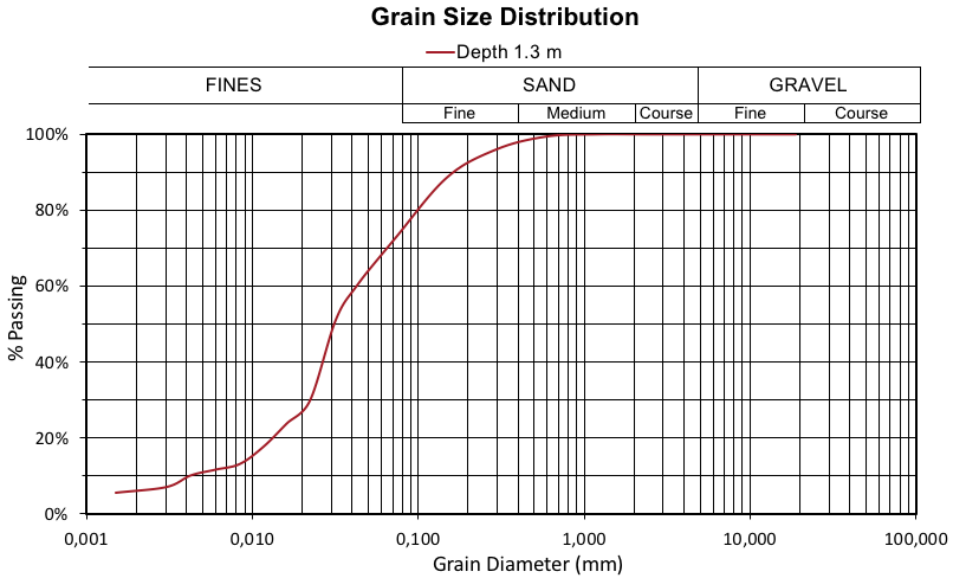

Figure A.1: Grain size distribution curve from 1.3 m

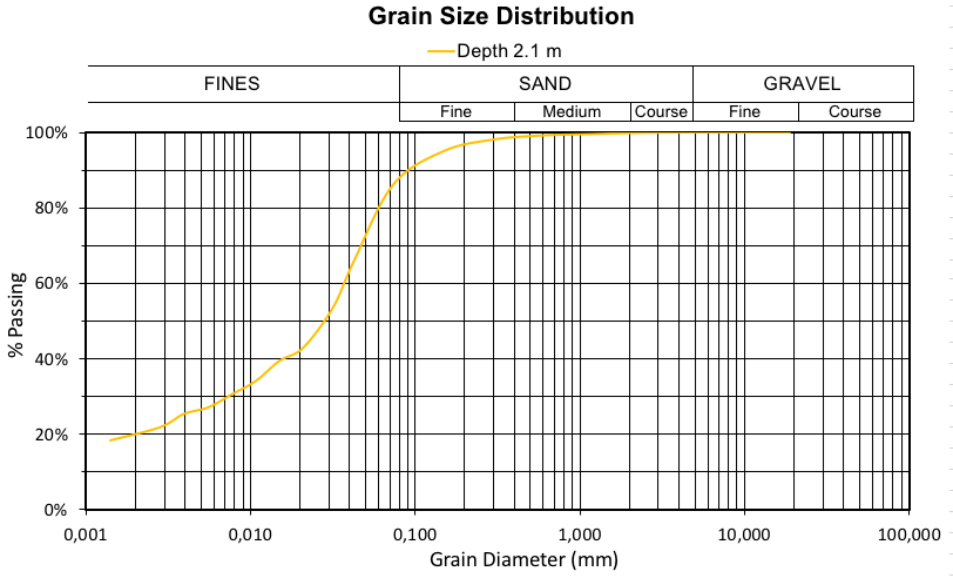

Figure A.2: Grain size distribution curve from 2.1 m

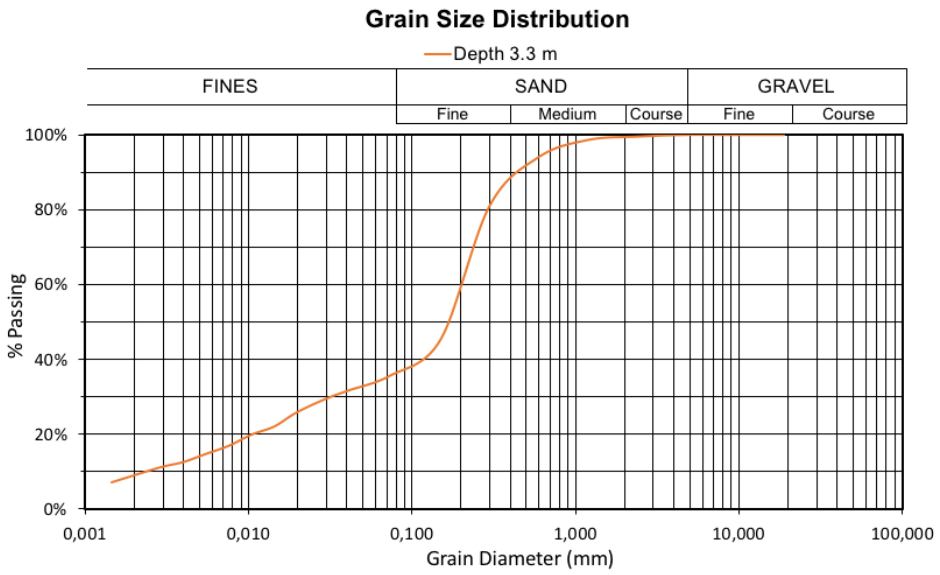

Figure A.3: Grain size distribution curve from 3.3 m

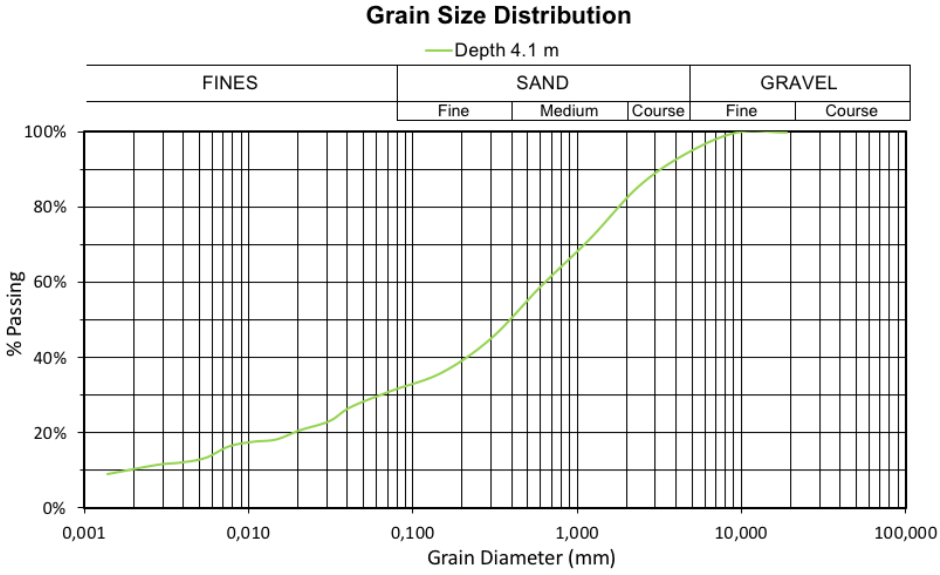

Figure A.4: Grain size distribution curve from 4.1 m

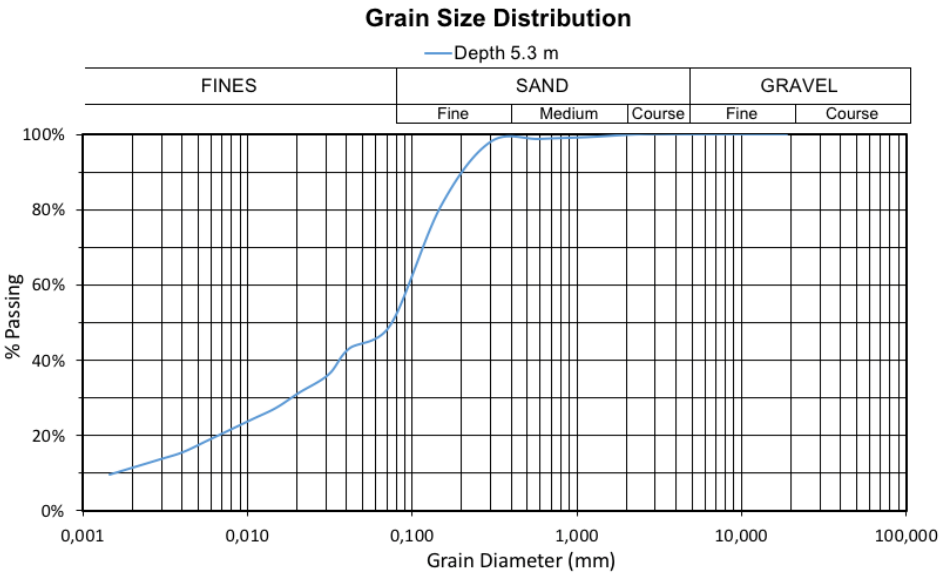

Figure A.5: Grain size distribution curve from 5.3 m

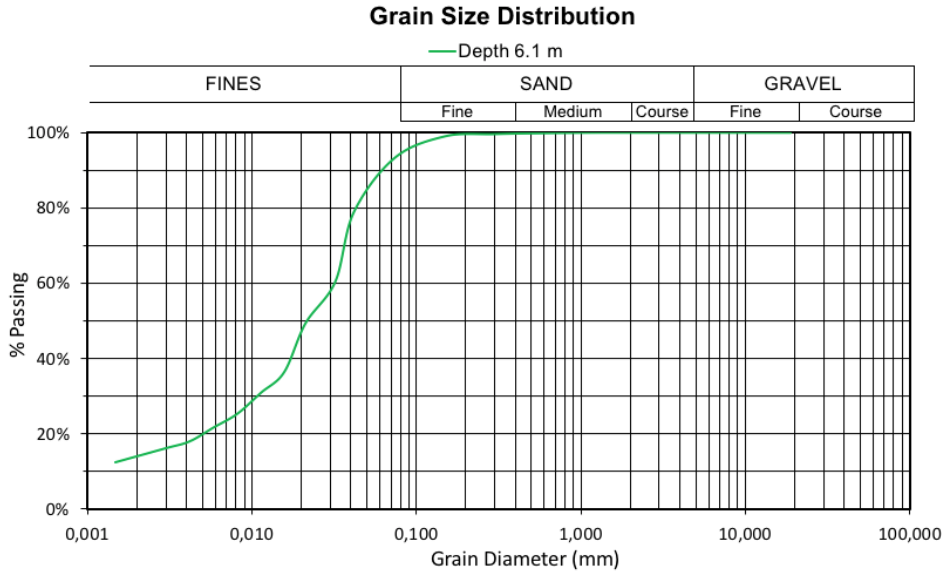

Figure A.6: Grain size distribution curve from 6.1 m

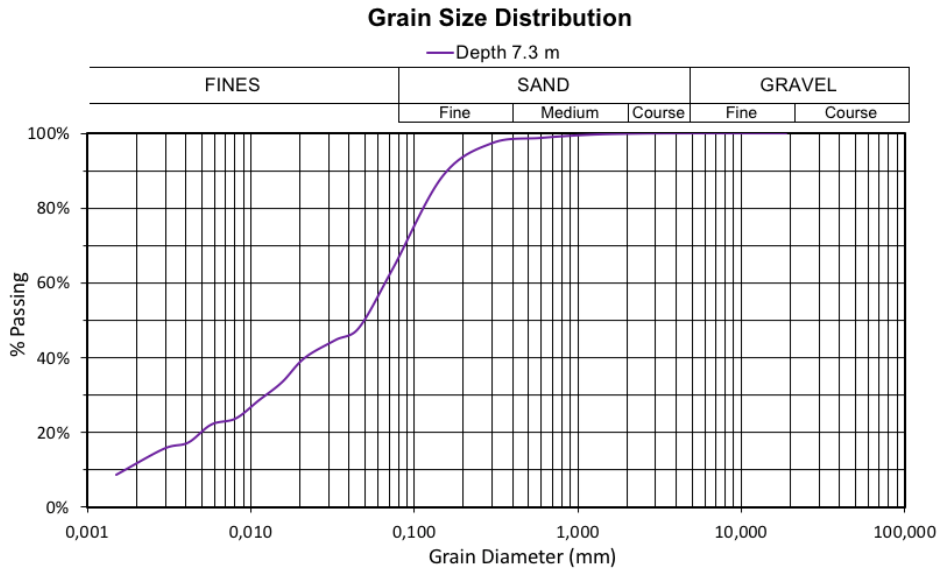

Figure A.7: Grain size distribution curve from 7.3 m

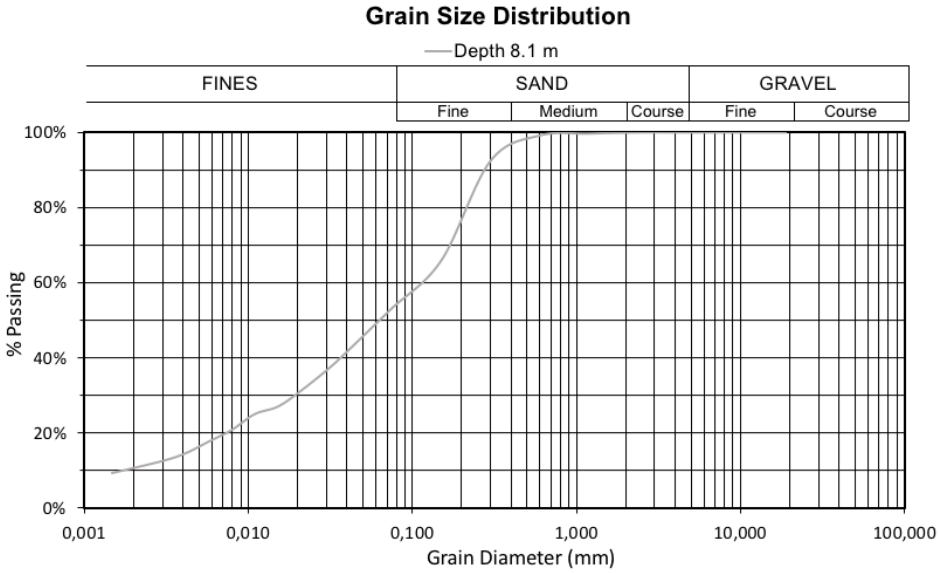

Figure A.8: Grain size distribution curve from 8.1 m

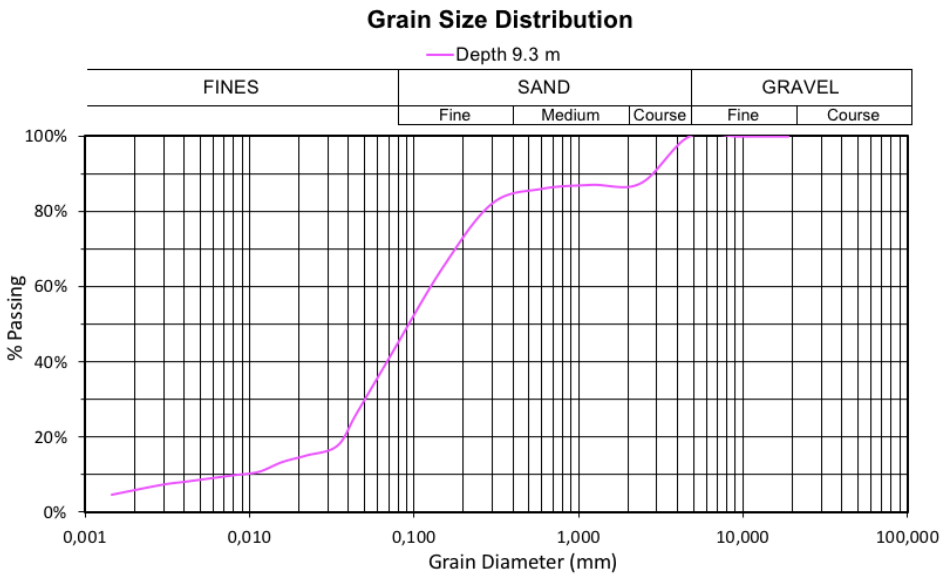

Figure A.9: Grain size distribution curve from 9.3 m

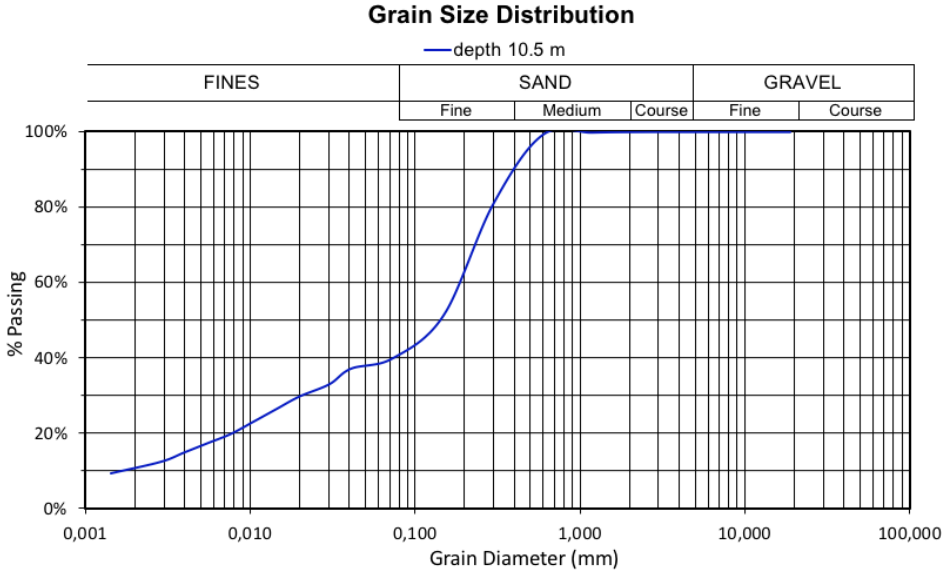

Figure A.10: Grain size distribution curve from 10.5 m

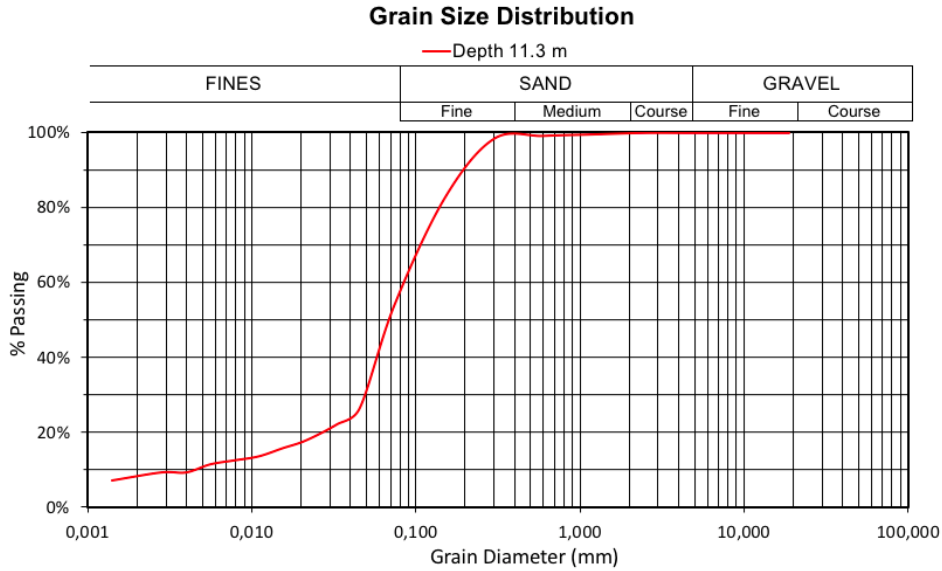

Figure A.11: Grain size distribution curve from 11.3 m

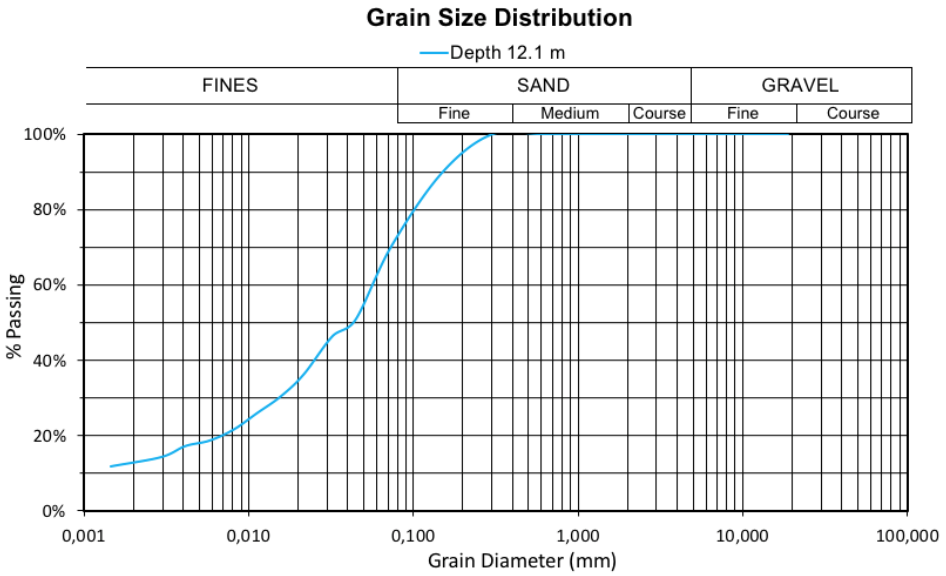

Figure A.12: Grain size distribution curve from 12.1 m

Grain Size Distribution Summary

Table A.4: Soil characteristics after ASTM requirements.

Depth [m]	C_u	C_c	% Gravel	% Sand	% Fines
1.3	10	0	0	27	73
2.1	11	4	0	14	86
3.3	80	2	0	64	36
4.1	300	4	5	64	31
5.3	67	3	0	51	49
6.1	5	0	0	7	93
7.3	44	1	0	36	64
8.1	80	2	0	47	53
9.3	22	3	0	58	42
10.5	130	1	0	60	40
11.3	19	7	0	46	54
12.1	9	0	0	30	70

Note: Particle - size limits (after ASTM D2488); Gravel 75mm - 4.75mm, Sand 4.75mm - 0.0075mm, Fines $<$ 0.0075 mm.

Coefficient of Uniformity:

$$C_u = \frac{D_{60}}{D_{10}} \tag{A.1}$$

Coefficient of Curvature:

$$C_c = \frac{(D_{30})^2}{(D_{10})(D_{60})} \tag{A.2}$$

Appendix B

PLAXIS Model; Calculations and Results

Thermal properties of solid particles

In PLAXIS the input parameters for soil are separated into the components of unfrozen soil; solids, air and water. Hence, the measured thermal conductivity and volumetric heat capacity needs to be solved for the corresponding values for solids. Equation B.2 is used for thermal conductivity-

$$k = (1-n)k_s + nS_r k_w + n(1-S_r)k_{air} \tag{B.1}$$

Equation B.1 is used for specific heat capacity.

$$\rho c = (1-n)\rho_s c_s + nS_r \rho_w c_w + n(1-S_r)\rho_{air} c_{air} \tag{B.2}$$

The equations are solved for c_s and k_s, equations B.3 and B.4, respectively.

$$k_s = \frac{k - nS_r k_w - n(1-S_r)k_{air}}{(1-n)} \tag{B.3}$$

$$c_s = \frac{\rho c - nS_r \rho_w c_w - n(1-S_r)\rho_{air} c_{air}}{(1-n)\rho_s} \tag{B.4}$$

Table B.2 lists the values needed for the PLAXIS model. The measured thermal properties, C_{vu} and k (KD2 Pro measurements), and index properties porosity, n, and degree of

saturation, S_r, are used in equation B.3 and B.4 to find the thermal properties for solids. The values for air and water are valid for 20°C, and given in table B.1. Recall that: C_{vu} = ρc, where C_{vu} is the measured value in (MJ/m^{3}K).

Note that for depth 2.1 m and 3.3 m, the specific heat capacity and thermal conductivity are estimated values, due to the lack of results from KD2 Pro measurements. Both layers are given low thermal conductivity as a result of the porosity and high water content.

	Water
Density, ρ_w, [g/cm^3]	0.9982
Specific heat capacity, c_w, [kJ/kgK]	4.182
Thermal conductivity, k_w, [W/mK],	0.6065
	Air
Density, ρ_{air}, [g/cm^3]	0.0012041
Specific heat capacity, c_{air},[kJ/kgK],	0.7172
Thermal conductivity, k_{air}, [W/mK]	0.02587

Table B.1: Properties of water and air

	Layer 1	Layer 2	Layer 3
Bulk density, ρ, [g/cm^3]	1.51	1.12	1.27
Density of solids, ρ_s, [g/cm^3]	2.66	2.56	2.70
Unfrozen thermal conductivity, k_{un}, [W/m·K]	1.39	0.80	1.00
Unfrozen volumetric heat capacity C_{vu}, [MJ/m^{3}K]	3.28	3.02	2.88
Porosity, n, [-]	0.43	0.56	0.53
Degree of saturation, S_r, [-]	0.88	0.81	0.84
Thermal conductivity of solids, k_s, [W/mK]	1.98	2.52	2.33
Specific heat capacity of solids, c_s, [kJ/kgK]	6.93	6.49	5.13
	Layer 4	Layer 5	Layer 6
Bulk density, ρ, [g/cm^3]	1.99	1.67	1.62
Density of solids, ρ_s, [g/cm^3]	2.68	2.64	2.67
Unfrozen thermal conductivity, k_{un}, [W/mK]	138	1.41	1.43
Unfrozen volumetric heat capacity C_{vu}, [MJ/m^{3}K]	2.75	2.53	2.18
Porosity, n, [-]	0.26	0.37	0.39
Degree of saturation, S_r, [-]	0.73	0.78	0.77
Thermal conductivity of solids, k_s, [W/mK]	1.71	1.96	2.04
Specific heat capacity of solids, c_s, [kJ/kgK]	7.11	5.58	4.06
	Layer 7	Layer 8	Layer 9
Bulk density, ρ, [g/cm^3]	1.86	1.72	1.72
Density of solids, ρ_s, [g/cm^3]	2.69	2.69	2.56
Unfrozen thermal conductivity, k_{un}, [W/m·K]	1.51	1.53	1.55
Unfrozen volumetric heat capacity C_{vu}, [MJ/m^{3}K]	2.58	2.76	2.99
Porosity, n, [-]	0.31	0.36	0.33
Degree of saturation, S_r, [-]	0.87	0.85	0.92
Thermal conductivity of solids, k_s, [W/mK]	1.91	2.10	2.04
Specific heat capacity of solids, c_s, [kJ/kgK]	5.01	6.21	6.58
	Layer 10	Layer 11	Layer 12
Bulk density, ρ, [g/cm^3]	1.78	1.74	1.74
Density of solids, ρ_s, [g/cm^3]	2.70	2.66	2.71
Unfrozen thermal conductivity, k_{un}, [W/mK]	1.53	1.54	1.55
Unfrozen volumetric heat capacity C_{vu}, [MJ/m^{3}K]	2.73	2.69	2.66
Porosity, n, [-]	0.34	0.35	0.36
Degree of saturation, S_r, [-]	0.90	0.86	0.84
Thermal conductivity of solids, k_s, [W/mK]	2.01	2.08	2.07
Specific heat capacity of solids, c_s, [kJ/kgK]	5.37	5.88	4.89

Table B.2: PLAXIS input parameters

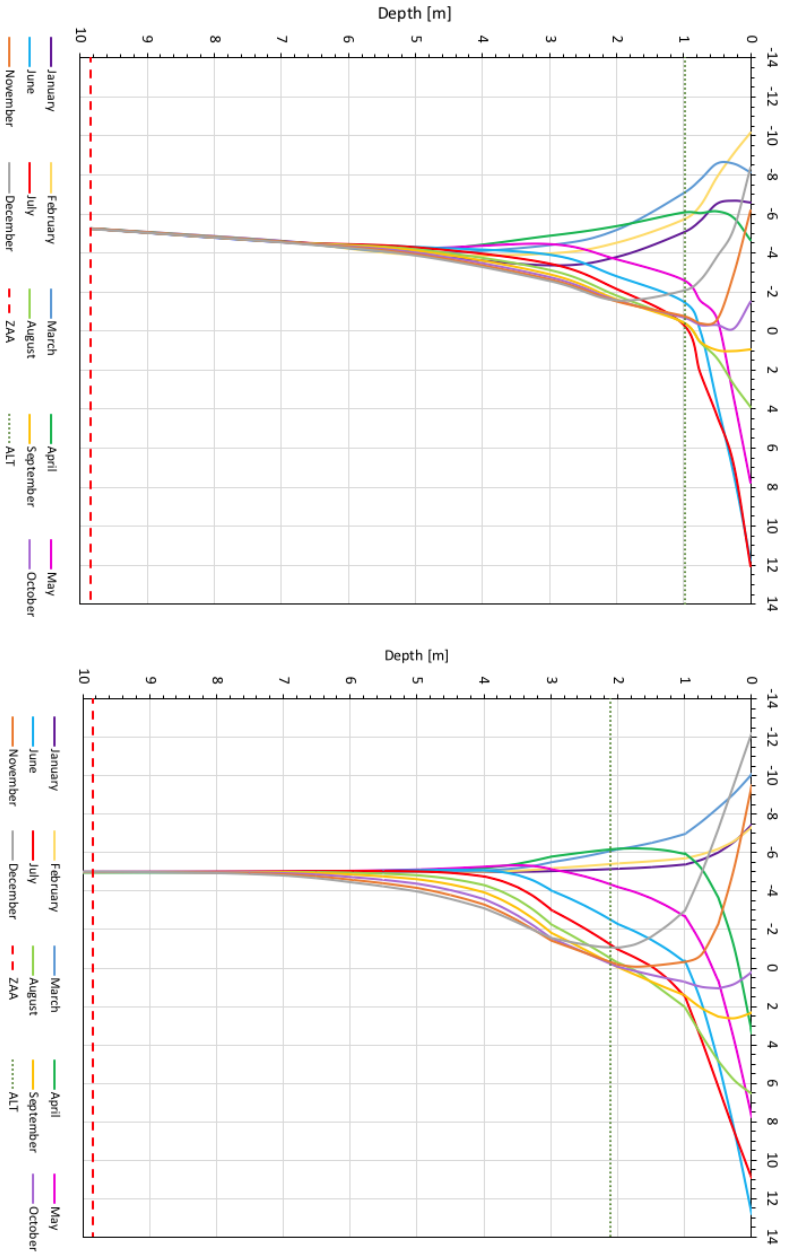

Figure B.1: Comparison of the measured and modelled ground temperature profile in 2016

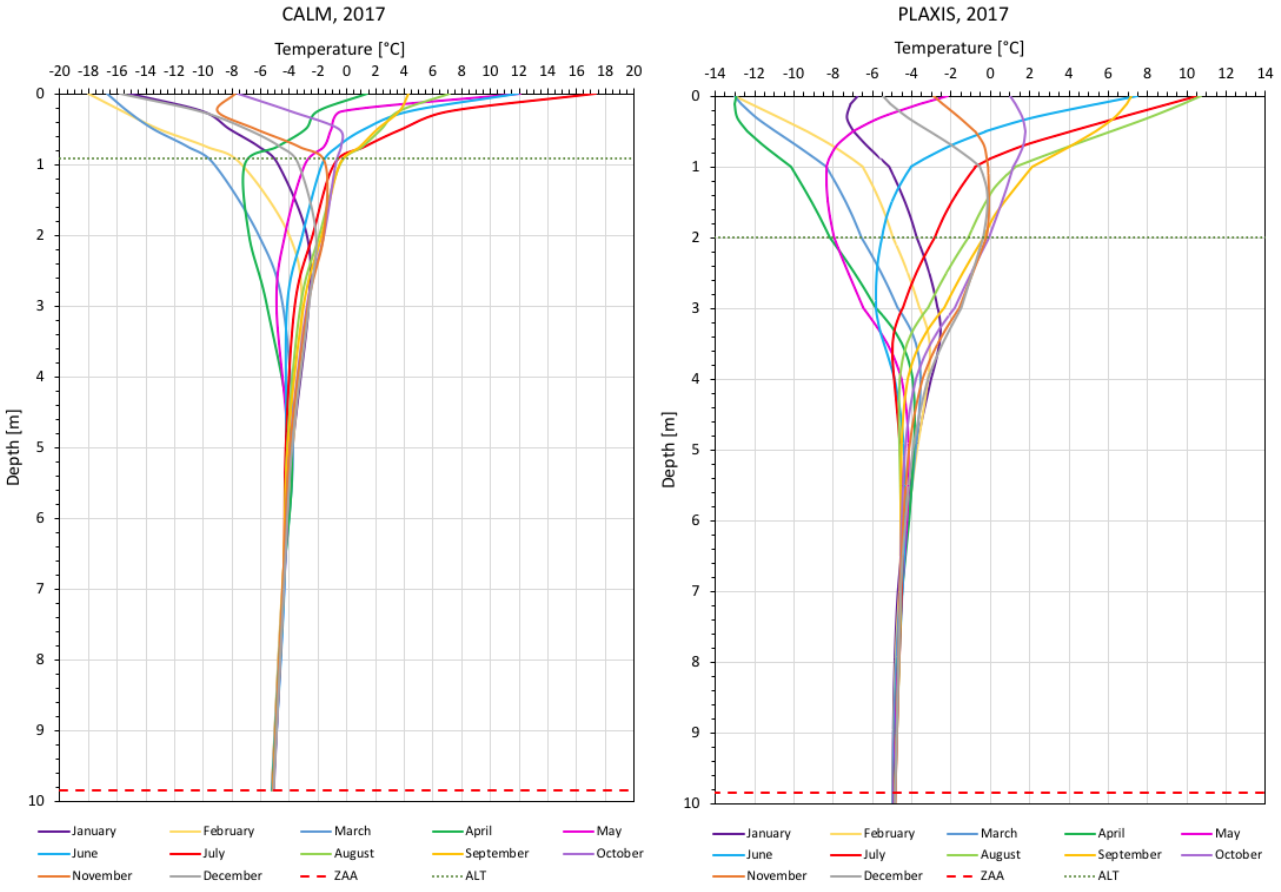

Figure B.2: Comparison of the measured and modelled ground temperature profile in 2017

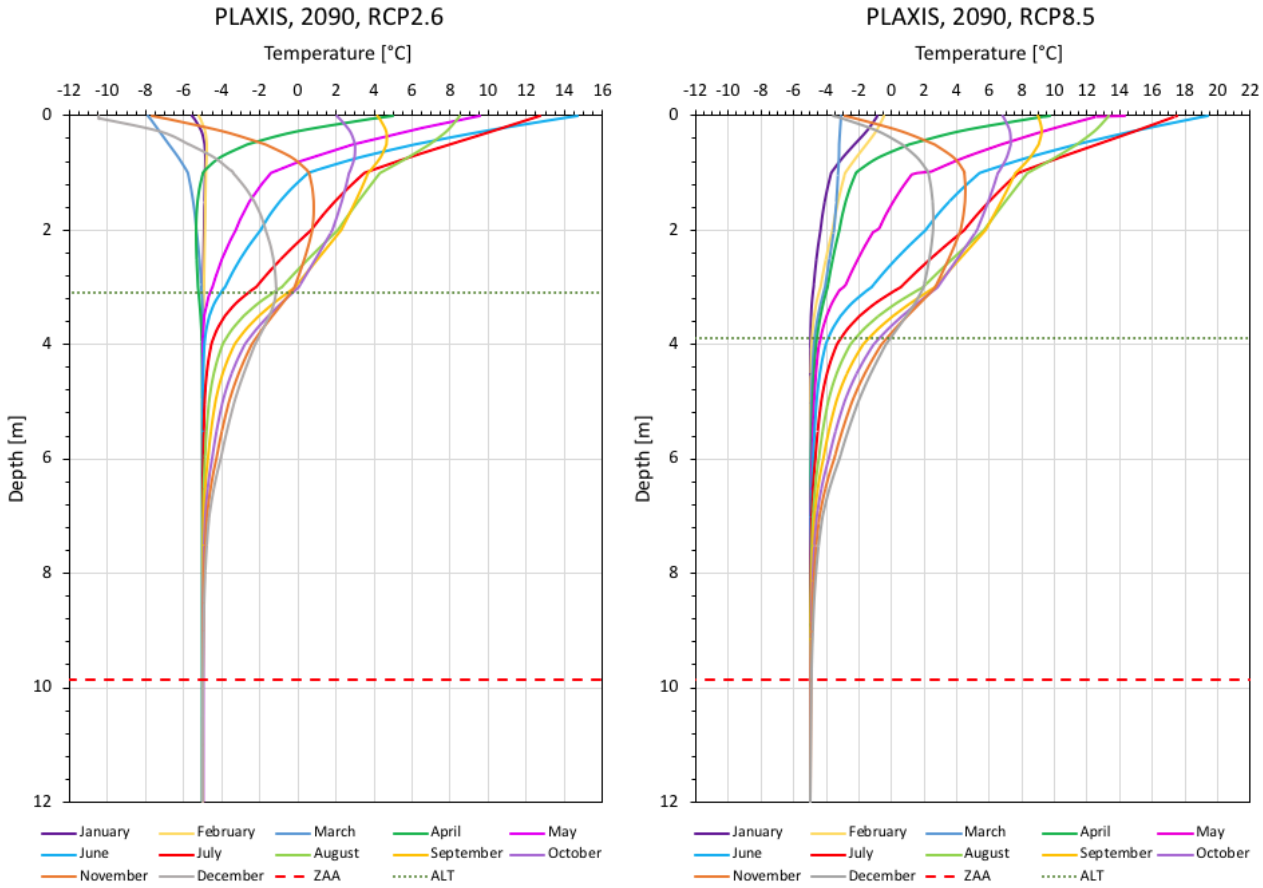

Figure B.3: Comparison of the two scenarios of ground temperature profile in 2090